Assessing a Wave Model à la SWAMP

W. Perrie and B. Toulany

Atlantic Oceanographic Laboratory
Ocean Science and Surveys, Atlantic
Department of Fisheries and Oceans

Bedford Institute of Oceanography
P.O. Box 1006
Dartmouth, Nova Scotia B2Y 4A2

August 1985

Canadian Technical Report of Hydrography and Ocean Sciences No. 61

36-0914/

Canadian Technical Report of Hydrography and Ocean Sciences

These reports contain scientific and technical information of a type that represents a contribution to existing knowledge but which is not normally found in the primary literature. The subject matter is generally related to programs and interests of the Ocean Science and Surveys (OSS) sector of the Department of Fisheries and Oceans.

Technical Reports may be cited as full publications. The correct citation appears above the abstract of each report. Each report will be abstracted in Aquatic Sciences and Fisheries Abstracts. Reports are also listed in the Department's annual index to scientific and technical publications.

Technical Reports are produced regionally but are numbered and indexed nationally. Requests for individual reports will be fulfilled by the issuing establishment listed on the front cover and title page. Out of stock reports will be supplied for a fee by commercial agents.

Regional and headquarters establishments of Ocean Science and Surveys ceased publication of their various report series as of December 1981. A complete listing of these publications and the last number issued under each title are published in the *Canadian Journal of Fisheries and Aquatic Sciences*, Volume 38: Index to Publications 1981. The current series began with Report Number 1 in January 1982.

Rapport technique canadien sur l'hydrographie et les sciences océaniques

Ces rapports contiennent des renseignements scientifiques et techniques qui constituent une contribution aux connaissances actuelles mais que l'on ne trouve pas normalement dans les revues scientifiques. Le sujet est généralement rattaché aux programmes et intérêts du service des Sciences et Levés océaniques (SLO) du ministère des Pêches et des Océans.

Les rapports techniques peuvent être considérés comme des publications à part entière. Le titre exact figure au-dessus du résumé du chaque rapport. Les résumés des rapports seront publiés dans la revue Résumés des sciences aquatiques et halieutiques et les titres figureront dans l'index annuel des publications scientifiques et techniques du Ministère.

Les rapports techniques sont produits à l'échelon régional mais sont numérotés et placés dans l'index à l'échelon national. Les demandes de rapports seront satisfaites par l'établissement auteur dont le nom figure sur la couverture et la page de titre. Les rapports épuisés seront fournis contre rétribution par des agents commerciaux.

Les établissements des Sciences et Levés océaniques dans les régions et à l'administration centrale ont cessé de publier leurs diverses séries de rapports depuis décembre 1981. Vous trouverez dans l'index des publications du volume 38 du *Journal canadien des sciences halieutiques et aquatiques*, la liste de ces publications ainsi que le dernier numéro paru dans chaque catégorie. La nouvelle série a commencé avec la publication du Rapport n° 1 en janvier 1982.

Canadian Technical Report of

Hydrography and Ocean Sciences No. 61

August 1985

ASSESSING A WAVE MODEL A LA SWAMP

by

W. Perrie and B. Toulany

Atlantic Oceanographic Laboratory
Ocean Science and Surveys, Atlantic
Department of Fisheries and Oceans

Bedford Institute of Oceanography
P.O. Box 1006
Dartmouth, Nova Scotia
Canada B2Y 4A2

©Minister of Supply and Services 1985

Cat. No. FS 97-18/61E ISSN 0711-6764

Correct citation for this publication:

Perrie, W. and Toulany, B. 1985. Assessing a wave model à la Swamp. Can. Tech. Rep. Hydrogr. Ocean Sci. 61: vi + 78 p.

ABSTRACT

Perrie, W. and Toulany, B. 1985. Assessing a wave model à la Swamp. Can. Tech. Rep. Hydrogr. Ocean Sci. 61: vi + 78 p.

The nonlinear discrete spectral model constructed by Resio (1981), hereafter denoted RESIO, is run for the sevel hypothetical wind fields used in the Sea Wave Modelling Project to intercompare 10 wave prediction models, SWAMP (1981). Results for each test are summarized graphically and a brief explanation of RESIO's behavior is given.

When RESIO's drag coefficient is tuned so that energy transfer with fetch matches JONSWAP data, the duration-limited growth curves and the variation of peak frequency with fetch and duration also are in good agreement with JONSWAP.

RÉSUMÉ

Pierre, W. and Toulany, B. 1985. Assessing a wave model à la Swamp. Can. Tech. Rep. Hydrogr. Ocean Sci. 61: vi + 78 p.

Le modèle spectral discret non linéaire, construit par Resio (1981) et ci-après désigné RESIO, est appliqué aux sept champs de vent théoriques utilisés dans le Projet SWAMP (1981) de modélisation des vagues de mer pour comparer entre eux 10 modèles de prévision de vagues. Les résultats de chaque essai sont résumés graphiquement et une brève explication du comportement de RESIO est donnée.

Lorsque le coefficient de traînée de RESIO est choisi pour que le transfert d'énergie avec le fetch corresponde aux données de JONSWAP, les courbes de croissance en un temps limité et la variation de la fréquence maximale en fonction du fetch et du temps sont aussi en bon accord avec JONSWAP.

TABLE OF CONTENTS

	PAGE
ABSTRACT	iii
TABLE OF CONTENTS	iv
LIST OF ILLUSTRATIONS	v
LIST OF TABLES	vi
1. INTRODUCTION	1
2. TEST CASES	7
2.1 INTRODUCTION	7
2.2 SYMBOLS AND DEFINITIONS	7
2.2.1 SYMBOLS	7
2.2.2 DEFINITIONS OF DIMENSIONAL QUANTITIES	8
2.2.3 DEFINITIONS OF NON-DIMENSIONAL QUANTITIES	9
2.3 TEST DESCRIPTIONS	9
2.3.1 CASE II: FETCH AND DURATION LIMITED GROWTH	9
2.3.2 CASE I: FREE PROPAGATION	12
2.3.3 CASE III: SLANTING FETCH	14
2.3.4 CASE IV: HALF-PLANE WIND FIELD	19
2.3.5 CASE VII: 90° CHANGE IN WIND DIRECTION	23
2.3.6 CASE V: DIAGONAL FRONT	26
2.3.7 CASE VI: STATIONARY AND MOVING HURRICANE	27
3. SUMMARY	33
ACKNOWLEDGEMENTS	34
REFERENCES	35
FIGURES	37 - 78

LIST OF ILLUSTRATIONS

		PAGE
FIGURES II.1 - II.21	Model Response to Case II.	37
FIGURES I.1 - I.8	Model Response to Case I.	49
FIGURES III.1 - III.16	Model Response to Case III.	51
FIGURES IV.1 - IV.15	Model Response to Case IV.	56
FIGURES VII.1 - VII.14	Model Response to Case VII.	60
FIGURES V.1 - V.10	Model Response to Case V.	64
FIGURES VI.1 - VI.45	Model Response to Case VI.	67

LIST OF TABLES

			PAGE
TABLE	1.1	Models used in intercomparison study.	2 & 3
TABLE	1.2	Source functions, coupled discrete (CD) models.	4
TABLE	II.1	Ratios of drag coefficient used in renormalized Figs. II.6 - II.9 to original drag coefficient used in Figs. II.2 - II.5.	13
TABLE	III.1	Energy and frequency ratios for selected points: Case III/PM.	17
TABLE	III.2	Energy and frequency ratios for selected fetches: Case III/Case II.	18
TABLE	IV.1	Ratios of the windsea energies in Case IV to the pure fetch-limited Case II for points A,B (cf. Fig. IV.1).	21
TABLE	IV.2	Relative energies, mean frequencies and mean directions of swell in the calm half-plane at $X^* = Y^* = 1.01 \times 10^7$, point C. The quantities in the windy half-plane (subscript B) are at $(X^*, Y^*) = (.34 \times 10^7, 1.01 \times 10^7)$, point B.	22
TABLE	VII.1	Model classification for Case VII.	25
TABLE	VI.1	Wave model attributes for Case VI. (hurricane wind field).	30
TABLE	VI.2	Wave model results for Case VI.	31

1. INTRODUCTION

Early in 1979 a wave model intercomparison study was proposed by a few researchers to clarify the interrelations existing among various recent models developed for real time forecasting, wave statistics compilation and hindcast studies. The idea was enthusiastically welcomed and finally 10 modelling groups from the USA, Japan and Europe participated in what is now known as the SWAMP study. Part I, the principal results and conclusions, was presented in the proceedings of the IUCRM Symposium on Wave Dynamics and Radio Probing of the Ocean Surface, Miami 1981. Part II is a comprehensive set of diagrams representing the main results of all models involved.

Here, we repeat the test cases for the MEDS/BIO "RESIO" model, intercomparing its response with that of the SWAMP models. In this sense we calibrate and categorize RESIO.

Table 1.1 lists RESIO and the SWAMP models and their classes (decoupled propagation DP, coupled hybrid CH, coupled discrete CD: RESIO is CD). Discussion of the CD models is continued in Table 1.2, using F to represent the 2-D spectrum, B the Miles wind input factor, A the Phillips constant, and S_{nl}, the nonlinear transfer. B is reduced from its value in DP models, in accord with Snyder et al. (1981), whereas A is important in triggering growth in the BMO model. All models (except EXACT-NL) include some limiting saturation spectrum, dependent on the particular parameterization of nonlinear energy transfer in the forward face and peak regions of the windsea spectrum and in the windsea-swell transition region. Parameterizations also limit how well the model can do, given a quickly evolving directional windsea-swell system. In actuality CH models are dynamically similar to CD models.

TABLE 1.1. Models used in intercomparison study.

MODEL ABBREVIATION	INSTITUTION	APPLICATION	MODEL CLASS	SPATIAL REPRESENTATION
MRI	Meteorological Research Institute Japanese Meteorological Agency, Tsukuba	operational forecast, N. Pacific, regional wave statistics	DP	grid points
VENICE	Inst. Studio Dinamica Grandi Masse	regional wave statistics	DP	characteristics to output points only
NOWAMO	Norwegian Meteorological Institute	operational forecast, NE Atlantic	CH	wind sea, grid points: swell, characteristics to output points only
GONO	KMMI, De Bilt	operational forecast, North Sea	CH	wind sea, grid points: swell, characteristics to output points only
TOHOKU	Geophys. Institute, Tohoku University, Sendai	regional wave statistics	CH	grid points
HYPA	Institut für Meereskunde, Hamburg	regional wave statistics, (test operational forecast N. Atlantic and North Sea)	CH	wind sea, grid points: swell, characteristics
BMO	British Meteorlogical Office, Bracknell	operational forecast, Atlantic, North Sea, N. Pacific, Mediterranean. Regional wave statistics.	CD	grid points
SAIL	AOML, NOAA, Miami	regional wave statistics	CD	grid points
DNS	Scripps, La Jolla / NORDA, Bay St. Louis	regional wave statistics	CD	characteristics
EXACT-NL	Max-Planck-Institute of Meteorology	non-operational, one-dimensional integration only	CD	one-dimensional grid point

TABLE 1.1. CONT'D.

MODEL ABBREVIATION	INSTITUTION	APPLICATION	MODEL CLASS	SPATIAL REPRESENTATION
RESIO	Bedford Institute of Oceanography (developed by Don Resio, U.S. Army Engineer Waterways Experiment Station, Hydraulics Laboratory, Vicksburg, Miss.)	hindcast studies (at BIO), operational forecast at Atmospheric Environment Service	CD	grid points

TABLE 1.2. Source functions, coupled discrete (CD) models.

MODEL	LINEAR GROWTH	NONLINEAR TRANSFER	SATURATION SPECTRUM
BMO	$S_{in} = A + Bf$	Total net energy input computed from S_{in} and S_{ds}, where $S_{ds} = -f^2 E^{1/4} F$, then redistributed in accordance with JONSWAP form.	JONSWAP spectrum, saturation is included in nonlinear transfer parameterization.
SAIL	$S_{in} = BF$	Net source function inferred from JONSWAP growth curves is applied if greater than S_{in}.	Modified JONSWAP-type distribution. Saturation is accompanied by directional energy redistribution.
DNS	$S_{in} = BF$	EOF representation of exact S_{nl} computations computations as function of peak enhancement factor γ and directional spread $\Delta\theta$.	Pierson-Moskowitz spectrum with sea-state dependent saturation level.
EXACT-NL	$S_{in} = BF$	Exact computations.	Saturation specturm similar to observed spectrum generated by model with S_{in} and and S_{nl} as given and a dissipation function $S_{ds} = -(7.8)10^9(f^4/f_p^3)[E(2\pi f_p)^4/g^2]^6$
RESIO	$S_{in} = BF$	JONSWAP modified Kitaigorodskii-type	Saturation is attained when S_{in} puts more energy into central frequency bands than S_{nl} transfers out. S_{ds} is then operational. Modified JONSWAP - type distribution results.

It has been found to be important to tune RESIO's drag coefficient so that spectral energy growth matches the fetch-limited curves of JONSWAP. Then, not only duration-limited spectral energy growth curves, but also the fetch- and duration-limited behavior of peak frequency match JONSWAP.

CH and CD (second generation) and DP (first generation) models have fundamentally different pictures of spectral energy balance and space and time variables in the development of a windsea. If a DP model is tuned to a CH or CD model for fetch-limited growth, then it will develop 1.5 to 2.0 times faster than these for duration-limited growth.

DP models differ from CH and CD models in the development of the windsea spectrum. For fetch- or duration-limited growth cases, the former yield a nested family of spectral curves with no overshoot. For more complex wind fields, DP models lead to a more diverse selection of spectral distributions. This follows from the independence with which different wave components evolve along different rays. Thus, dependent on assumed directional distributions of the growth coefficients, these models are quite sensitive to fetch variations and propagation direction.

Second generation models are limited by their parameterization of nonlinear energy transfer, S_{nl}, which dominates shape and growth of windsea spectra. Models perform satisfactorily for standard fetch and duration limited growth situations for which the parameterizations were designed. SWAMP tests involve extreme conditions of rapidly changing wind, beyond the ability of the few degrees of freedom of the parameterizations. This restricts CD models in particular from giving a complete, discretized 2-D windsea spectrum beyond the calibre of that produced by a parametric CH model. The same constraints apply to prediction of a directional

distribution: greater accuracy of CD models does not follow from greater detail.

In the analysis of test results, it is important to normalize individual model renults by the corresponding fetch-limited growth results if basic features distinguishing the models are to be recognized. Otherwise, variations in basic fetch-limited growth rates of the different models can mask variations associated with different wind field geometries. The surprise is that most models are calibrated on fetch-limited growth data, and more data exist for the growth case than for any other. Diversity issues from the use of U_{10} or $U_{19.5}$ or U_*, etc. as the more fundamental boundary layer parameter, and to scatter in the drag coefficient utilized. Furthermore, there is not an agreed-upon boundary layer model relating surface velocities to the geostrophic winds which, via atmospheric models, are in practice used to drive the waves.

Integrating these many differences in model class and assumption implies major discrepanices in complex wind fields, such as Case VI. The tests were of course chosen to reveal and emphasize critical elements of the models. Slowly varying wind fields more typical of nature allow the models greater agreement. On the other hand, wave models are needed for extreme event forecasts. Reliable performance of the models in these situations, for which direct measurements are desperately sparse, must be regarded as questionable.

2. TEST CASES

2.1 INTRODUCTION

This section describes in detail the model test conditions and the common outputs accepted by all SWAMP participants. The description is intended to match documentation used for SWAMP, that a guide to the manner in which RESIO responds to the standard set of test cases may become clear.

2.2 SYMBOLS AND DEFINITIONS

2.2.1 SYMBOLS

c_g	group velocity
E	total variance
E_{PM}	total variance of the Pierson-Moskowitz spectrum
f	frequency
$\overline{f}$	mean frequency
f_p	spectral peak frequency
f_{PM}	peak frequency of P-M spectrum
$F(f)$	one-dim. variance density spectrum
F_{max}	maximum value of the variance density spectrum
$F_{PM}(f)$	one-dim. P-M spectrum
$F(f,\theta)$	two-dim. variance density spectrum
g	gravitational acceleration
H_s	significant wave height
n	number of time steps
T (or t)	time variable

$T_{45}°$	time for which mean direction of a given frequency band has turned by 45° (case VII)
Δt	time step
U_*	friction velocity
U_{10}	wind speed at 10 m height
X,Y (or x,y)	Cartesian space variables
Δx, Δy	grid spacings
α	Phillips' "constant"
θ	wave direction
$\overline{\theta}$	mean wave direction
θ_o	local wind direction
C_d	drag coefficient

2.2.2 DEFINITIONS OF DIMENSIONAL QUANTITIES

$$\alpha_{PM} = 0.0081$$

$$g = 9.806 \text{ m/s}^2$$

$$U_* = 0.855 \text{ m/s}$$

$$U_{10} = 20 \text{ m/s}$$

$$f_{PM} = 0.13(g/U_{10}) = 0.06374 \text{ Hz}$$

$$E_{PM} = 5^{-1}\alpha_{PM}\, g^2(2\pi f_{PM})^{-4} = 6.0552 \text{ m}^2$$

$$H_s = 4\, E^{1/2}$$

$$F_{PM}(f) = \alpha_{PM}\, g^2(2\pi)^{-4}\, f^{-5} \exp\{-5/4(f_{PM}/f)^4\}$$

$$F_{PM}(f_{PM}) = \alpha_{PM}\, g^2(2\pi)^{-4}\, (f_{PM})^{-5} \exp(-5/4) = 136.1 \text{ m}^2/\text{Hz}$$

$$F_{PM}(f,\theta) = F_{PM}(f)\, \frac{2}{\pi} \cos^2(\theta - \theta_o), \text{ for } |\theta - \theta_o| < \frac{\pi}{2}$$

$$F_{PM}(f,\theta) = 0, \text{ for } \left|\theta - \theta_o\right| > \frac{\pi}{2}$$

$$F_{PM}(f_{PM},\theta_o) = 86.64 \text{ m}^2/\text{Hz.rad}$$

$$\bar{f} = \frac{1}{E} \int_o^{2\pi} \int_o^{\infty} f\, F(f,\theta)\, df\, d\theta$$

$$\bar{\theta} = \arg \int_o^{2\pi} \int_o^{\infty} e^{i\theta} F(f,\theta)\, df\, d\theta, \text{ with } \theta \text{ measured c.w. from North}$$

2.2.3 DEFINITIONS OF NON-DIMENSIONAL QUANTITIES

$$E^* = E \frac{g^2}{U_*^4}$$

$$f_p^* = f_p \frac{U_*}{g}$$

$$T^* = T \frac{g}{U_*}$$

$$X^* = X \frac{g}{U_*^2}$$

$$f_{PM}^* = 5.5575 \times 10^{-3}$$

$$E_{PM}^* = 1.0896 \times 10^{3}$$

2.3 TEST DESCRIPTIONS

2.3.1 CASE II: FETCH AND DURATION LIMITED GROWTH

With an initially calm sea, a wind of U_{10}=20 m/s (corresponding U_* = 0.855 m/s) is turned on at T=0. The wind direction is perpendicular to a boundary, say to the west. The western (windward) boundary is land. The energy at this boundary remains zero for T>0. All other boundaries are commonly perfectly absorbing. RESIO has solid wall boundaries. The test is run until model results reach stationarity.

Figures

II.1 Fully developed equilibrium spectra at ≈1000 km fetch (——)RESIO ((— — —)RESIO with tuned C_d to match fetch-limited JONSWAP).

II.2 Non-dimensional fetch-limited growth curves for total energy E*.

II.3 Non-dimensional fetch-limited growth curves for peak frequency f_p*.

II.4 Non-dimensional duration-limited growth curves for total energy E*.

II.5 Non-dimensional duration-limited growth curves for peak frequency f_p*.

II.6 Renormalized fetch-limited growth curves for total energy E*. The white band represents the JONSWAP growth curve ±5%. The arrows indicate the direction along which the curves are shifted by redefining Cd.

II.7 Renormalized fetch-limited growth curves for the peak frequency f_p*.

II.8 Renormalized duration-limited growth curves for the total energy E*.

II.9 Renormalized duration-limited growth curves for the peak frequency f_p*.

II.10 $F(f)/F_{PM}(f_{PM})$ vs. f* with X* as family parameter, at stationary state.

II.11 $F(f)/F_{PM}(f_{PM})$ vs. f* with T* as family parameter, at X = 1012.5 km.

II.12 Contours of E/E_{PM} vs. X* and T*.

II.13 Contours of f/f_{PM} vs. X* and T*.

II.14 E* vs. X* with T* as family parameter.

II.15 E* vs. T* with X* as family parameter.

II.16 f_p* vs. X* with T* as family parameter.

II.17 f_p* vs. T* with X* as family parameter.

II.18 - II.21 Contours of $F(f,\theta)/F(f,\theta)_{max}$ vs. f* and θ at 187.5 and 1012.5 km fetchs and 6 and 36 hrs. time.

Commentary

Fetch-and duration-limited growth curves are the basic calibration plots for parameterization used in all the models. The surprise is the variety of growth curves the models exhibit given this simple test case. There is a spread of a factor of 2. The very high peak for RESIO in Fig. II.1 and the comparatively high growth curves in Figs. II.2 and II.4 imply a poorly tuned drag coefficient C_d. When this is tuned to match JONSWAP for fetch-limited growth, both these plots and the f_p* curves of Figs. II.3 and II.5 achieve a good fit to JONSWAP, as shown in Figs. II.6-II.9.

Unlike EXACT-NL and to some extent TOHOKU, which continue to evolve in analogous plots to Figs. II.10 and II.11, slowly transferring energy to still lower frequencies after $f_p<f_{PM}$, RESIO has a termination point. Data do not definitively say whether or not this should occur. The required very large scale uniform wind fields and large fetch almost never exist when wave experiments are under way. As in all models, RESIO exhibits a sharp peak, a steep low frequency forward face for $f<f_p$, and a more slowly decreasing high frequency tail proportional to f^{-5}. A subdued overshoot is evident.

Like most second generation models, RESIO uses a frequency independent directional distribution. SAIL has a Mitsuyasu (1975) inspired f/f_{PM} dependency; EXACT-NL has an explicit computation from the energy balance equation. As seen in Figs. II.18-II.21, with increasing fetch the angular

range of RESIO narrows slightly, the peak steepens and moves to lower frequency with increasing time.

Diversity of response, in this test, may be attributed to use of U_* as opposed to U_{10} etc. as the basic boundary layer parameter. The way to model the planetary boundary layer, relating U_* or U_{10} to geostrophic velocities, is not universally agreed upon. Notice that in Table II.1, C_d'/C_d, the ratio of tuned drag coefficient used in the renormalization to untuned drag coefficient, is ≈0.79 for RESIO and 1.52 for SAIL. Presumably both base their planetary boundary layer modelling on Cardone (1969). A reanalysis of C_d data, or a carefully executed CASP (Canadian Atlantic Storm Project) experiment could perhaps give a more definitive growth curve for fetch- and duration-limited cases.

2.3.2 CASE I: FREE PROPAGATION

This, basically a pure swell propagation experiment, was to provide a comparison of the numerical advection schemes of discrete spectral models. A discussion did not appear in SWAMP because although all models yielded acceptable numerical approximations to pure advection of infinitely narrow band spectral components, none of the current numerical forward advection schemes properly handle spatial dispersion for the propagation of finite sized spectral bins of real finite resolution discrete spectral models. The test simply disconnects the wind from the analogous situation, in space and time, of Case II above.

TABLE II.1. Ratios of drag coefficient C'_d used in renormalised Figs. II.6 - II.9 to original drag coefficient C_d used in Figs. II.2 - II.5.

MODEL	$\frac{C'_d}{C_d}$ (from E* - x* growth curves)
MRI	1.05
VENICE	1.44
NOWAMO	0.96
GONO	1.30
TOHOKU	1.00
HYPA	1.00
BMO	1.04
SAIL	1.52
DNS	1.00
EXACT-NL	1.17
RESIO	0.79

Figures

I.1 - I.4 $F(f,\theta)/F(f,\theta)_{max}$ vs. f* and θ at 1012.5 and 112.5 km fetchs and various times.

I.5 - I.6 $F(f)/F_{PM}(f_{PM})$ vs. f* at 1012.5 and 112.5 km fetchs with T* as family parameter.

I.7 E* vs. T* with X* as a family parameter.

I.8 f_p* vs. X* with T* as a family parameter.

Commentary

Figs. I.1 and I.2 show little spottiness as opposed to Figs. I.3 and I.4 where it is pronounced. The former is quite sharply peaked at the beginning of the test, as seen in Fig. I.5, whereas the latter, Fig. I.6, is not. This agrees with the discussion on numerical forward advection schemes as presented in SWAMP, appendix B, for example. At large fetch, E* remains high until all propagation from shorter fetch is complete, and then decreases. f_p* follows this pattern. The former is Fig. I.7, the latter, I.5 and I.8.

2.3.3 CASE III: SLANTING FETCH

This test starts with the same configuration as Case II, except that the wind now blows diagonally (45°) across the box ocean, and that both southern and western boundaries are land. The remaining conditions are subject to the conditions of Case II. The test is run until the model reaches stationarity.

Figures

III.1 - III.2 So-called "Custer diagram" of E/E_{PM} and $\bar{\theta}$ vs. X* and Y*, stationary state.

III.3 f_p/f_{PM} vs. X* and Y*, stationary state.

III.4 $F(f)/F_{PM}(f_{PM})$ vs. f* with distance from the origin with $D^*=[(X^*)^2 + (Y^*)^2]^{1/2}$ as the family parameter corresponding to about the same coordinates as above [these may be compared with Case II plots at fetches ≈100, 400, 1000 km] at selected times.

III.5 - III.8 $F(f)/F_{PM}(f_{PM})$ vs. f* with T* as family paramter at coordinates (X,Y) = (37,37), (112,112), (337,337) and (712,787) km respectively.

III.9 Lake Ontario data; from Donelan (1985). Mean direction of waves at the spectral peak versus mean wind direction (approach bearing in both cases). The broken line is the line of perfect agreement; the solid line has been deduced from similarity considerations using fetch averaged over 30° (±15°) about the wave approach direction. The inset demonstrates the relative insensitivity to choice of averaging over 60° (solid) or not at all (broken).

III.10 Location of RESIO and SWAMP models in E_{III}/E_{II} vs. f_{pIII}/f_{pII}) parameters plane at point F (located on Fig. III.1). Unit length arrows indicate mean wave direction.

III.11 - III.16 $F(f,\theta)/F(f,\theta)_{max}$ vs. f* and θ for the steady state, at coordinates (X,Y) = (112,112), (262,112), (337,337), (712,112), (712,337) and (712,787) km respectively.

Commentary

It is important to correctly model this test case, slanting fetch, because it happens all the time. This probes the directional response of a given model.

Unlike most other SWAMP models, which show reduced growth along the diagonal, RESIO's growth, as seen in Figs. III.4-III.8, is quite similar to Case II. The effects of geometry are of course evident at off diagonal points. Nondimensional energies and frequencies for RESIO and SWAMP models are given in Table III.1 and Fig. III.10 at locations A,B,C and F located on Fig. III.1. Table III.2 normalizes the data by values predicted in Case II for the same parallel fetch. Normalization emphasizes the effect of wind field geometry, negating fetch-limited growth characteristics associated with different models. Fig. III.9, from Donelan (1985) provides the variation of wave direction at the spectral peak with wind direction. When Lake Ontario's axis is the wind direction, waves and wind have the same orientation. Otherwise, the peak shifts direction to longer fetch as in Fig. III.14.

RESIO as seen in Figs. III.11-III.16, is similar to CD models SAIL and DNS in skewing its directional distribution as distance from the diagonal increases. This reflects the model's ability to track individual windsea components and couple them nonlinearly. It may thus be expected that these CD models would show a rather low growth rate on Table III.1. RESIO, with the hyper growth characteristics seen in Case II, stands out of course as the highest model, and only when normalized gives good agreement, in Table III.2 and Fig. III.10, with other models.

Large differences are manifest in the 2-D directional distributions in responding to asymmetric geometry, among all the models. Like MRI and

TABLE III.1. Energy and frequency ratios for selected points: Case III/PM.

MODEL (Δx, Δt)	E_{III}/E_{PM}			f_{pIII}/f_{PM}		
POSITION (x, y) (km)	B (375, 375)	C (750, 375)	A (750, 750)	B (375, 375)	C (750, 375)	A (750, 750)
MRI 40,60	0.45	0.50	0.59	1.59	1.54	1.48
VENICE 75,30	0.53	0.60	0.71	1.39	1.34	1.25
NOWAMO 75,90	0.62	0.71	1.34	1.94	1.70	<1.60
GONO 75,90	0.57	0.60	0.78	1.30	1.30	1.19
TOHOKU 25,30	0.45	0.48	0.70	1.37	1.32	1.05
HYPA 25,15	0.59	0.71	0.90	1.33	1.30	1.07
BMO 25,20	0.63	0.70	0.90	1.25	1.20	0.91
SAIL 37.5,60	0.53	0.85	1.00	1.25	1.13	0.95
DNS 50,20	0.45	0.48	0.72	1.40	1.34	1.25
JONSWAP N/A	0.57	x	1.23	1.14	x	0.91
RESIO 75,45	1.04	1.16	1.405	1.23	1.21	1.10

* (Δx, Δt) refer to model grid spacing (km) and time step (min).

TABLE III.2. Energy and frequency ratios, for selected fetches, Case III/Case II.

MODEL	E_{III}/E_{II}				f_{pIII}/f_{pII}		
	POSITION (x,y) (km)	B (375, 375)	C (750, 375)	A (750, 750)	B (375, 375)	C (750, 375)	A (750, 750)
MRI		0.88	0.99	0.97	1.03	1.00	1.00
VENICE		0.91	0.86	0.95	0.98	1.01	0.98
NOWAMO		x	1.33	1.30	0.76	0.80	0.84
GONO		0.90	0.83	1.04	1.05	1.09	1.02
TOHOKU		0.92	0.75	0.95	1.04	1.10	0.91
HYPA		0.84	0.73	0.91	1.04	1.12	0.96
BMO		0.83	0.73	0.90	0.97	1.17	0.91
SAIL		0.56	0.85	1.00	1.23	0.96	0.84
DNS		0.82	0.70	0.96	1.09	1.13	1.11
RESIO		0.87	0.97	0.97	1.09	1.08	1.05

VENICE, DP first generation models, and SAIL and DNS, second generation, RESIO can roughly simulate detailed 2-D spectra like the data of Donelan (1985). However nonlinear transfer in all these models (except EXACT-NL) is simply parameterized without much respect for subtle complexities. Thus directional fine structure is wrong, as indicated by a significant divergence in the predictions. Data are needed to verify the test.

2.3.4 CASE IV: HALF-PLANE WIND FIELD

A stationary wind of U_{10} = 20 m/s is turned on at T=0 over the left half-plane. The right half-plane remains calm. The wind blows offshore to the North, parallel to a north-south front as near as possible to X=500 km. Initial conditions are a calm sea. The southern boundary is land. All other boundaries are as in Case II.

Figures

IV.1 - IV.3	Custer diagram of E/E_{PM} and $\overline{\theta}$ vs. X* and Y* at 12 and 48 hrs.
IV.4	f/f_{PM} vs. X* and Y* at stationarity.
IV.5 - IV.8	$F(f)/F_{PM}(f_{PM})$ vs. f* with Y* as family parameter at X = 262, 562, 487 and 787 Km respectively.
IV.9 - IV.14	$F(f,\theta)/F(f,\theta)_{max}$ vs. f* and θ at coordinates (X,Y) = (487,37), (487,262), (562,487), (562,712), (637,37) and (787,262) km respectively.
IV.15	Model locations in the parameter plane spanned by the values of (E_{IV}/E_{II}) at points A and B (Fig. IV.1).

IV.16 Model locations in parameter plane of E_C/E_B vs. $\bar{f}_C/\bar{f}_B$ for points B and C in Fig. IV.1; $\bar{f}$ is the mean frequency averaged over the spectrum. Arrows denote the mean swell direction at point C.

Commentary

RESIO exhibits a smooth transition in crossing the front in Figs. IV.1 - IV.3 similar to DNS and VENICE and in contrast to BMO. Energy and direction of the swell field come largely from the directional distribution of windsea in the forced half-plane. Thus RESIO yields a swell field traveling at small angles to the wind and decaying with increasing lateral distance from the front.

Table IV.1 and Fig. IV.15 give a measure of the effect of geometry. Growth rates at points A and B in Fig. IV.1, along the centre line of the windy half-plane, are normalized by the corresponding Case II situation. Differences in E_{IV}/E_{II} among the models arise from directional coupling of the windsea, as in the Case II discussion. Similarly Table IV.2 and Fig. IV.16 for point C apply to swell.

The 2-D spectra, for example at (562,487) km, Fig. IV.11, near point C show appropriate skewing but with ≈10 times the energy level reflecting RESIO's hyper growth characteristics. As in the windy half-plane, swell predictions do not group readily into model classes, but reflect individual features in growth rates and angular distributions in the windsea, whence the swell radiates.

Little variation is evident in Fig. IV.16 regarding frequency ratios and mean directions. This is the relative contribution of swell components propagating at a small angle to the wind from less developed

TABLE IV.1. Ratios of the windsea energies in Case IV on the pure fetch-limited development in Case II for the points A, B (cf. Fig. IV.1).

MODEL	A: $X^* = 0.34 \times 10^7$, $Y^* = 0.40 \times 10^7$			B: $X^* = 0.34 \times 10^7$, $Y^* = 1.01 \times 10^7$		
	E_{IV}/E_{PM}	E_{II}/E_{PM}	E_{IV}/E_{II}	E_{IV}/E_{PM}	E_{II}/E_{PM}	E_{IV}/E_{II}
MRI	0.39	0.42	0.93	0.51	0.58	0.88
VENICE	0.45	0.54	0.83	0.66	0.76	0.87
NOWAMO	0.37	0.38	0.97	1.00	1.21	0.83
GONO	0.47	0.47	1.00	0.67	0.68	0.99
TOHOKU	0.35	0.35	1.00	0.63	0.63	1.00
HYPA	0.39	0.39	1.00	0.98	0.98	1.00
BMO	0.46	0.49	0.94	0.90	0.92	0.98
SAIL	0.42	0.76	0.55	0.99	1.00	0.99
DNS	0.37	0.43	0.86	0.57	0.73	0.78
RESIO	0.76	0.85	0.894	1.26	1.35	0.93

TABLE IV.2. Relative energies, mean frequencies and mean directions of swell in the calm half-plane at $X^* = Y^* = 1.01 \times 10^7$, point C. The quantities in the windy half-plane (subscript B) are taken at $(X^*, Y^*) = (0.34 \times 10^7, 1.01 \times 10^7)$, point B.

MODEL	E_C/E_B	$\overline{f}_C/\overline{f}_B$	$\overline{\theta}_C - \overline{\theta}_B$
MRI	0.24	1.05	39°
VENICE	0.11	1.19	30°
NOWAMO	<0.05	1.18	45°
GONO	0.14	0.97	47°
TOHOKU	0	x	x
HYPA	0.18	1.24	45°
BMO	0.10	1.22	47°
SAIL	0.13	1.26	35°
DNS	0.17	1.06	45°
RESIO	0.167	1.145	37°

windsea regions near the coast, compared to components at larger angles to the wind from further developed windsea at larger fetches. Growth rate is seen to compete with directional spread.

The lateral wind field boundary affects wave growth in the interior of the wind field in much the same way as angled boundaries affect wave growth along the diagonal (Case III). Waves propagating at an angle to the wind have less fetch than the standard Case II fetch-limited situation. Discrete models with broad spreading functions are affected because they follow windsea component evolution.

2.3.5 CASE VII: 90° CHANGE IN WIND DIRECTION

A stationary wind of U_{10} = 20 m/s is blowing to the North over an infinite ocean. At T=0 the wind turns instantly from North to West. Consider 2 cases: an initial state (at T=0) equal to a fully developed windsea as developed by the model for times T<0, and an initial state equal to a half developed sea state (at which $f_p = .26\ g/U_{10}$ which is $2f_{PM}$). The ocean and wind fields are regarded as spatially uniform by using appropriate boundaries, or big enough boundaries, etc. so that no boundary effects enter. The problem is one-dimensional and depends on time only.

Figures

VII.1 - VII.4 Contours of $F(f,\theta)/F(f,\theta)_{max}$ at (X,Y)=(487,562) km and 0, 3, 6, 9 hrs; half developed sea.

VII.5 - VII.10 Contours of $F(f,\theta)/F(f,\theta)_{max}$ at (X,Y)=(487,562) km and 0, 3, 6, 9, 12, 15 hrs; fully developed sea.

VII.11 - VII.12 Contours of $F(f,\theta)/F(f,\theta)_{max}$ at (X,Y)=(787,712) km and 12, 15 hrs; fully developed sea.

VII.13 - VII.14 Evolutions of windsea (13) and swell (14) peak spectral densities after the change in wind direction at t=0 for an initially half-developed windsea.

Commentary

Directional relaxation is composed of energy input to a new windsea by the wind, attenuation of swell, and weak nonlinear interactions which transfer energy from swell to windsea. Different simulations of these processes by different wave models yield significant deviations in respective outputs. Windsea-swell coupling is critically tested because of the large directional change. Additional directional response mechanisms, involving interactions within the windsea spectrum itself and important for a continuously turning wind vector, have no bearing here.

The scatter among SWAMP models (see model classification in Table VII.1) and RESIO's hyper growth ability are amazingly clear in Fig. VII.13. The extended response for fully developed sea test is illustrated in Figs. VII.5-VII.10 as opposed to the faster reaction of Figs. VII.1-VII.4.

Exact computations of nonlinear energy transfer for a number of superimposed swell and windsea spectra indicate weak coupling except when the swell and windsea frequencies are comparable. The transition region is also fairly sensitive to relative propagation directions, as can be seen in the EXACT-NL case. Within this model, with the 90° shift, new windsea is generated at high frequencies. Windsea-swell coupling becomes important at ≈ 6 hrs., when the two peak frequencies are about equal. Thence new

TABLE VII.1. Model classification for Case VII.

WINDSEA-SWELL INTERACTION	SUB-CLASS	MODELS	MODEL CLASS
decoupled	with swell dissipation	VENICE	DP
	without significant swell dissipation	MRI TOHOKU	DP CH
coupled	frequency criterion	HYPA	CH
	frequency-direction criterion	SAIL RESIO DNS BMO GONO NOWAMO	CD CD CD CD CH CH
	continuous coupling, more strongly frequency than directionally dependent	EXACT-NL	CD

windsea grows as in Case II, swell decays by dissipation and absorption into the windsea when the latter's peak frequency becomes comparable to the former's. RESIO's behavior is similar, as seen in all the VII Figs.

In common practice, the critical process of nonlinear windsea-swell coupling is parametrized from simpler spectral distributions in an ad hoc manner: a general operator parameterization is called for.

2.3.6 CASE V: DIAGONAL FRONT

A front runs diagonally from southwest to northeast across a 1000 km square grid. The southern boundary is land. All other initial and boundary conditions are as in Case II. At T=0, a wind of U_{10} = 20 m/s to the North below the front, and to the West above the front is turned on. For grid points on the diagonal, the wind is to the North, so the front lies between the main diagonal line of grid points and the next line of points above (to the North of) the main diagonal.

Figures

V.1	Custer diagram of E/E_{PM} and $\bar{\theta}$ vs. X* and Y* at stationarity.
V.2	f_p/f_{PM} vs. X* and Y* at stationarity.
V.3 - V.4	$F(f)/F_{PM}(f_{PM})$ vs. f* with Y* as family paramter for 3 points near X = 300 km and 3 points near 750 km.
V.5 - V.8	$F(f,\theta)/F(f,\theta)_{max}$ vs. f* and θ at (X,Y) = (637,787), (112,337), (262,337) and (712,787) km respectively.
V.9	Relaxation of mean wave direction $\bar{\theta}$ as function of fetch X* along an EW section at Y* = 1.07×10^7. Note that fetch increases to the right (decreasing X*).

V.10 Total wave energy E/E_{PM} as function of fetch X* along an EW section at Y* = 1.07×10^7. Note that fetch increases to the right (decreasing X*).

Commentary

In many respects RESIO is similar to SAIL. Figs. V.1-V.2 show uniform growth downwind from the southern boundary with some eastern edge/oblique front effects. As the windsea crosses the front to become NW sector swell, some relaxation to the new windsea direction is evident. Some models are much more abrupt, as in the intercomparison Fig. V.9. As in Fig. V.10, DNS shows a relatively high energy shift.

Discrepancies among the models reflect windsea-swell coupling, slanting fetch growth for new windsea in the NW sector, swell decay, and numerical modelling of front discontinuties. Figs. V.5-V.8 show the 2-D spectral variation of RESIO, reflecting a continuous gentle transition of windsea to swell across the front.

As in Case VII, swell-windsea coupling is tested. The complexity is augmented by generation of new windsea beyond the front under slanting fetch-limited conditions as in Case III, and propagation of a spatially inhomogeneous wave field into a front. The principal processes of this case are computable, as in the EXACT-NL model so no arbitrary parameterization is needed. If the front is moving, the case tests a commonly observed basic wind field.

2.3.7 CASE VI: STATIONARY AND MOVING HURRICANE

Using idealized hurricane wind fields (modelled after the synthetic wind fields prepared by the NOAA Atlantic Oceanographic and Meteorological

Labs, two test cases are run: a stationary storm and a storm translating to the North (Y-direction) at 15 m/s. The storms are defined on coordinates $0 \leq X \leq 1300$ km, $0 \leq Y \leq 1700$ km. The eye of the stationary storm is at (x,y) = (650,1400); the eye of the moving storm is at the same coordinates after 24 hours. The Ross hurricane model described in SWAMP II is followed for initial and boundary conditions throughout the run. The moving storm's eye is started at 1296 km south of (650,1400) even if this is off the computing grid.

Figures

(a) Stationary storm

VI.1	Wind field vs. X and Y.
VI.2	$\overline{f}$ vs. X and Y at 24 hrs.
VI.3 - VI.4	Custer diagrams of significant wave height H_s and $\overline{\theta}$ vs. X and Y at 24 hrs.
VI.5 - VI.8	$F(f)/F_{PM}(f_{PM})$ vs. f with D as family parameter, distance from the eye of the storm in SE, NE, NW and SW directions respectively at 36 hrs.
VI.9 - VI.24	Contours of $F(f,\theta)/F(f,\theta)_{max}$ vs. f and θ at coordinates (X,Y) = (387,1137), (462,1212), (537,1287), (612,1362), (687,1437), (762,1512), (837,1587), (912,1662), (912,1137), (837,1212), (762,1287), (687,1362), (612,1437), (537,1512), (462,1587) and (387,1662) Km respectively at 36 hrs.

VI.45 Positions of significant wave height H_s, for different models. Arrows point in the mean wave direction $\bar{\theta}$ and are proportional to H_s in length.

(b) Moving storm

VI.25 - VI.28 Wind field vs. X and Y at 0, 6, 12, 18 hrs. respectively.

VI.29 - VI.32 Custer diagram of significant wave height H_s, and $\bar{\theta}$ vs. X and Y at 12, 15, 18, 21 hrs.

VI.33 - VI.44 Contours of $F(f,\theta)/F(f,\theta)_{max}$ vs. f and θ at coordinates (X,Y) = (612,1437), (612,1362), (687,1437), and (687,1362) km and 9, 12, 15 hrs.

Commentary

The considerable differences among models reflect differences in experimental conditions, documented in Table VI.1. The test is a composite of all the specialized aspects of earlier tests, and is designed to reveal differences in parameterizing these aspects. All models respond predictably with respect to regions of highest waves, general wave directions (Table VI.2), superposition of windsea and swell and the diversity of response does not readily allow grouping by class (DP, CH, CD).

The maximum energy in the inner region ($\lesssim$ 100 km) of the stationary storm is very sensitive to coupling between wind and wave directions. Models with rapid directional relaxation and weak swell radiation produce the highest wave heights, given the swirling wind. The growth curves of Case II are not seen.

TABLE VI.1. Wave Model attributes for Case VI (hurricane wind field).

	MRI	VENICE	NOWAMO	GONO	TOHOKU	HYPA	BMO	SAIL	DNS	RESIO
Grid size x (km) y (km)	1280 1720	3200 4500	1300 1700	1400 1800	1320 1720	780 1200	1600 1680	1350 2700	800 1000	1050 975
Grid spacing (km)	40	50	75	40	40	30	40	37.5	40	75
Time step (hrs)	1.0	0.67	1.5	0.5	1.0	0.25	0.5	1.0	1.0	0.75
Boundary Conditions	Yes	No	Yes	No	x	Yes	No	No	Yes	No
Initial conditions, moving storm	Yes, (1/2 energy)	No	Yes	(did not run)	Yes	No	No	Yes	No	No
Initial conditions, stationary storm	Yes (1/2 energy)	No	Yes	Yes	Yes	No	No	Yes	No	No

TABLE VI.2. Wave model results for Case VI.

Stationary

	MRI	VENICE	NOWAMO	GONO	TOHOKU	HYPA	BMO	SAIL	DNS	RESIO
H_s maximum (m)	14	11	14	16	13	8	25	14	10	16
Bearing from (eye)	NE	NE	NE	NE	W	NE	NE	NE	NE	NE
Distance (km)	80	90	50	60	80	100	50	50	60	53
Distance $H_s/2$	325	240	450	250	260	>500	150	400	>500	318
$\overline{f}$ at $(H_s)_{max}$	.08	.09	.11	.08	.08	.10	.07	.08	.10	.085
$\overline{\theta}$ at $(H_s)_{max}$	NW	NW	NW	NW	S	NNW	NW	NW	NW	NW

Moving

	MRI	VENICE	NOWAMO		TOHOKU		HYPA		BMO	SAIL	DNS	RESIO
H_s maximum (m)	16	15	9		10		10		14	20	9	13
Bearing	ESE	SE	NE	SSE	SE	SE	SE	SSE	SE	SE	SE	SE
Distance (km)	60	100	50	275	175	400	120	220	200	90	200	53
Distance $H_s/2$	325	525	400	700	x	700	x	650	650	375	600	318
$\overline{f}$ at $(H_s)_{max}$	.07	.08	.12	.11	.10	.08	.10	.10	.08	.07	.10	.10
$\overline{\theta}$ at $(H_s)_{max}$	N	N	NW	NE	NNE	NNE	NNE	NNE	NNE	NNE	NNE	NNE

Outer regions (≈ 350 km) of the stationary storm manifest a locally inner region. Response varies with windsea-swell coupling and windsea generation in the inner regions.

All models shift the region of maximum wave heights from NE to SE in the moving case relative to the stationary case. This is the usual group velocity quasi-resonance seen when storm propagation matches wave group velocity.

Because of variations in grid domain, spacing, time step, initial and boundary conditions, plus the complexity of the test, the picture is inconclusive. The SWAMP group has recommended an intercomparison study using hurricane winds and directional wave spectra.

3. SUMMARY

RESIO responds competitively to the tests, with respect to other models participating in SWAMP and, particularly with respect to other coupled discrete second generation models. One point that is important concerns the drag coefficient. As strikingly seen in Case II and at least implicitly evident in all cases, it is essential to tune the drag coefficient such that RESIO matches the fetch-limited JONSWAP results. The duration-limited growth curves and the variation of peak frequency with fetch and duration then also agree well with JONSWAP. This takes one single perspective of JONSWAP results. Other responses of the model more or less meet expectations. A second point where further work could be an improvement is the model's behavior under rapidly changing winds. This is true for the SWAMP models generally. A study using actual winds and data seems essential to finally assess a given model.

ACKNOWLEDGEMENTS

We would like to thank Drs. Fred Dobson and Peter Smith for many useful discussions and for reviewing the manuscript. Fouad Majaess worked very hard to help us with the graphical work.

OERD funding sustained us.

REFERENCES

CARDONE, V.J. 1969. Specification of the Wind Distribution in the Marine Boundary Layer for Wave Forecasting. Ph.D. Thesis N.Y.U. 131 pp. Report TR-69-1, Geophys. Sci. Labn., N.Y.U. Available from NTIS AD #702-490.

DONELAN, M.A. 1985. Directional Spectra of Wind-Generated Waves. In Press in Roy. Soc. of Lond. Phil. Trans.

HASSELMANN, K., BARNETT, T.P., BOUWS, E., CARLSON, H., CARTWRIGHT, D.E., ENKE, K., EWING, J.A., GIENAPP, H., HASSELMANN, D.E., KRUSEMAN, P., MEERBURG, A., MULLER, P., OLBERS, D.J., RICHTER, K., SELL, W., and WALDEN, H. 1973. Measurements of Wind-Wave Growth and Swell Decay during the Joint North Sea Wave Project (JONSWAP). Dtsch. Hydrogr. Z. A8 (Suppl), 12.

MITSUYASU, H., TASAI, F., SUHARA, T., MIZUNO, S., OHKUSU, M., HONDA, T. and RIKIISHI, K. 1980. Observations of the Power Spectrum of Ocean Waves Using a Cloverleaf Buy. J. Phys. Oceanogr. 10, 286-296.

RESIO, D.T. 1981. The Estimation of Wind-Wave Generation in a Discrete Spectral Model. J. Phys. Oceanogr. 11, 510-525.

SNYDER, R.L., DOBSON, F.W., ELLIOTT, J.A., and LONG, R.B. 1981. Array Measurements of Atmospheric Pressure Fluctuations above Surface Gravity Waves. J. Fluid Mech. 102, 1-59.

SWAMP: ALLENDER, J.H., BARNETT, T.P., BERTOTTI, L., BRUINSMA, J., CARDONE, V.J., CAVALERI, L., EPHRAUMS, J.J., GOLDING, B., GREENWOOD, A., GUDDAL, J., GUNTHER, H., HASSELMANN, K., HASSELMANN, S., JOSEPH, P., KAWAI, S., KOMEN, G.J., LAWSON, L., LINNE, H., LONG, R.B., LYBANON, M., MAELAND, E., ROSENTHAL, W., TOBA, Y., UJI, T., DE VOOGT, W.J.P. 1982. Sea Wave Modelling Project (SWAMP), An Intercomparison Study of Wind-Wave Prediction Models; Part 2, A Compilation of Results, KNMI Pub. 161.

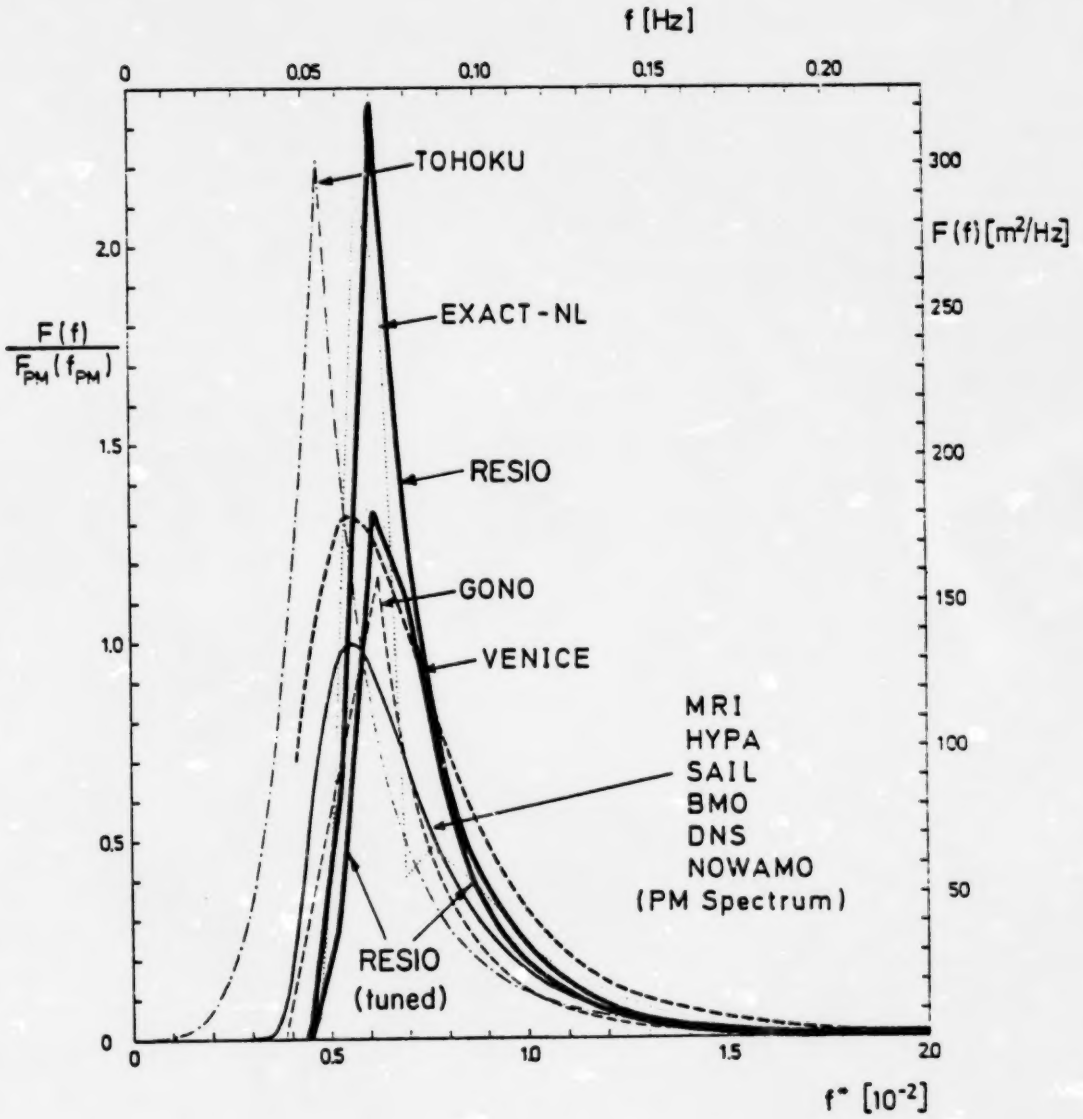
f [Hz]
0
0.05
0.10
0.15
0.20
TOHOKU
EXACT-NL
RESIO
GONO
VENICE
MRI
HYPA
SAIL
BMO
DNS
NOWAMO
(PM Spectrum)
RESIO
(tuned)
F(f)
F_PM(f_PM)
F(f) [m²/Hz]
300
250
200
150
100
50
2.0
1.5
1.0
0.5
0
0.5
1.0
1.5
2.0
f* [10⁻²]

II.1

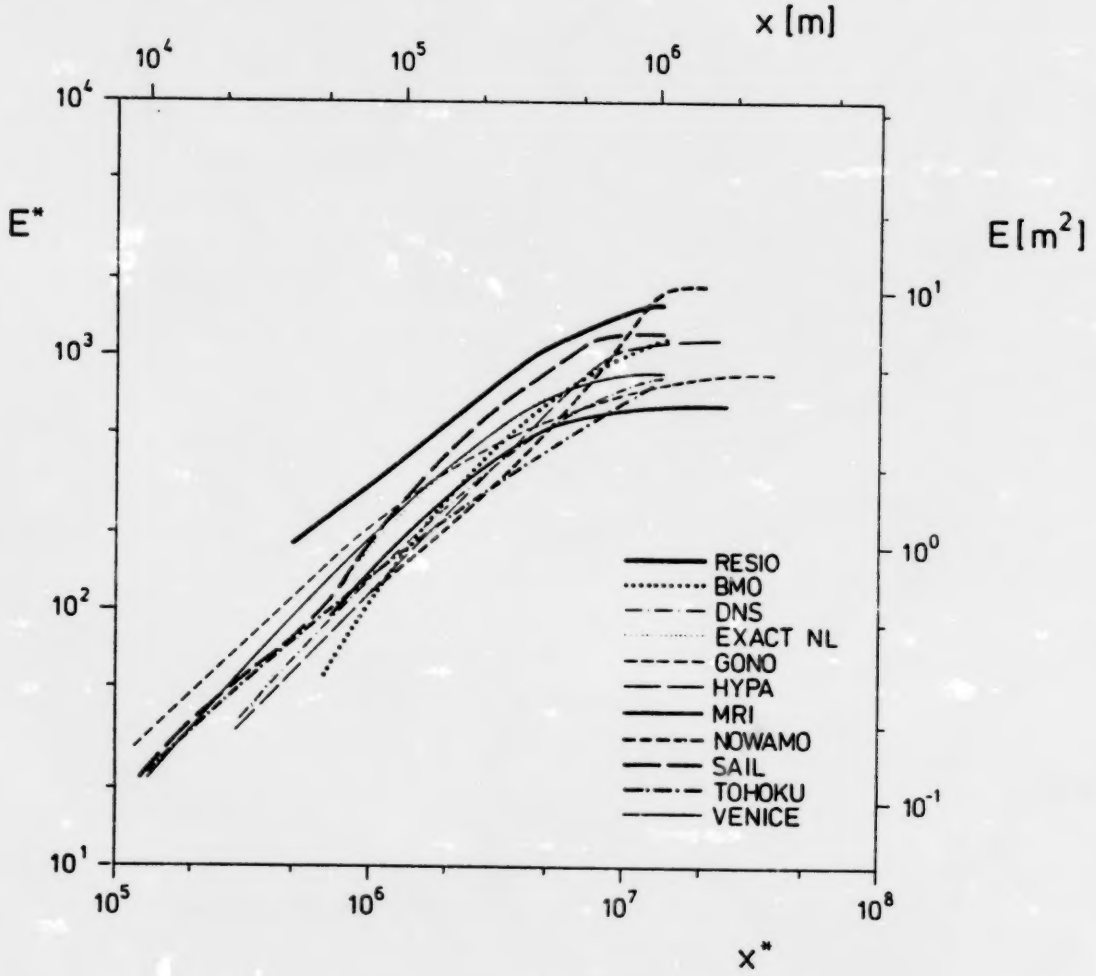
x [m]
10^4
10^5
10^6
E*
E[m²]
10^4
10^3
10^2
10^1
10^1
10^0
10^{-1}
RESIO
BMO
DNS
EXACT NL
GONO
HYPA
MRI
NOWAMO
SAIL
TOHOKU
VENICE
10^5
10^6
10^7
10^8
x*

II.2

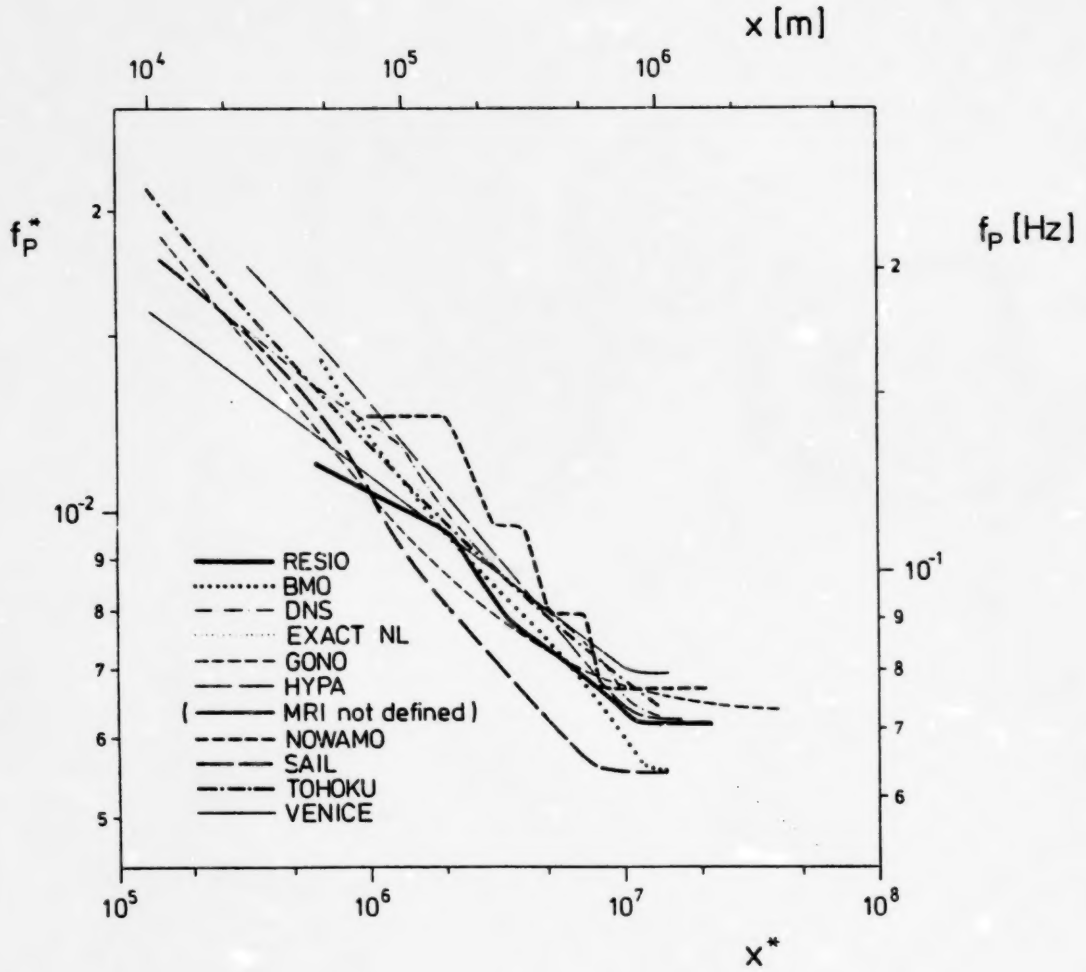
x [m]
10^4
10^5
10^6
f_P^*
f_P [Hz]
2
10^{-2}
9
8
7
6
5
10^{-1}
RESIO
BMO
DNS
EXACT NL
GONO
HYPA
(MRI not defined)
NOWAMO
SAIL
TOHOKU
VENICE
10^5
10^6
10^7
10^8
x^*

II.3

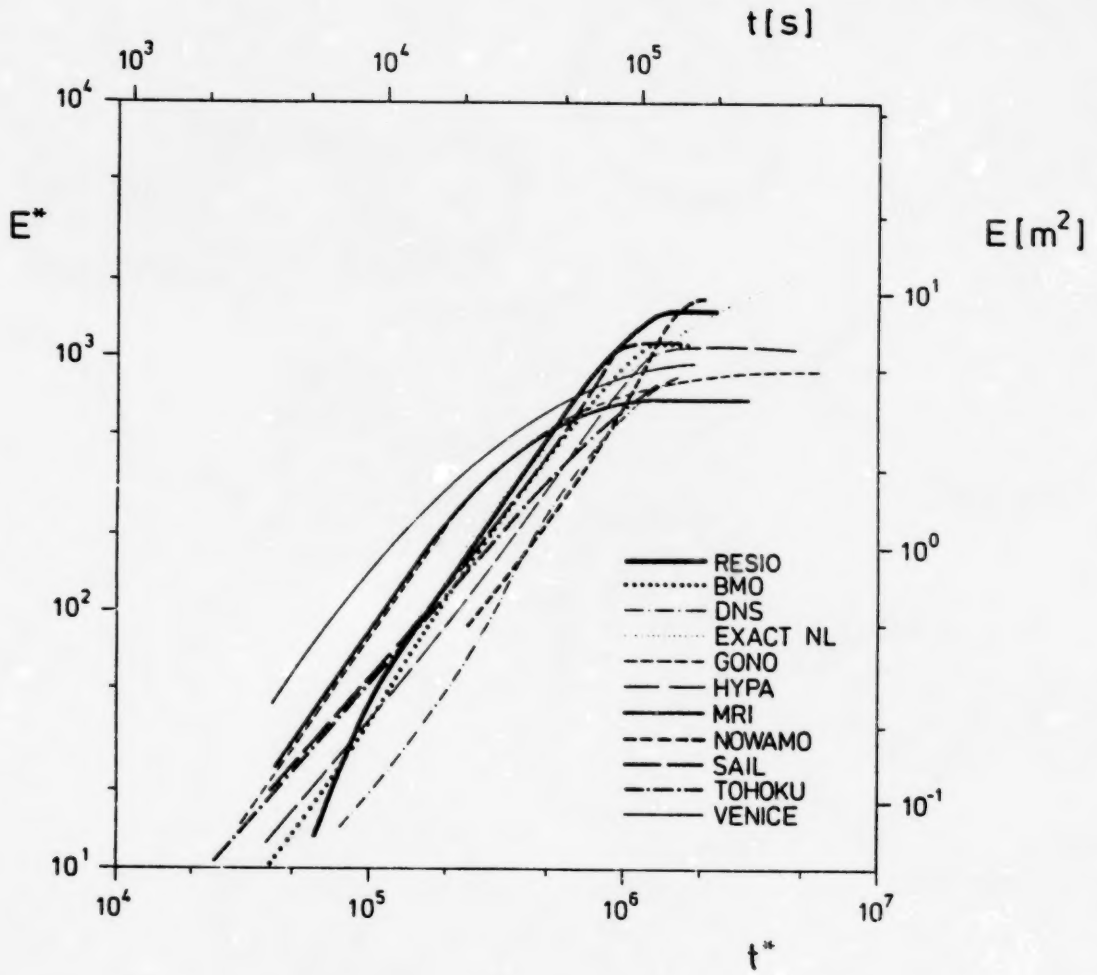
t[s]
10^3
10^4
10^5
10^4
10^3
10^2
10^1
E*
E[m²]
10^1
10^0
10^{-1}
RESIO
BMO
DNS
EXACT NL
GONO
HYPA
MRI
NOWAMO
SAIL
TOHOKU
VENICE
10^4
10^5
10^6
10^7
t*

II.4

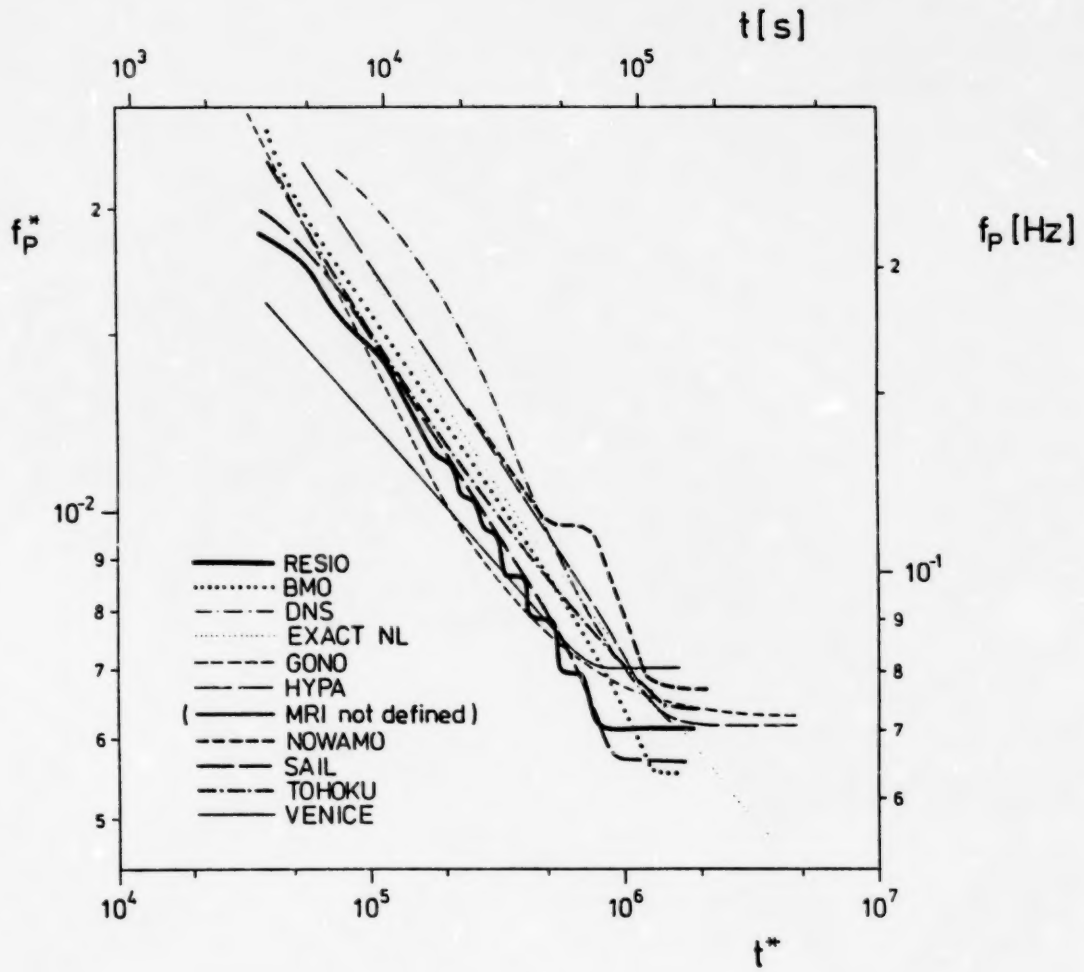
t[s]
10^3
10^4
10^5
f_P^*
f_P [Hz]
10^{-2}
10^{-1}
RESIO
BMO
DNS
EXACT NL
GONO
HYPA
(MRI not defined)
NOWAMO
SAIL
TOHOKU
VENICE
10^4
10^5
10^6
10^7
t^*

II.5

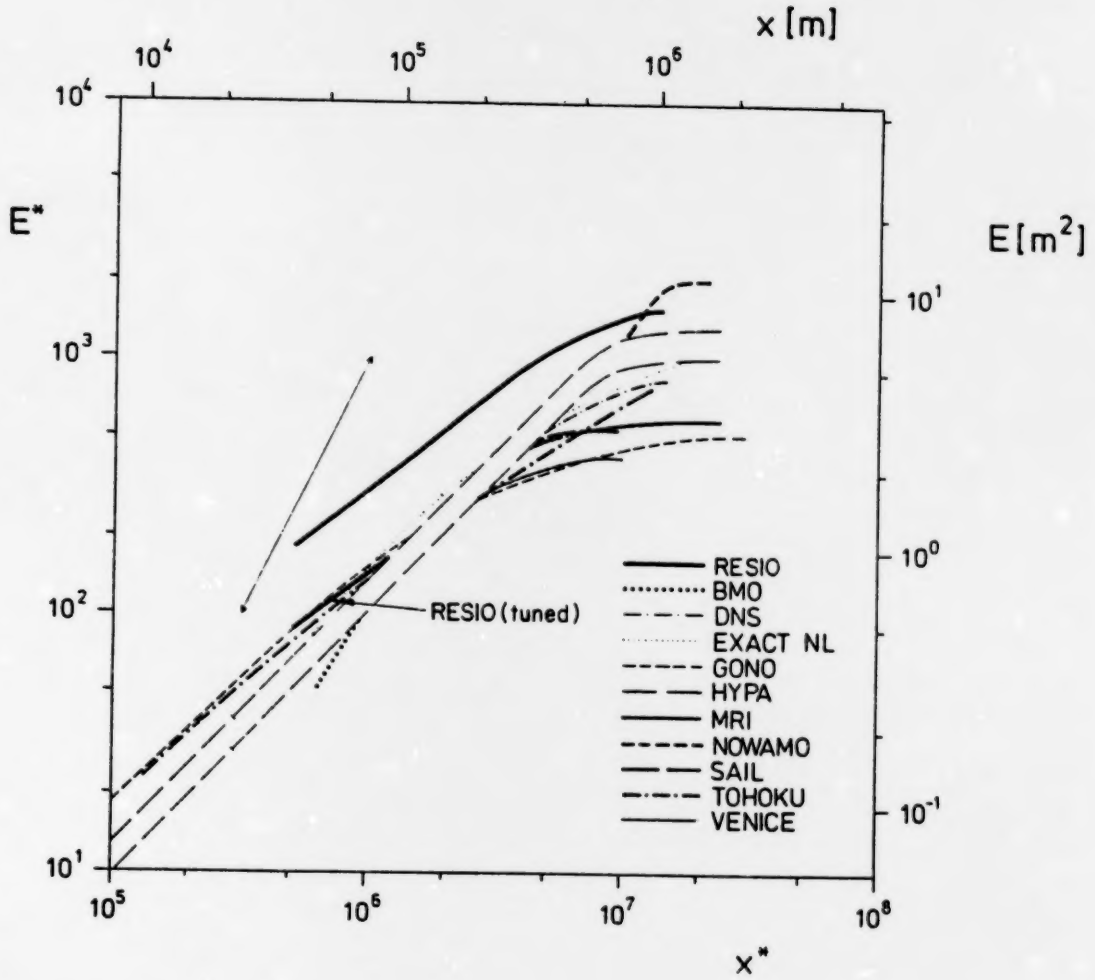
x [m]
10^4
10^5
10^6
E*
E[m²]
10^4
10^3
10^2
10^1
10^1
10^0
10^{-1}
RESIO (tuned)
RESIO
BMO
DNS
EXACT NL
GONO
HYPA
MRI
NOWAMO
SAIL
TOHOKU
VENICE
10^5
10^6
10^7
10^8
x*

II.6

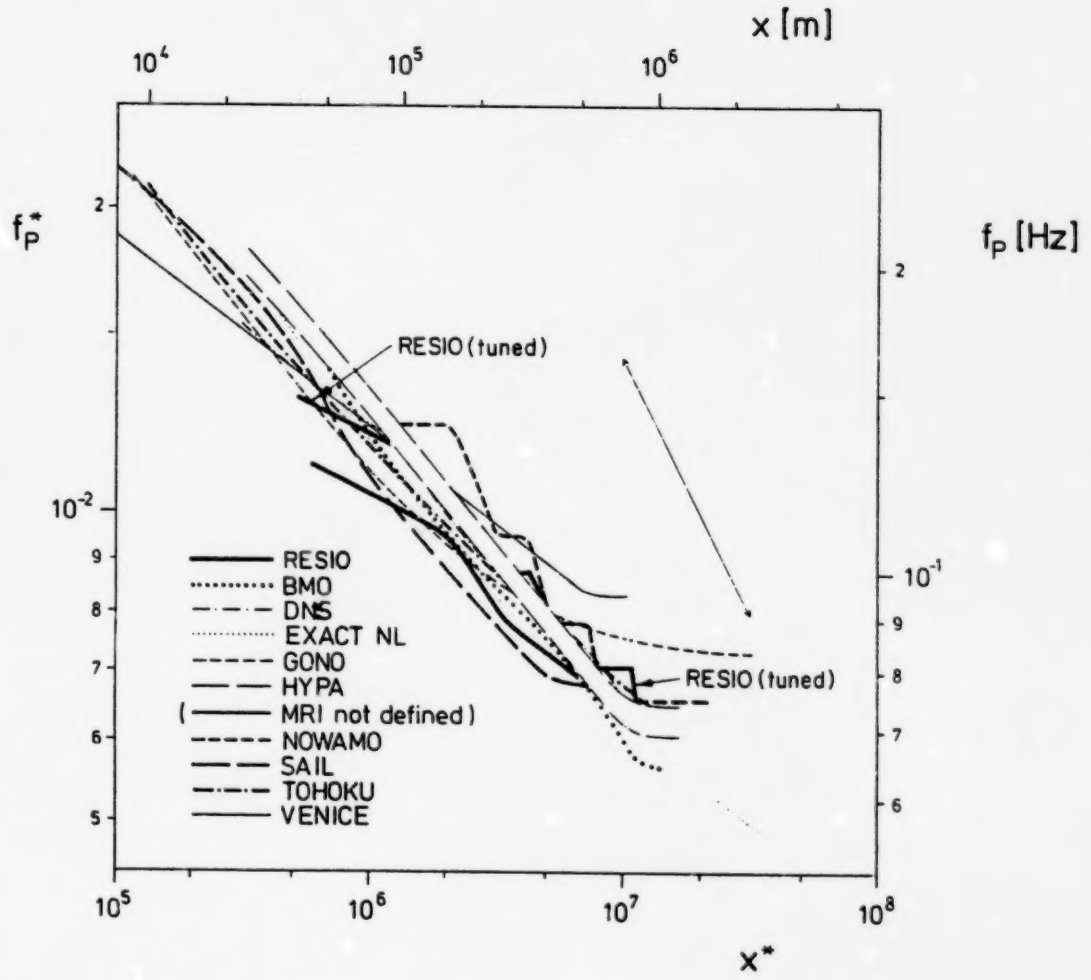
x [m]
10^4
10^5
10^6
f_P^*
f_P [Hz]
RESIO (tuned)
RESIO (tuned)
RESIO
BMO
DNS
EXACT NL
GONO
HYPA
MRI not defined)
NOWAMO
SAIL
TOHOKU
VENICE
10^{-2}
10^{-1}
10^5
10^6
10^7
10^8
x^*

II.7

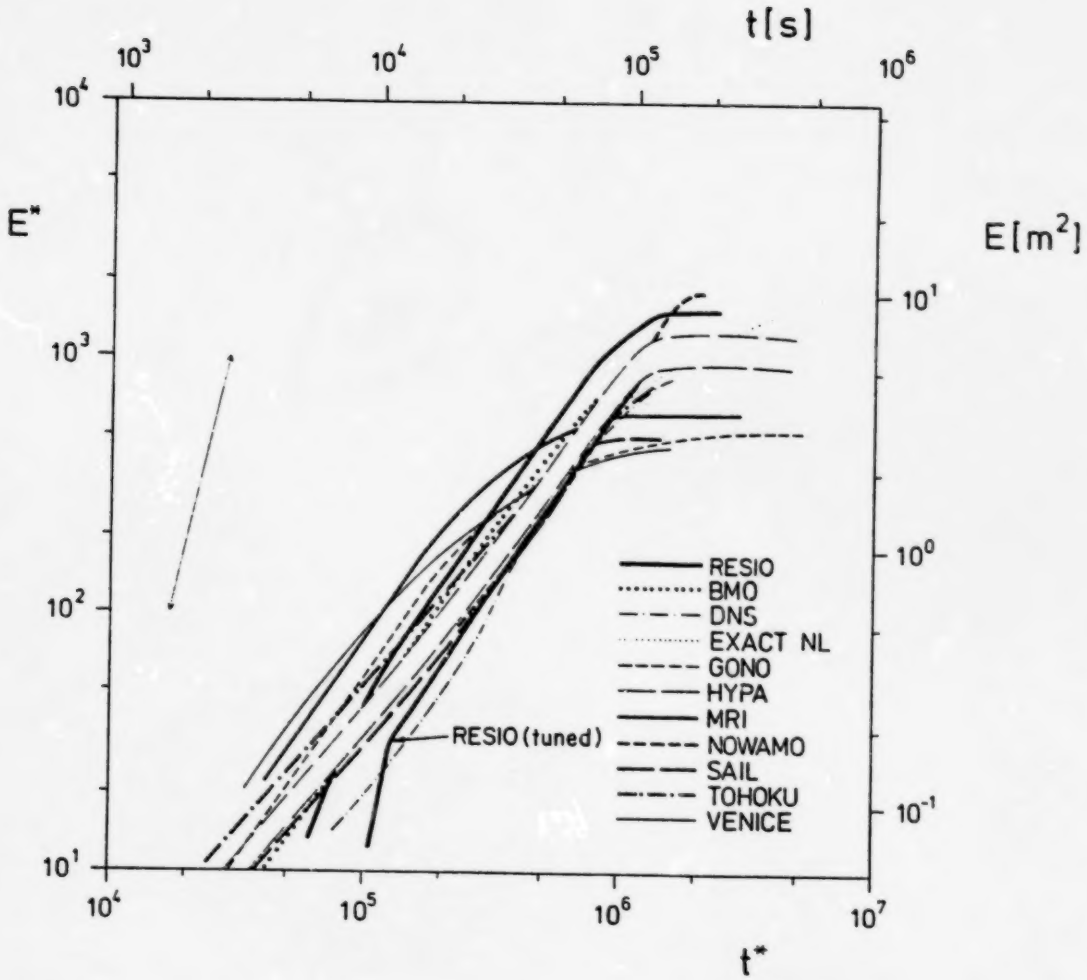
t[s]
10^3
10^4
10^5
10^6
10^4
10^3
10^2
10^1
E*
E[m²]
10^1
10^0
10^{-1}
RESIO
BMO
DNS
EXACT NL
GONO
HYPA
MRI
NOWAMO
SAIL
TOHOKU
VENICE
RESIO (tuned)
10^4
10^5
10^6
10^7
t*

II.8

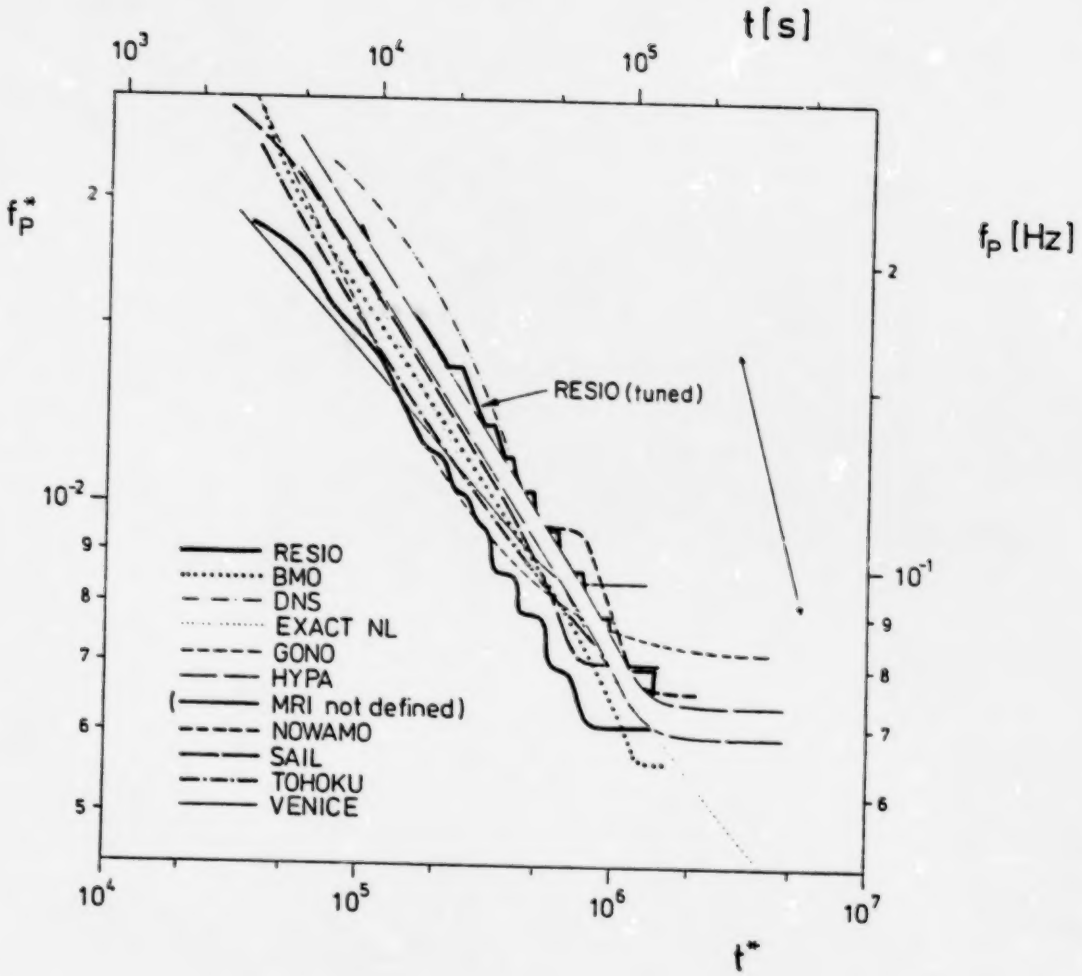
t[s]
10^3
10^4
10^5
f_P^*
f_p [Hz]
RESIO (tuned)
RESIO
BMO
DNS
EXACT NL
GONO
HYPA
(MRI not defined)
NOWAMO
SAIL
TOHOKU
VENICE
10^{-2}
10^{-1}
10^4
10^5
10^6
10^7
t^*

II.9

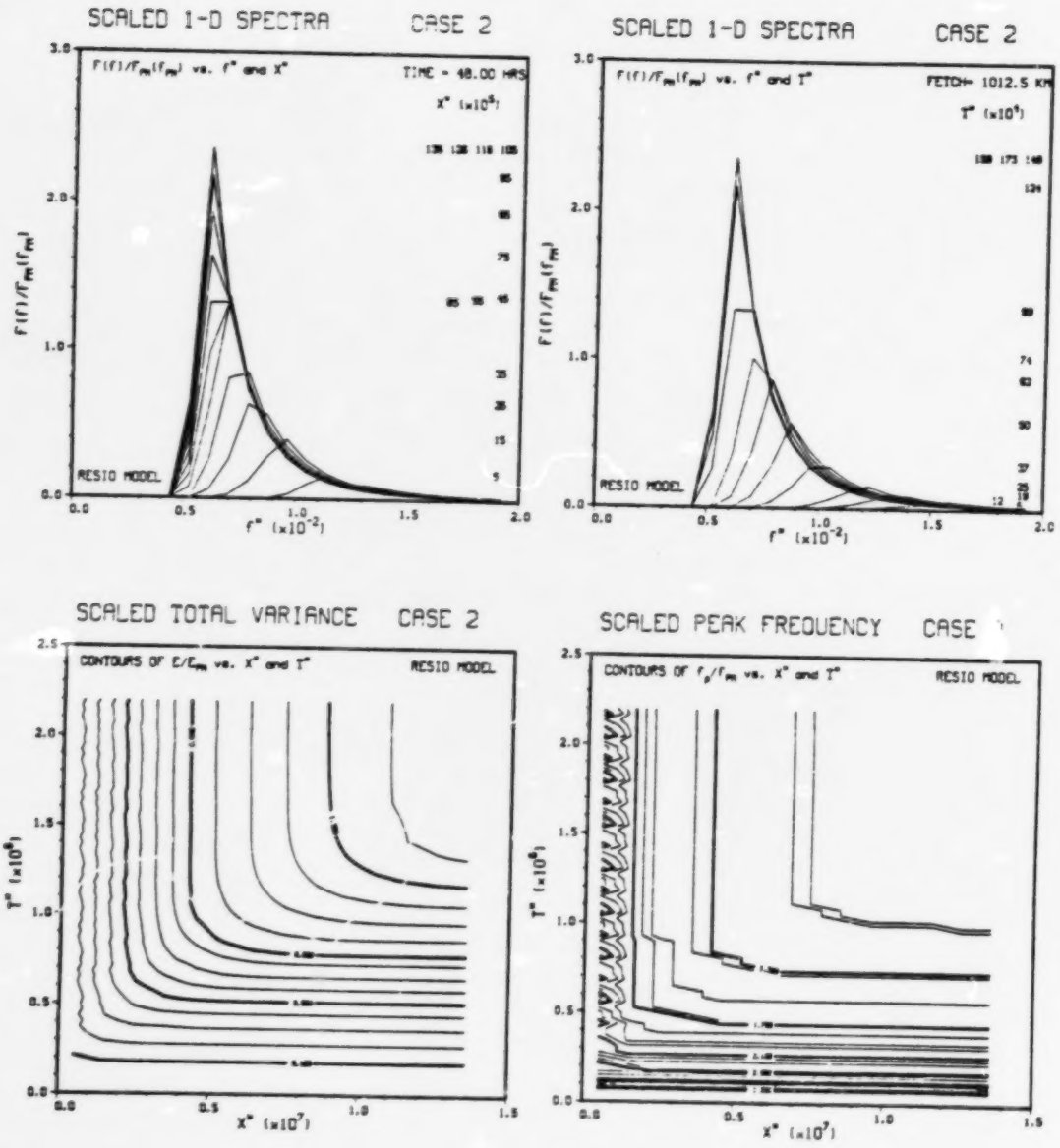
SCALED 1-D SPECTRA CASE 2
SCALED 1-D SPECTRA CASE 2
RESIO MODEL
RESIO MODEL
SCALED TOTAL VARIANCE CASE 2
SCALED PEAK FREQUENCY CASE
CONTOURS OF E/E_PM vs. X* and T*
CONTOURS OF f_p/f_PM vs. X* and T*
RESIO MODEL
RESIO MODEL
X* (x10^7)
X* (x10^7)

II.10 - II.13

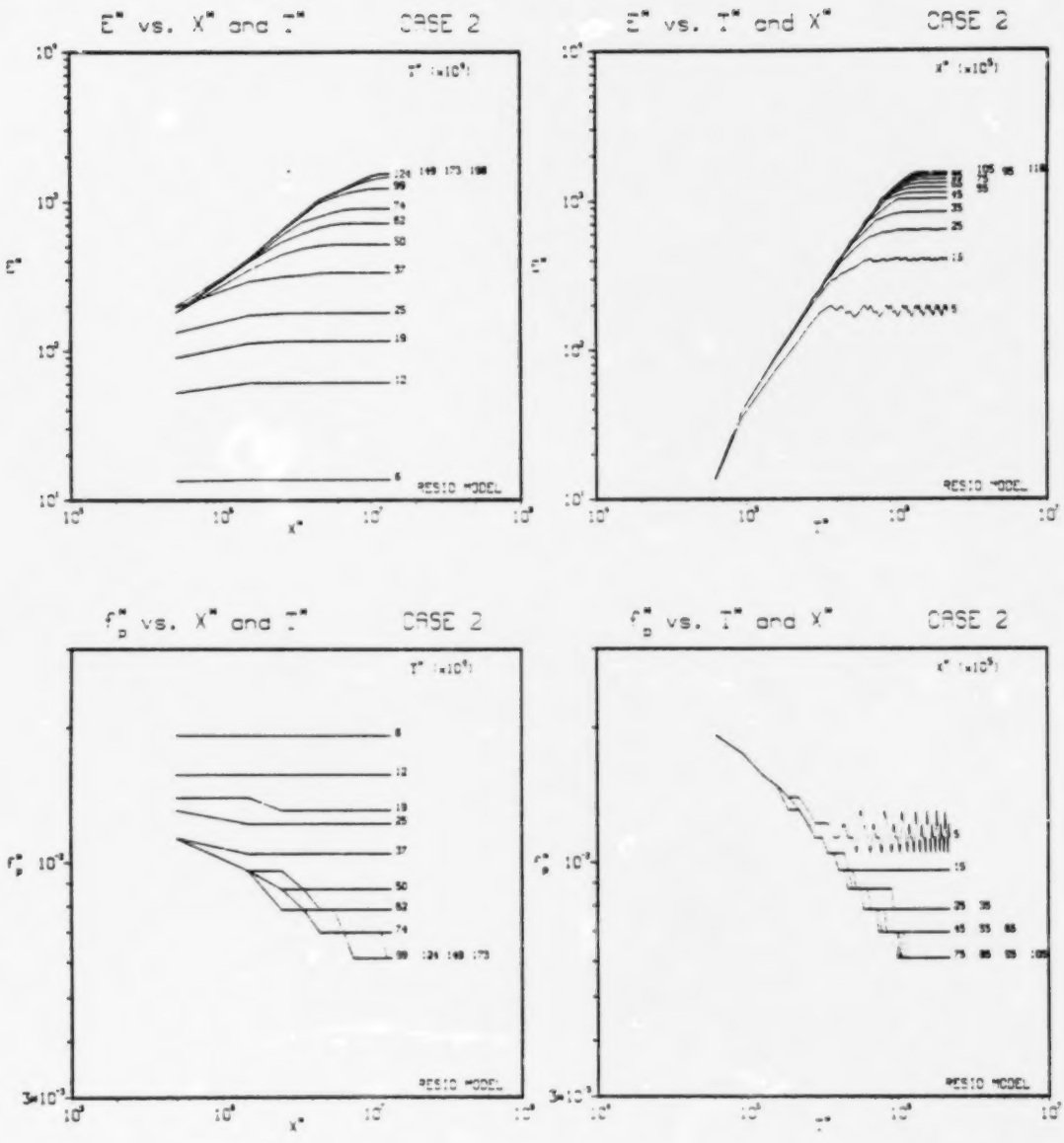
E* vs. X* and T*
CASE 2
T* (×10⁵)
E*
X*
RESID MODEL
E* vs. T* and X*
CASE 2
X* (×10⁵)
E*
T*
RESID MODEL
f_p* vs. X* and T*
CASE 2
T* (×10⁵)
f_p*
X*
RESID MODEL
f_p* vs. T* and X*
CASE 2
X* (×10⁵)
f_p*
T*
RESID MODEL

II.14 - II.17

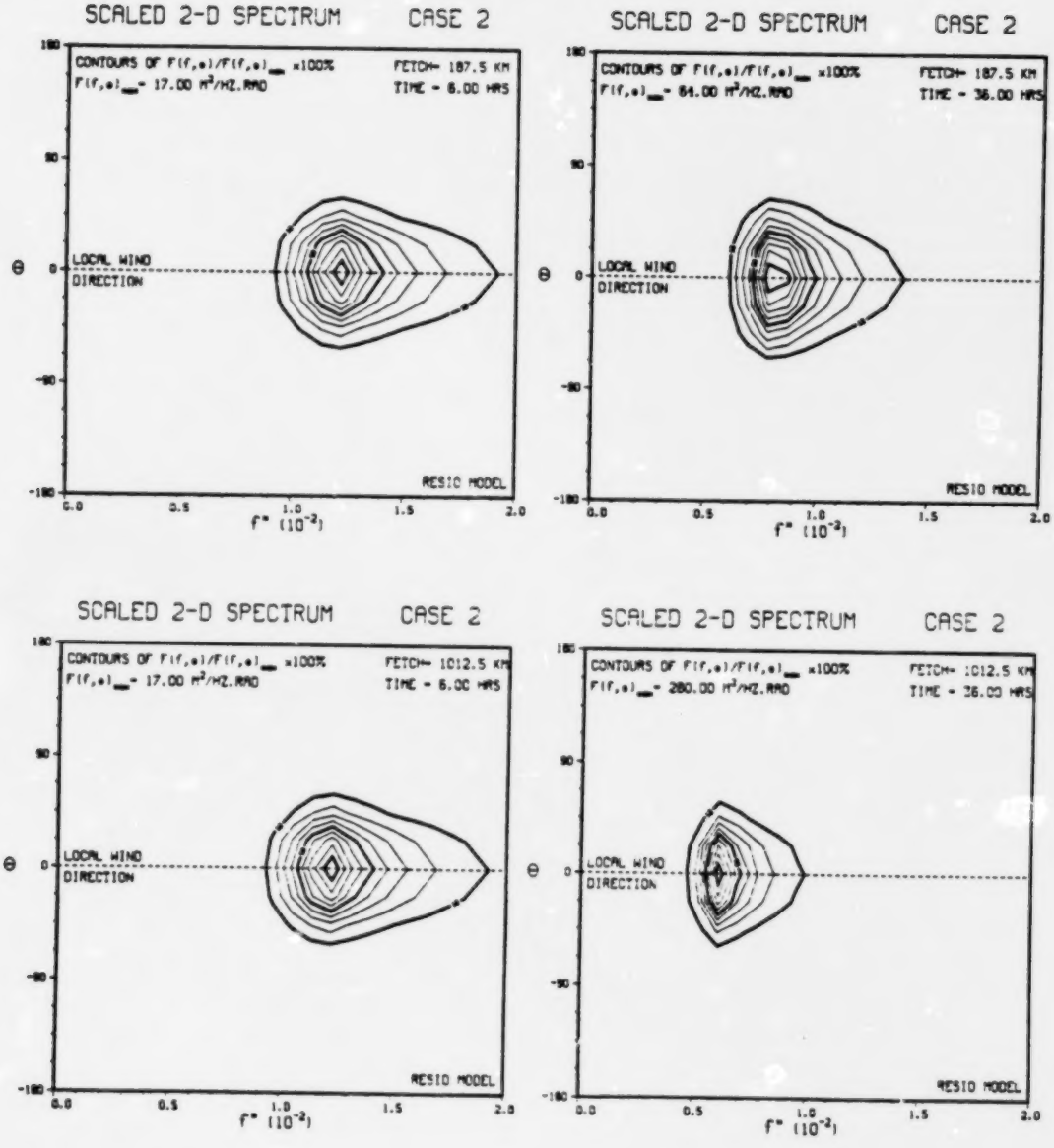
SCALED 2-D SPECTRUM CASE 2
CONTOURS OF F(f,θ)/F(f,θ)max ×100%
F(f,θ)max = 17.00 M²/HZ.RAD
FETCH = 187.5 KM
TIME = 6.00 HRS
LOCAL WIND DIRECTION
RESIO MODEL
f* (10⁻²)
SCALED 2-D SPECTRUM CASE 2
CONTOURS OF F(f,θ)/F(f,θ)max ×100%
F(f,θ)max = 64.00 M²/HZ.RAD
FETCH = 187.5 KM
TIME = 36.00 HRS
LOCAL WIND DIRECTION
RESIO MODEL
f* (10⁻²)
SCALED 2-D SPECTRUM CASE 2
CONTOURS OF F(f,θ)/F(f,θ)max ×100%
F(f,θ)max = 17.00 M²/HZ.RAD
FETCH = 1012.5 KM
TIME = 6.00 HRS
LOCAL WIND DIRECTION
RESIO MODEL
f* (10⁻²)
SCALED 2-D SPECTRUM CASE 2
CONTOURS OF F(f,θ)/F(f,θ)max ×100%
F(f,θ)max = 280.00 M²/HZ.RAD
FETCH = 1012.5 KM
TIME = 36.00 HRS
LOCAL WIND DIRECTION
RESIO MODEL
f* (10⁻²)

II.18 - II.21

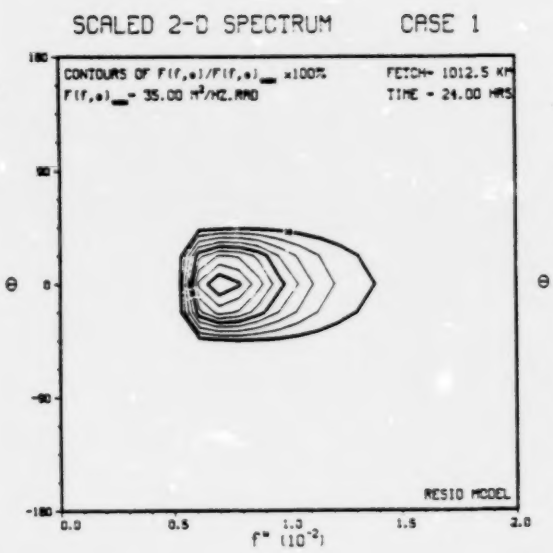
SCALED 2-D SPECTRUM CASE 1
CONTOURS OF F(f,θ)/F(f,θ)max ×100%
F(f,θ)max = 35.00 M²/HZ.RAD
FETCH= 1012.5 KM
TIME = 24.00 HRS
RESIO MODEL
θ
f* (10⁻²)

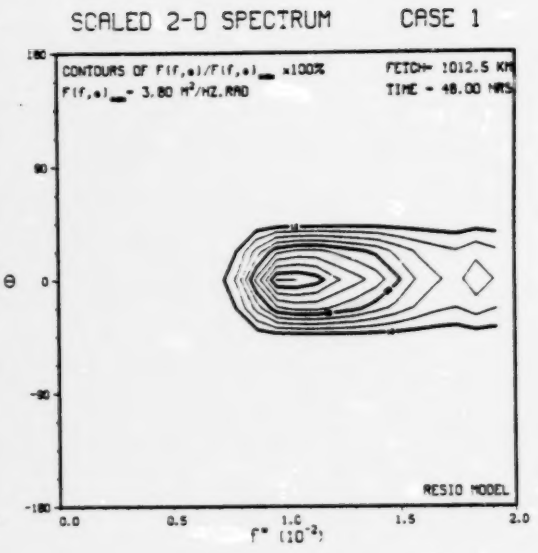
SCALED 2-D SPECTRUM CASE 1
CONTOURS OF F(f,θ)/F(f,θ)max ×100%
F(f,θ)max = 3.80 M²/HZ.RAD
FETCH= 1012.5 KM
TIME = 48.00 HRS
RESIO MODEL
θ
f* (10⁻²)

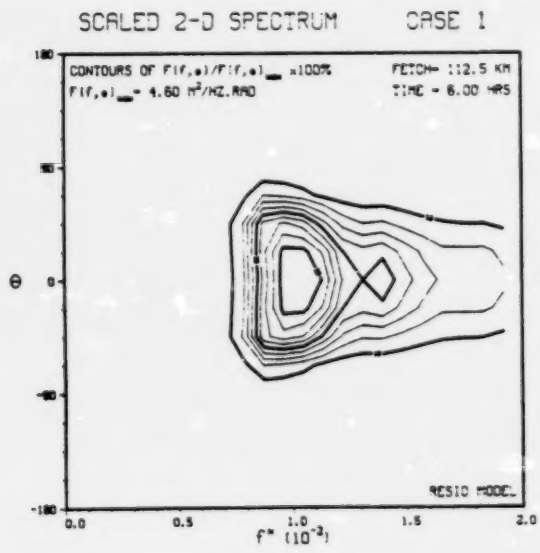
SCALED 2-D SPECTRUM CASE 1
CONTOURS OF F(f,θ)/F(f,θ)max ×100%
F(f,θ)max = 4.60 M²/HZ.RAD
FETCH= 112.5 KM
TIME = 6.00 HRS
RESIO MODEL
θ
f* (10⁻²)

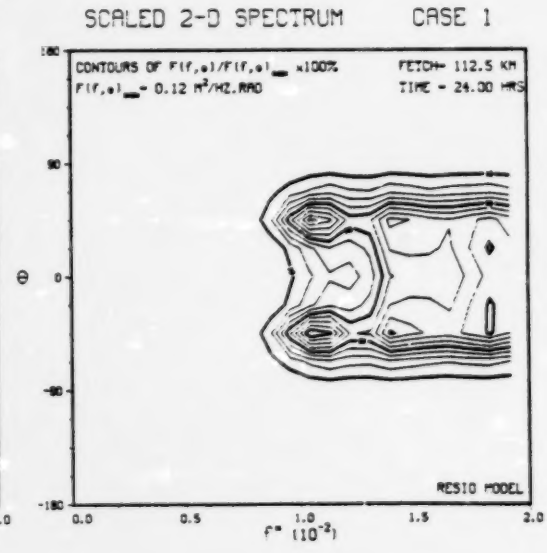
SCALED 2-D SPECTRUM CASE 1
CONTOURS OF F(f,θ)/F(f,θ)max ×100%
F(f,θ)max = 0.12 M²/HZ.RAD
FETCH= 112.5 KM
TIME = 24.00 HRS
RESIO MODEL
θ
f* (10⁻²)

I.1 - I.4

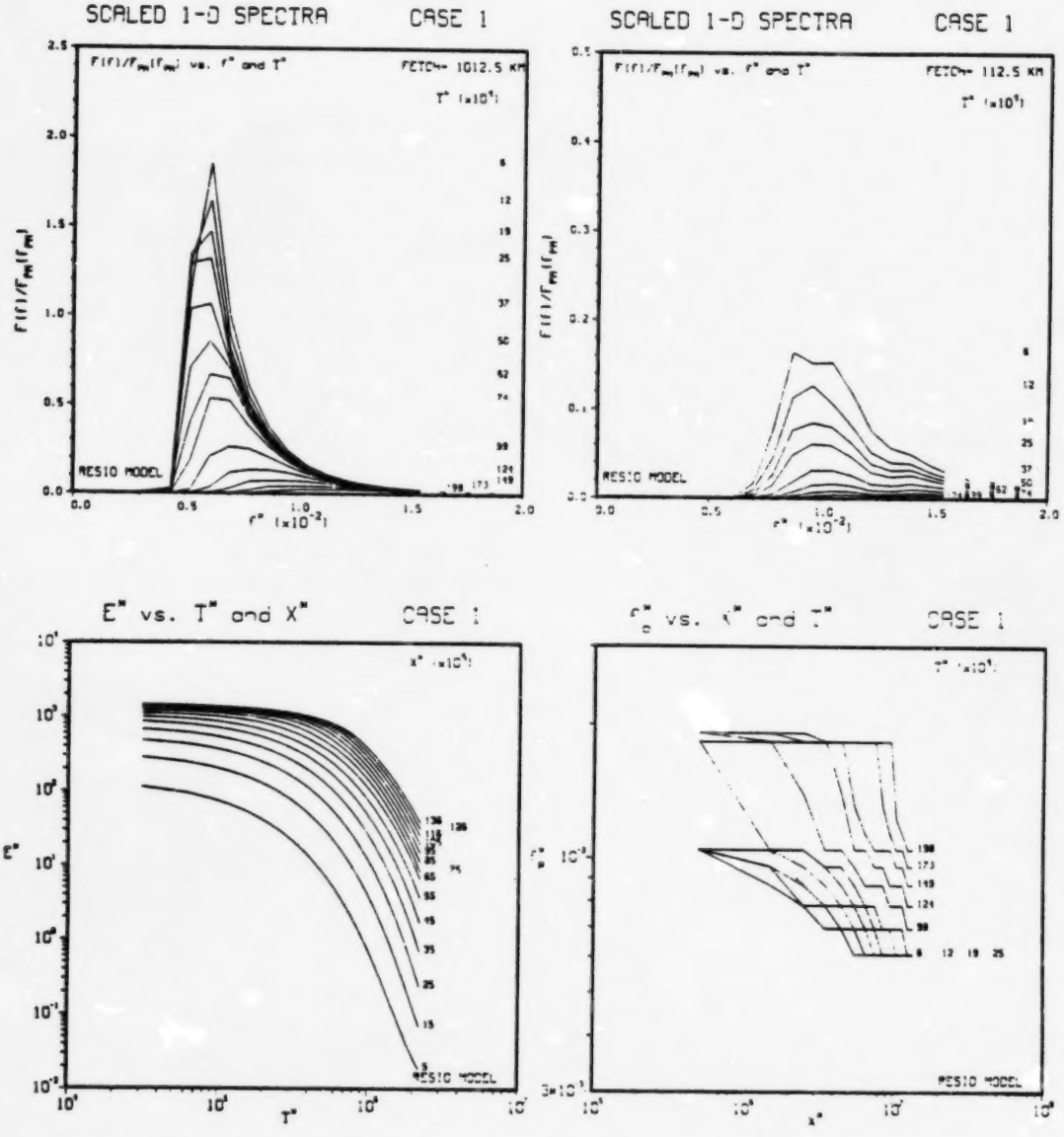
SCALED 1-D SPECTRA CASE 1
SCALED 1-D SPECTRA CASE 1
RESID MODEL
RESID MODEL
E* vs. T* and X*
CASE 1
RESID MODEL

I.5 - I.8

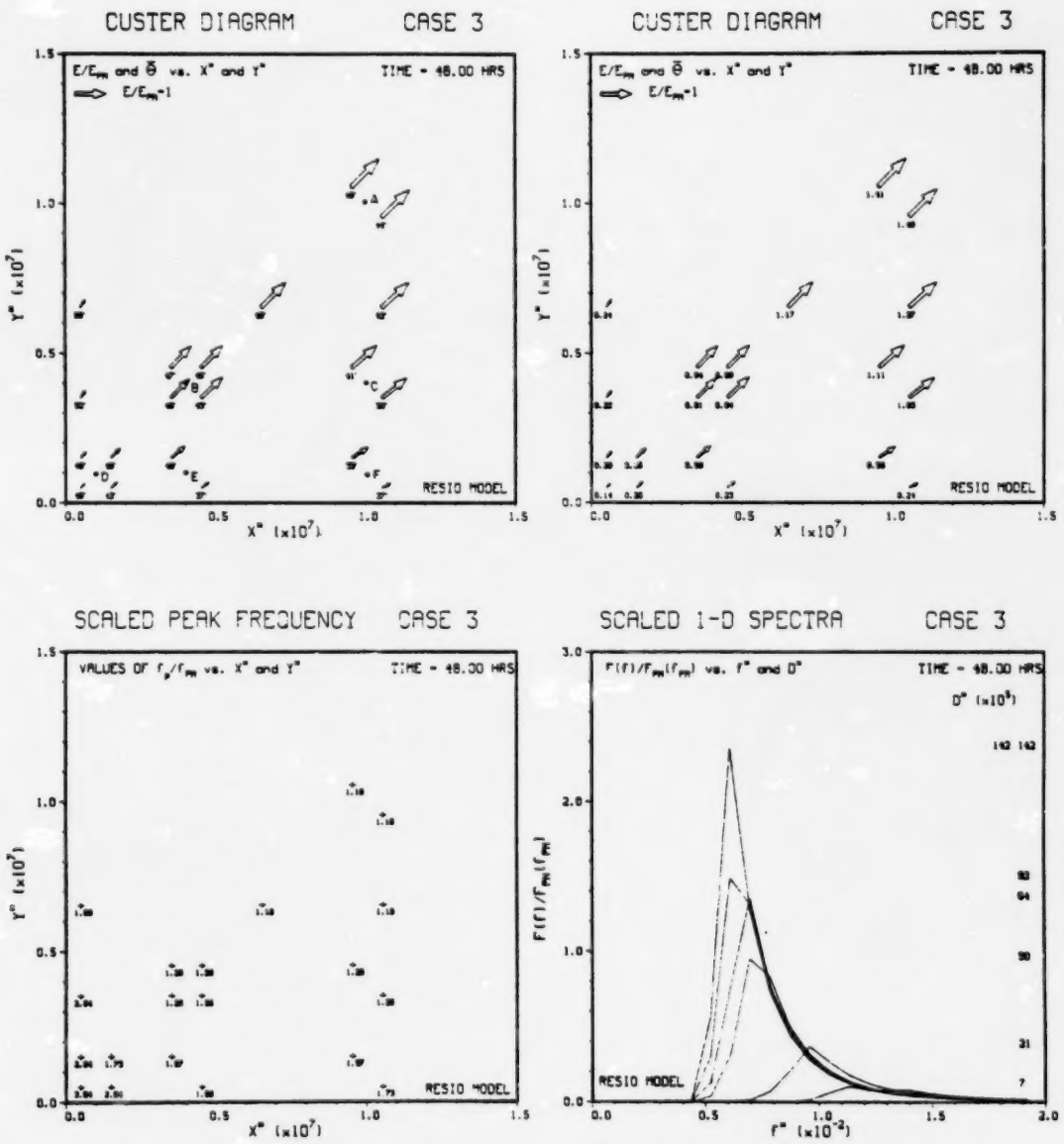
CUSTER DIAGRAM CASE 3
TIME = 48.00 HRS
RESIO MODEL
CUSTER DIAGRAM CASE 3
TIME = 48.00 HRS
RESIO MODEL
SCALED PEAK FREQUENCY CASE 3
TIME = 48.00 HRS
RESIO MODEL
SCALED 1-D SPECTRA CASE 3
TIME = 48.00 HRS
RESIO MODEL

III.1 - III.4

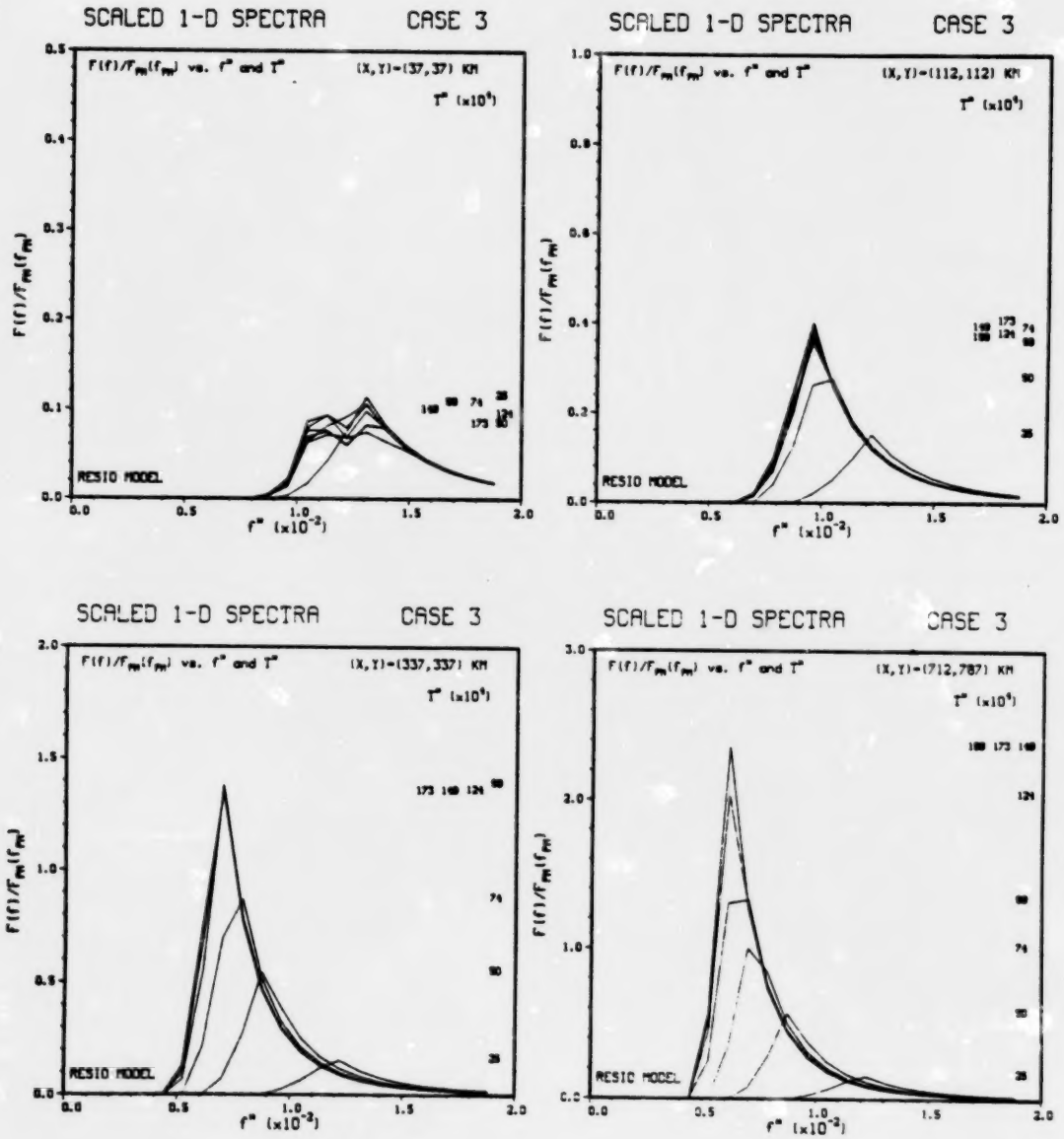
SCALED 1-D SPECTRA CASE 3
F(f)/F_m(f_m) vs. f* and T*
(X,Y)=(37,37) KM
(X,Y)=(112,112) KM
(X,Y)=(337,337) KM
(X,Y)=(712,787) KM
T* (x10^4)
RESID MODEL
f* (x10^-2)
F(f)/F_m(f_m)

III.5 - III.8

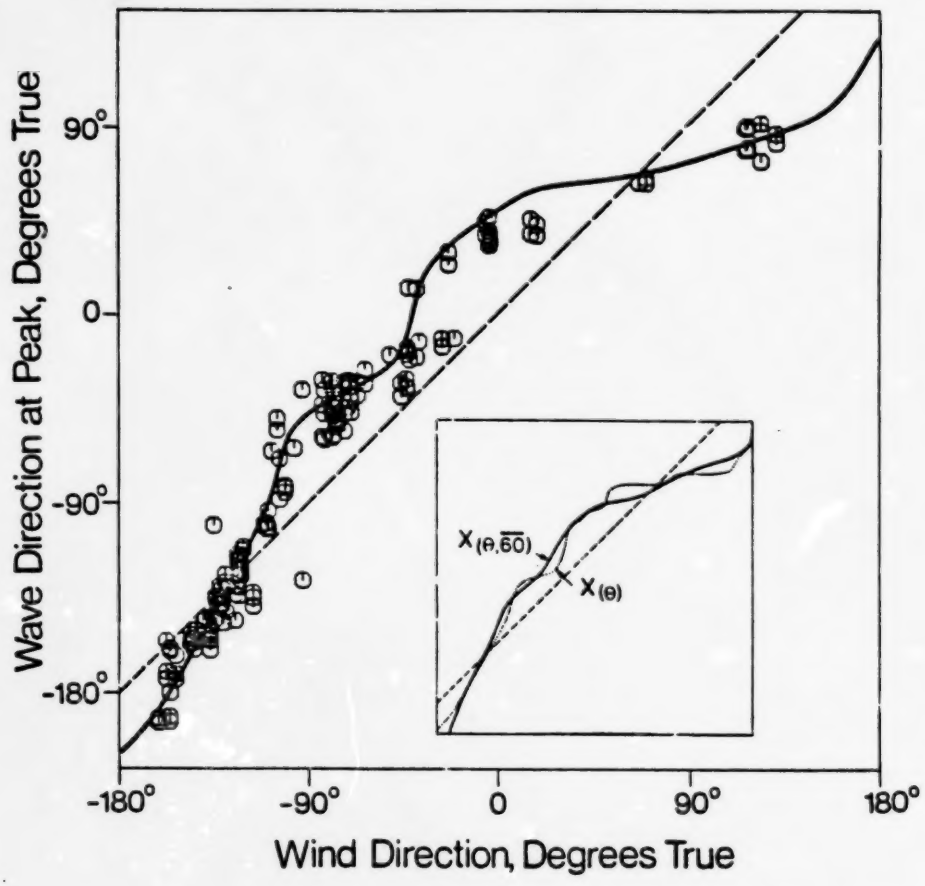
Wave Direction at Peak, Degrees True
90°
0
-90°
-180°
-180°
-90°
0
90°
180°
Wind Direction, Degrees True
X(θ,60)
X(θ)

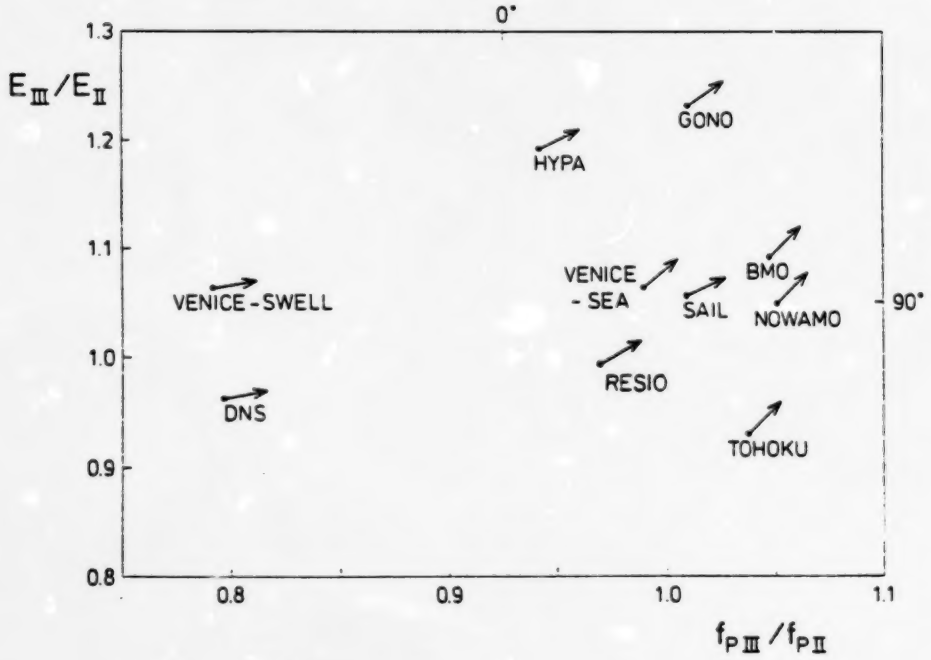
0°
90°
E III / E II
1.3
1.2
1.1
1.0
0.9
0.8
0.8
0.9
1.0
1.1
f P III / f P II
GONO
HYPA
VENICE - SEA
BMO
SAIL
NOWAMO
VENICE - SWELL
RESIO
DNS
TOHOKU

III.9 - III.10

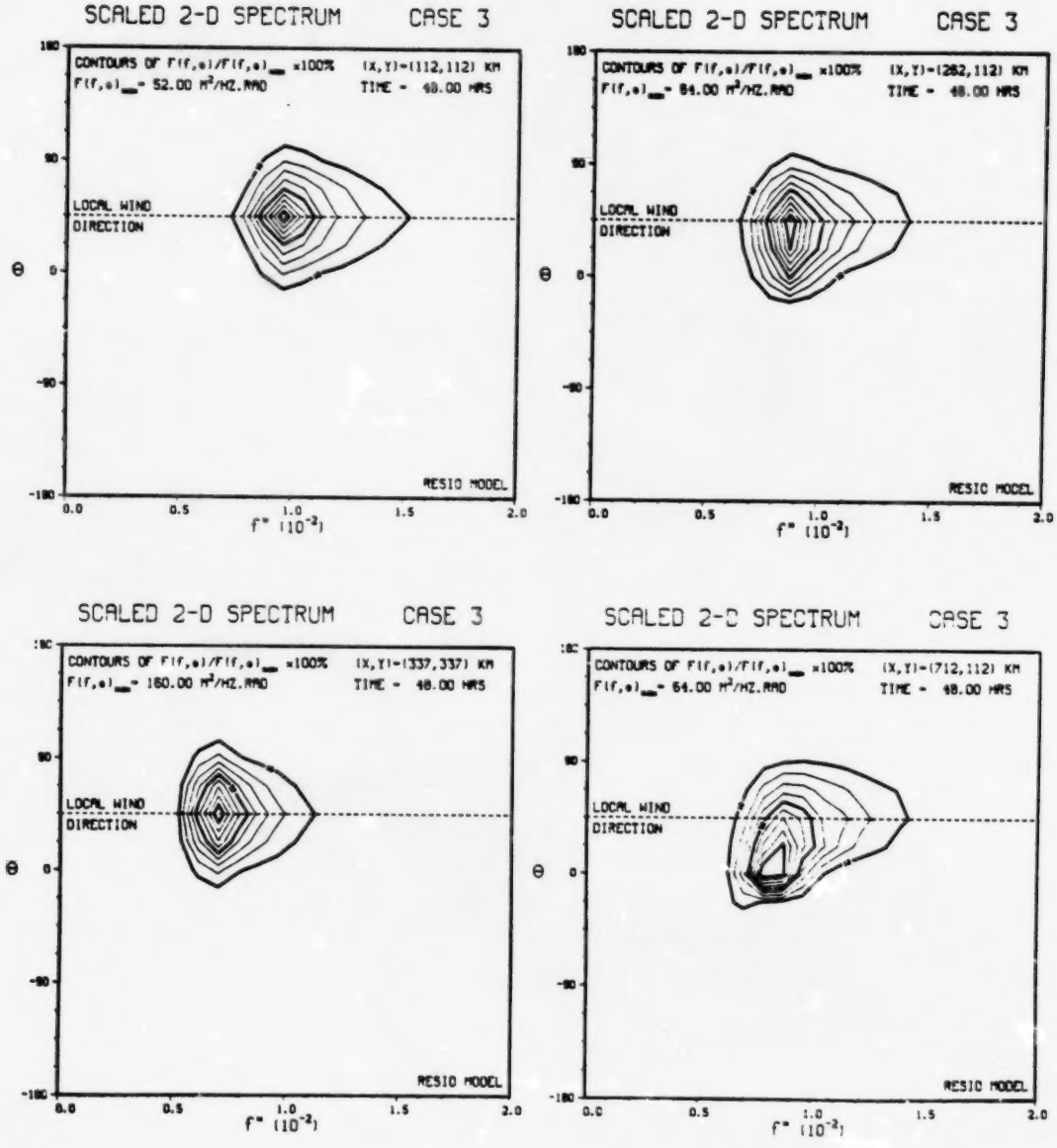
SCALED 2-D SPECTRUM CASE 3
CONTOURS OF F(f,θ)/F(f,θ)max ×100%
F(f,θ)max = 52.00 M²/HZ.RAD
(X,Y)=(112,112) KM
TIME = 48.00 HRS
LOCAL WIND DIRECTION
RESIO MODEL
θ
f* (10⁻²)
SCALED 2-D SPECTRUM CASE 3
CONTOURS OF F(f,θ)/F(f,θ)max ×100%
F(f,θ)max = 84.00 M²/HZ.RAD
(X,Y)=(262,112) KM
TIME = 48.00 HRS
LOCAL WIND DIRECTION
RESIO MODEL
θ
f* (10⁻²)
SCALED 2-D SPECTRUM CASE 3
CONTOURS OF F(f,θ)/F(f,θ)max ×100%
F(f,θ)max = 160.00 M²/HZ.RAD
(X,Y)=(337,337) KM
TIME = 48.00 HRS
LOCAL WIND DIRECTION
RESIO MODEL
θ
f* (10⁻²)
SCALED 2-D SPECTRUM CASE 3
CONTOURS OF F(f,θ)/F(f,θ)max ×100%
F(f,θ)max = 64.00 M²/HZ.RAD
(X,Y)=(712,112) KM
TIME = 48.00 HRS
LOCAL WIND DIRECTION
RESIO MODEL
θ
f* (10⁻²)

III.11 - III.14

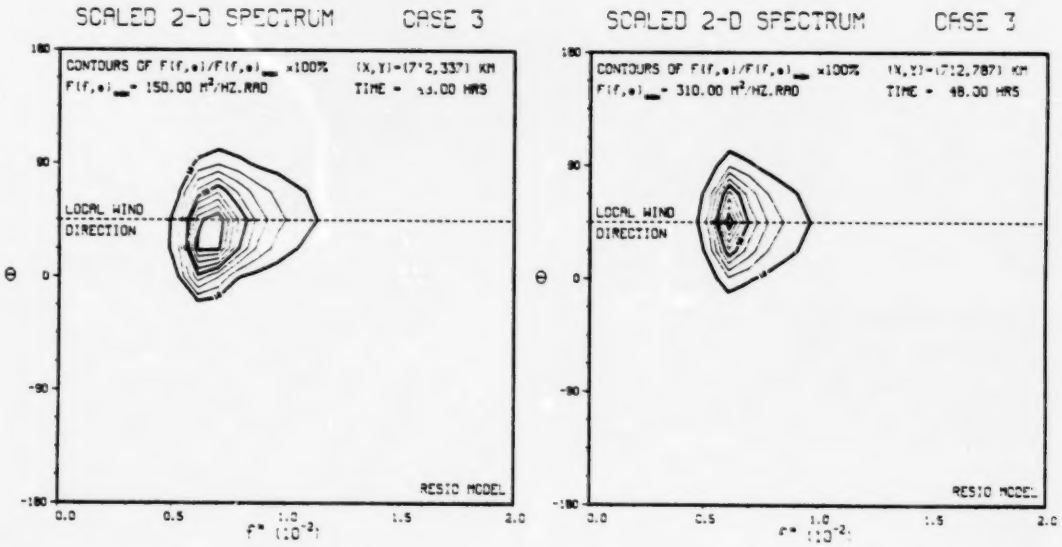
SCALED 2-D SPECTRUM CASE 3
CONTOURS OF F(f,θ)/F(f,θ)max ×100%
F(f,θ)max = 150.00 M²/HZ.RAD
(X,Y)=(712,337) KM
TIME = 48.00 HRS
LOCAL WIND DIRECTION
RESIO MODEL
θ
f* (10⁻²)
SCALED 2-D SPECTRUM CASE 3
CONTOURS OF F(f,θ)/F(f,θ)max ×100%
F(f,θ)max = 310.00 M²/HZ.RAD
(X,Y)=(712,787) KM
TIME = 48.00 HRS
LOCAL WIND DIRECTION
RESIO MODEL
θ
f* (10⁻²)

III.15 - III.16

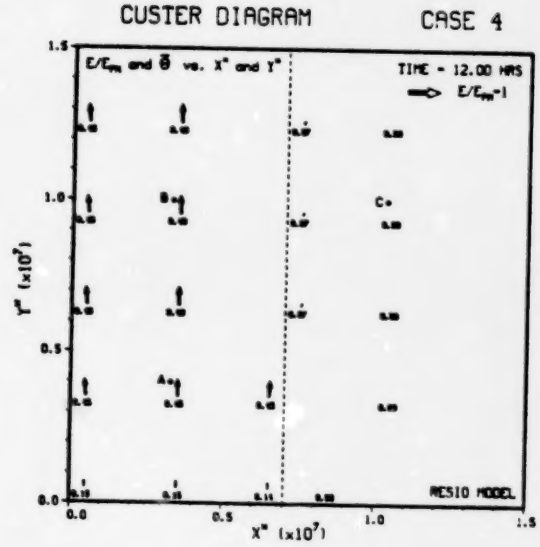
CUSTER DIAGRAM
CASE 4
TIME - 12.00 HRS
RESID MODEL
X* (x10⁷)
Y* (x10⁷)

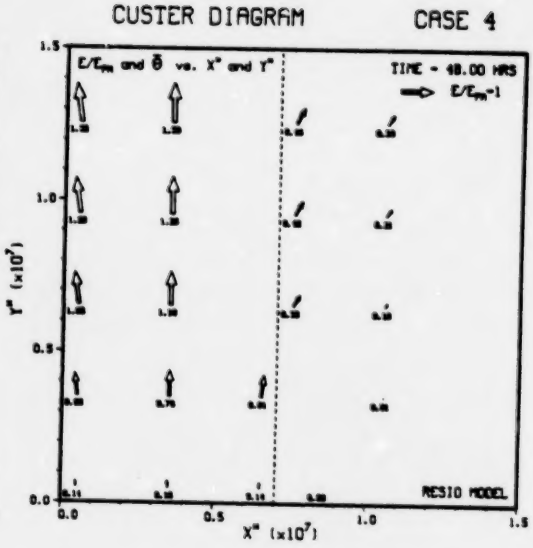
CUSTER DIAGRAM
CASE 4
TIME - 48.00 HRS
RESID MODEL
X* (x10⁷)
Y* (x10⁷)

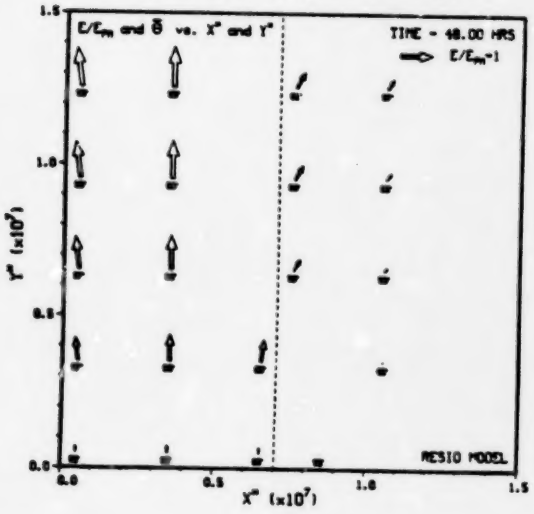
CUSTER DIAGRAM
CASE 4
TIME - 48.00 HRS
RESID MODEL
X* (x10⁷)
Y* (x10⁷)

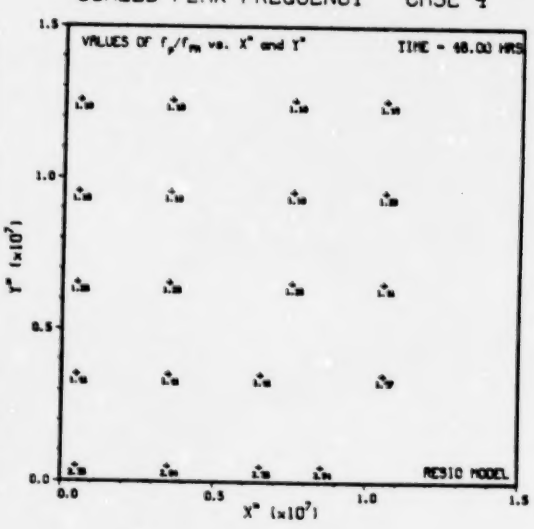
SCALED PEAK FREQUENCY
CASE 4
TIME - 48.00 HRS
RESID MODEL
X* (x10⁷)
Y* (x10⁷)

IV.1 - IV.4

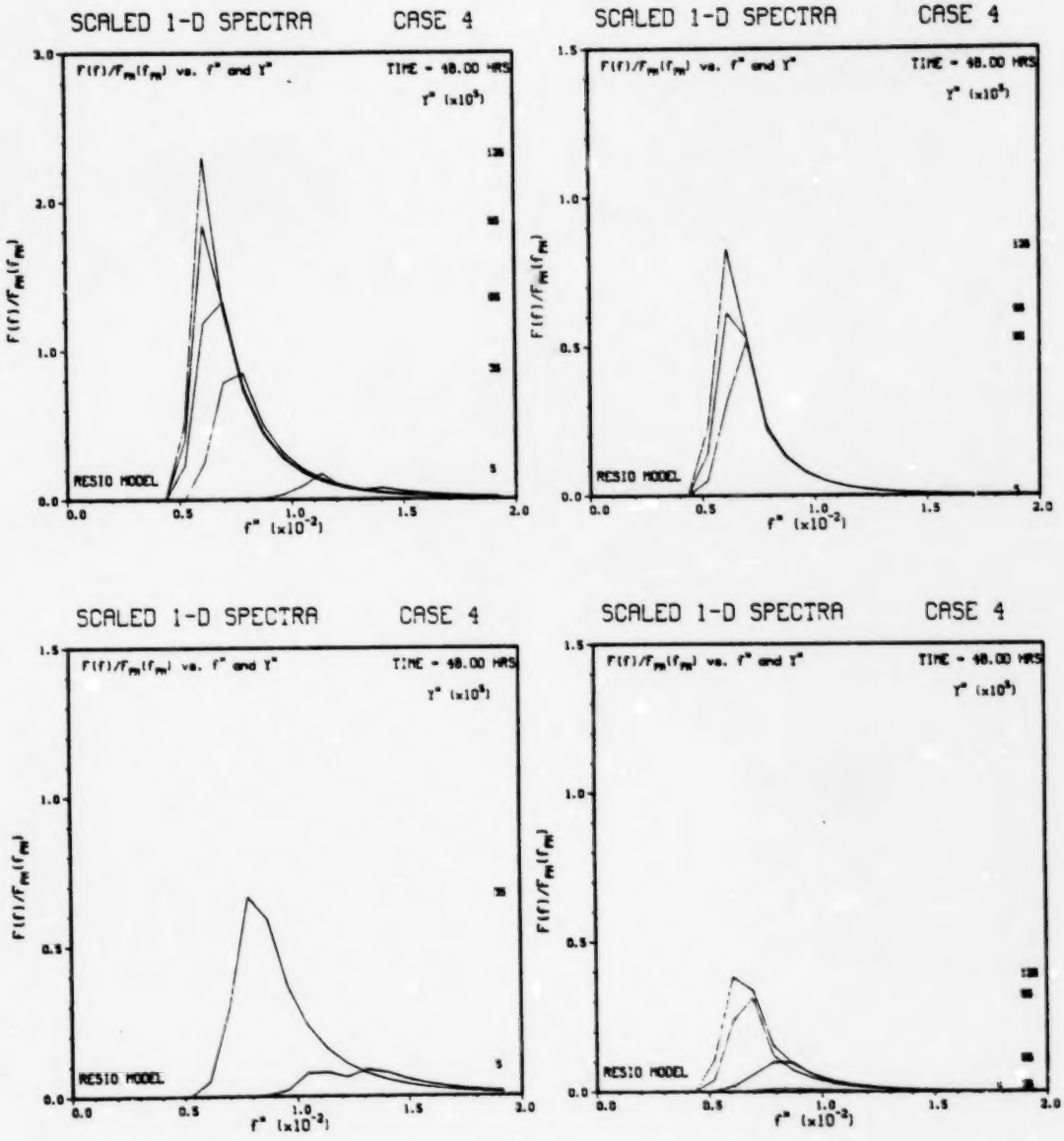
SCALED 1-D SPECTRA CASE 4
SCALED 1-D SPECTRA CASE 4
SCALED 1-D SPECTRA CASE 4
SCALED 1-D SPECTRA CASE 4
RESIO MODEL
TIME = 48.00 HRS

IV.5 - IV.8

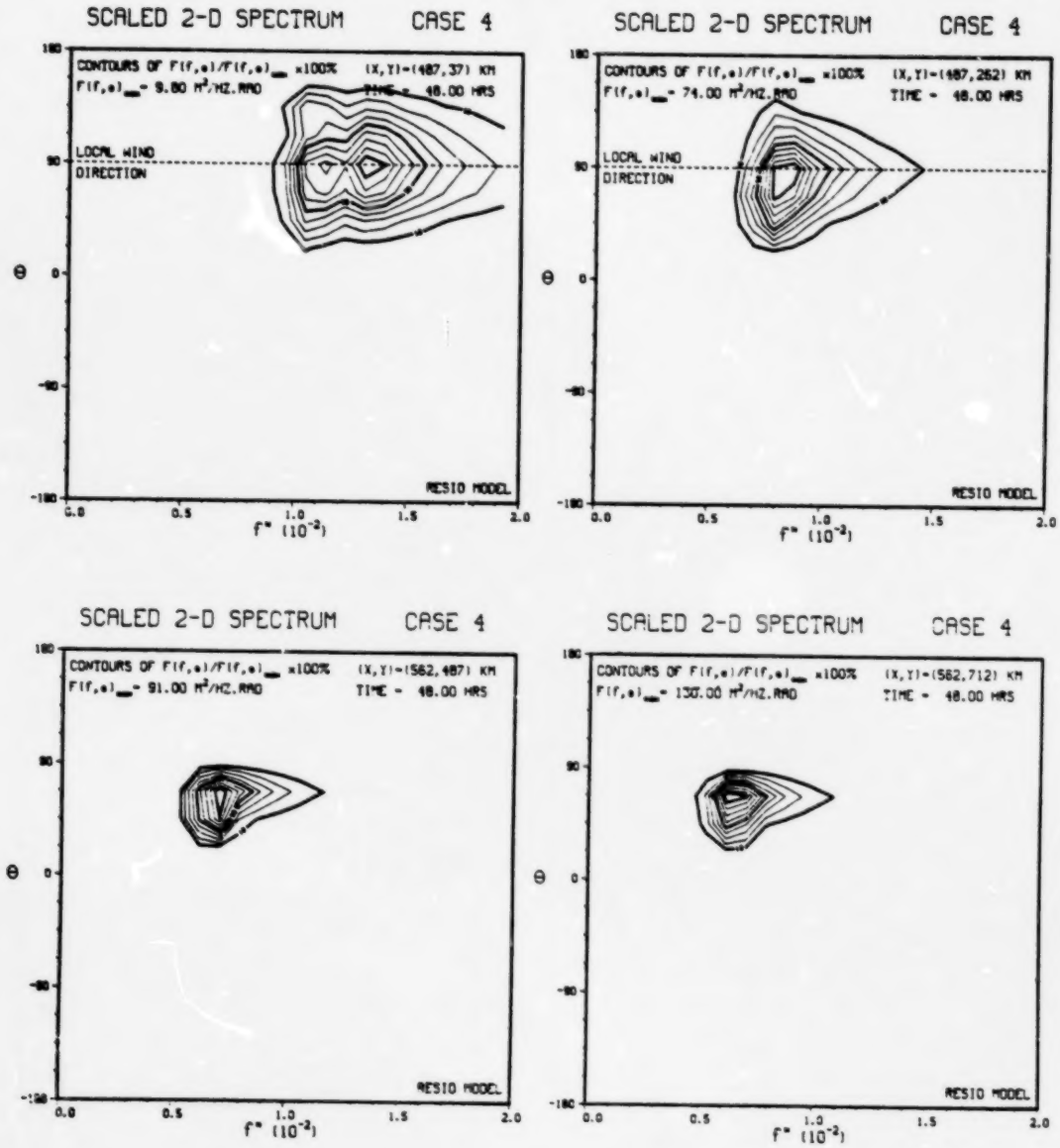
SCALED 2-D SPECTRUM CASE 4
CONTOURS OF F(f,θ)/F(f,θ)__ ×100%
F(f,θ)__ = 9.80 M²/HZ.RAD
(X,Y)=(487,37) KM
TIME = 48.00 HRS
LOCAL WIND DIRECTION
RESIO MODEL
θ
f* (10⁻²)
SCALED 2-D SPECTRUM CASE 4
CONTOURS OF F(f,θ)/F(f,θ)__ ×100%
F(f,θ)__ = 74.00 M²/HZ.RAD
(X,Y)=(487,262) KM
TIME = 48.00 HRS
LOCAL WIND DIRECTION
RESIO MODEL
θ
f* (10⁻²)
SCALED 2-D SPECTRUM CASE 4
CONTOURS OF F(f,θ)/F(f,θ)__ ×100%
F(f,θ)__ = 91.00 M²/HZ.RAD
(X,Y)=(562,487) KM
TIME = 48.00 HRS
RESIO MODEL
θ
f* (10⁻²)
SCALED 2-D SPECTRUM CASE 4
CONTOURS OF F(f,θ)/F(f,θ)__ ×100%
F(f,θ)__ = 130.00 M²/HZ.RAD
(X,Y)=(562,712) KM
TIME = 48.00 HRS
RESIO MODEL
θ
f* (10⁻²)

IV.9 - IV.12

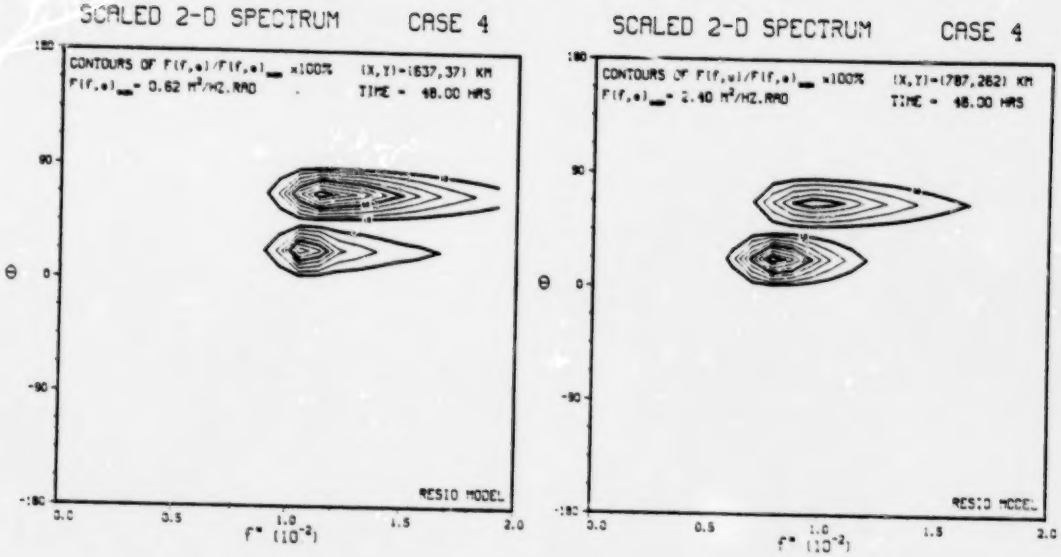
SCALED 2-D SPECTRUM CASE 4
CONTOURS OF F(f,θ)/F(f,θ)max ×100%
F(f,θ)max = 0.62 M²/HZ.RAD
(X,Y)=(637,37) KM
TIME = 48.00 HRS
RESIO MODEL
f* (10⁻²)
θ
SCALED 2-D SPECTRUM CASE 4
CONTOURS OF F(f,θ)/F(f,θ)max ×100%
F(f,θ)max = 2.40 M²/HZ.RAD
(X,Y)=(787,262) KM
TIME = 48.00 HRS
RESIO MODEL
f* (10⁻²)
θ

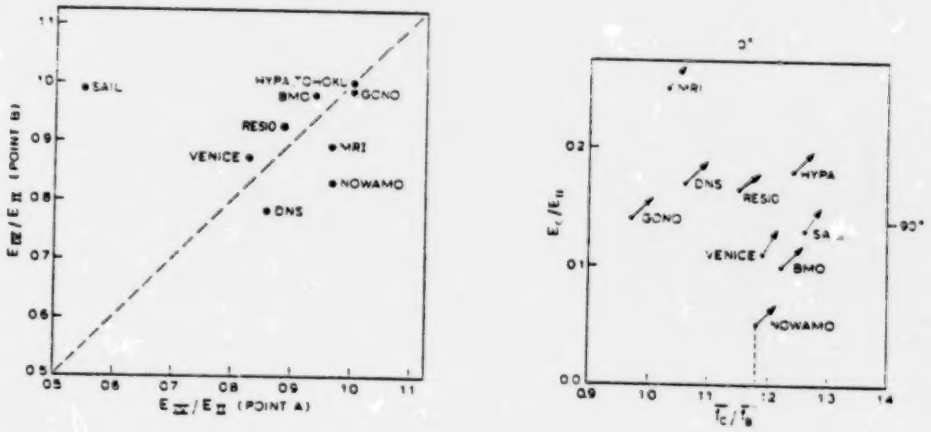
SAIL
HYPA TOHOKU
BMO
GONO
RESIO
VENICE
WRI
NOWAMO
DNS
E_II / E_II (POINT B)
E_II / E_II (POINT A)
0°
WRI
HYPA
DNS
RESIO
GONO
SA
VENICE
BMO
NOWAMO
90°
E_I / E_II
f_I / f_II

IV.13 - IV.16

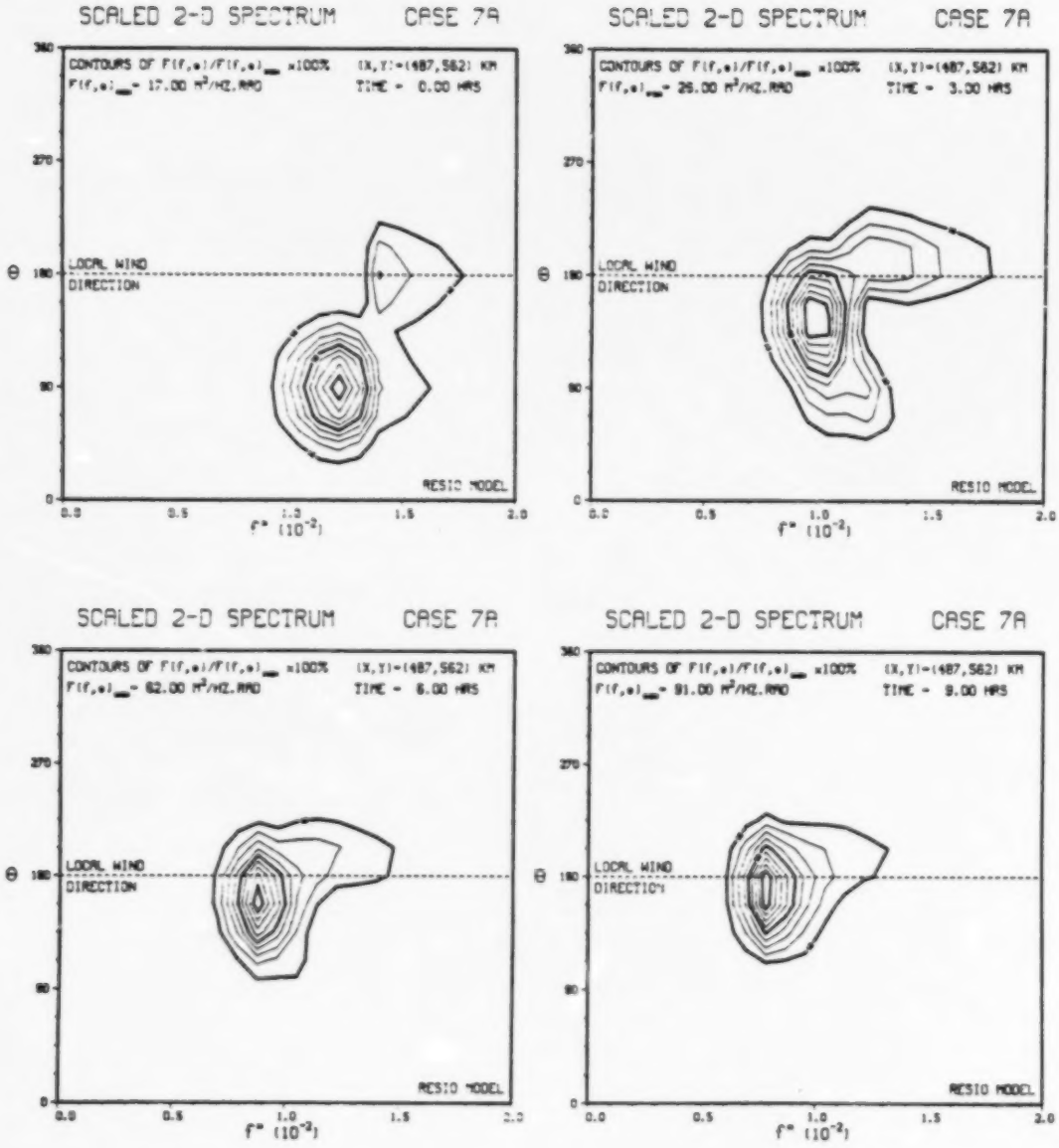
SCALED 2-D SPECTRUM CASE 7A
CONTOURS OF F(f,θ)/F(f,θ)max ×100%
F(f,θ)max = 17.00 M²/HZ.RAD
(X,Y)=(487,562) KM
TIME = 0.00 HRS
LOCAL WIND DIRECTION
RESIO MODEL
θ
f* (10⁻²)
SCALED 2-D SPECTRUM CASE 7A
CONTOURS OF F(f,θ)/F(f,θ)max ×100%
F(f,θ)max = 26.00 M²/HZ.RAD
(X,Y)=(487,562) KM
TIME = 3.00 HRS
LOCAL WIND DIRECTION
RESIO MODEL
θ
f* (10⁻²)
SCALED 2-D SPECTRUM CASE 7A
CONTOURS OF F(f,θ)/F(f,θ)max ×100%
F(f,θ)max = 62.00 M²/HZ.RAD
(X,Y)=(487,562) KM
TIME = 6.00 HRS
LOCAL WIND DIRECTION
RESIO MODEL
θ
f* (10⁻²)
SCALED 2-D SPECTRUM CASE 7A
CONTOURS OF F(f,θ)/F(f,θ)max ×100%
F(f,θ)max = 91.00 M²/HZ.RAD
(X,Y)=(487,562) KM
TIME = 9.00 HRS
LOCAL WIND DIRECTION
RESIO MODEL
θ
f* (10⁻²)

VII.1 - VII.4

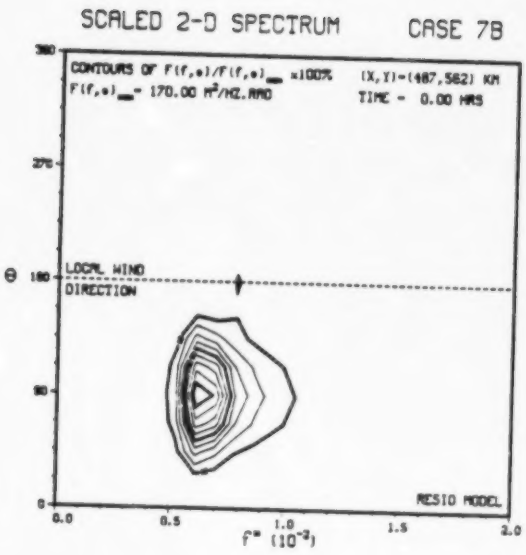
SCALED 2-D SPECTRUM CASE 7B
CONTOURS OF F(f,θ)/F(f,θ)max ×100%
F(f,θ)max = 170.00 M²/HZ.RAD
(X,Y)=(487,562) KM
TIME = 0.00 HRS
LOCAL WIND DIRECTION
RESID MODEL
θ
f* (10⁻²)

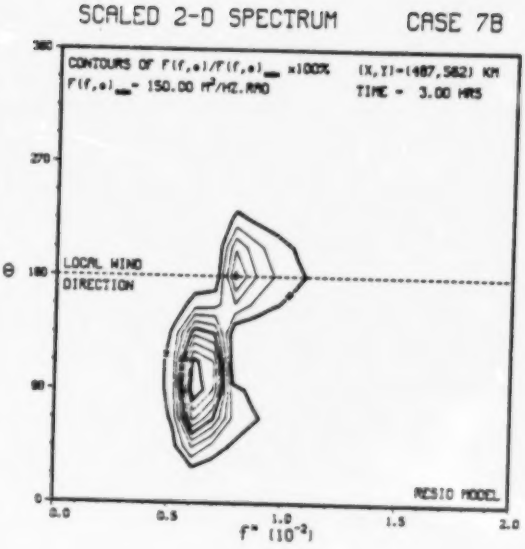
SCALED 2-D SPECTRUM CASE 7B
CONTOURS OF F(f,θ)/F(f,θ)max ×100%
F(f,θ)max = 150.00 M²/HZ.RAD
(X,Y)=(487,562) KM
TIME = 3.00 HRS
LOCAL WIND DIRECTION
RESID MODEL
θ
f* (10⁻²)

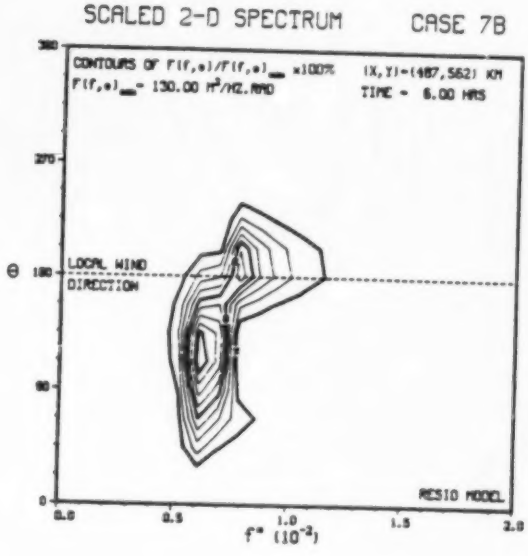
SCALED 2-D SPECTRUM CASE 7B
CONTOURS OF F(f,θ)/F(f,θ)max ×100%
F(f,θ)max = 130.00 M²/HZ.RAD
(X,Y)=(487,562) KM
TIME = 6.00 HRS
LOCAL WIND DIRECTION
RESID MODEL
θ
f* (10⁻²)

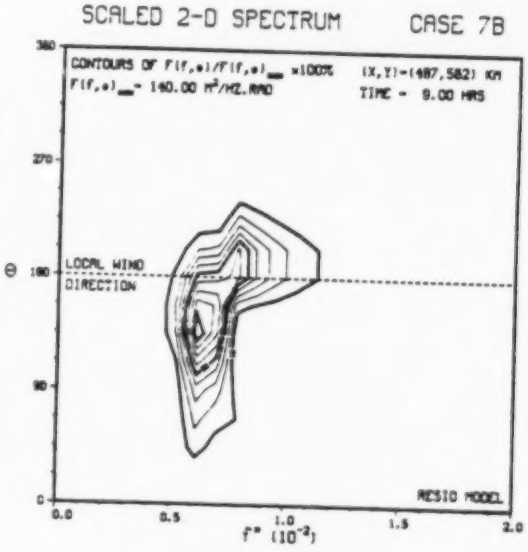
SCALED 2-D SPECTRUM CASE 7B
CONTOURS OF F(f,θ)/F(f,θ)max ×100%
F(f,θ)max = 140.00 M²/HZ.RAD
(X,Y)=(487,562) KM
TIME = 9.00 HRS
LOCAL WIND DIRECTION
RESID MODEL
θ
f* (10⁻²)

VII.5 - VII.8

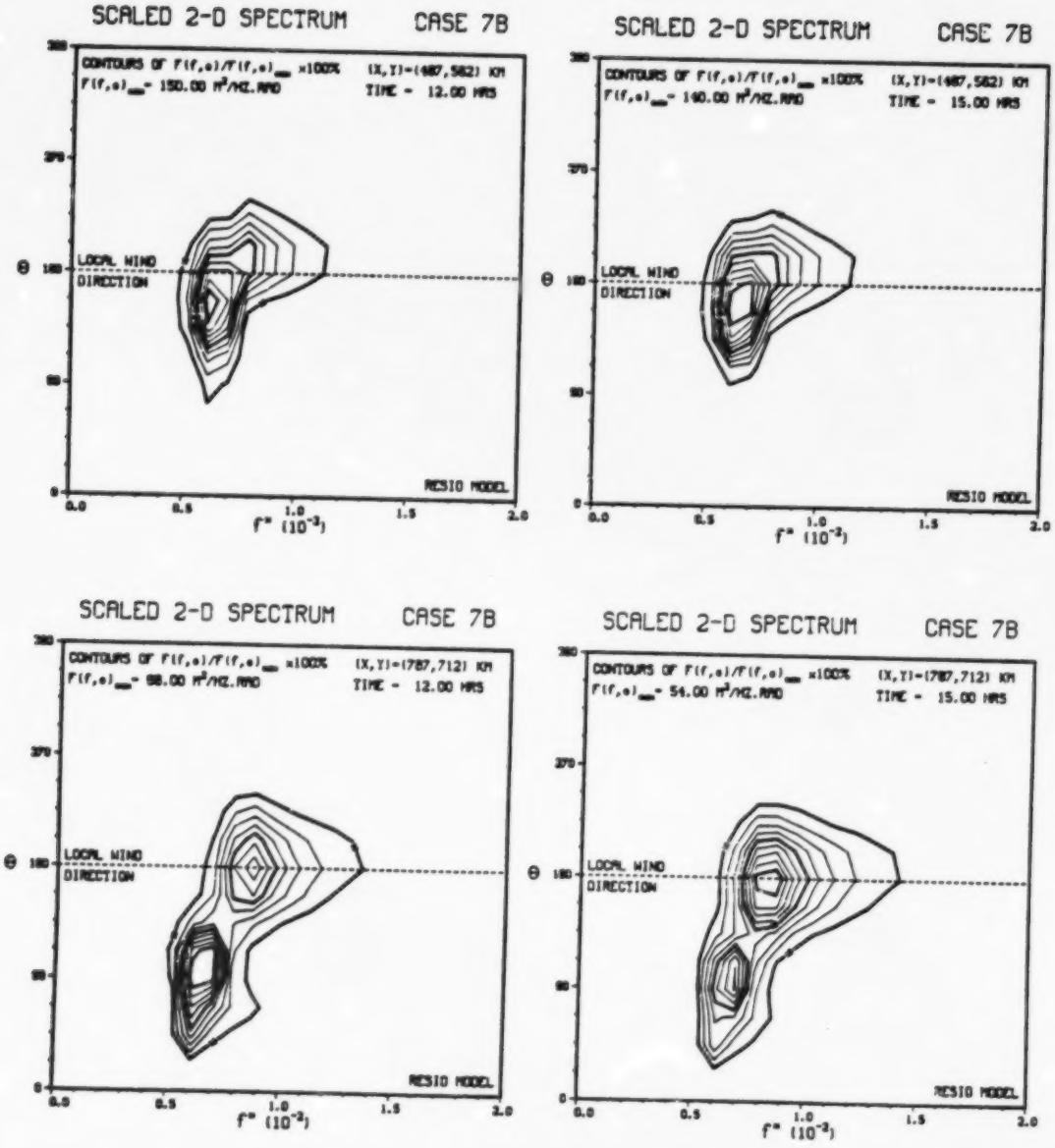
SCALED 2-D SPECTRUM CASE 7B
CONTOURS OF F(f,θ)/F(f,θ)max ×100%
F(f,θ)max = 150.00 M²/HZ.RAD
(X,Y)=(487,582) KM
TIME = 12.00 HRS
LOCAL WIND DIRECTION
RESID MODEL
f* (10⁻²)
SCALED 2-D SPECTRUM CASE 7B
CONTOURS OF F(f,θ)/F(f,θ)max ×100%
F(f,θ)max = 140.00 M²/HZ.RAD
(X,Y)=(487,582) KM
TIME = 15.00 HRS
LOCAL WIND DIRECTION
RESID MODEL
f* (10⁻²)
SCALED 2-D SPECTRUM CASE 7B
CONTOURS OF F(f,θ)/F(f,θ)max ×100%
F(f,θ)max = 98.00 M²/HZ.RAD
(X,Y)=(787,712) KM
TIME = 12.00 HRS
LOCAL WIND DIRECTION
RESID MODEL
f* (10⁻²)
SCALED 2-D SPECTRUM CASE 7B
CONTOURS OF F(f,θ)/F(f,θ)max ×100%
F(f,θ)max = 54.00 M²/HZ.RAD
(X,Y)=(787,712) KM
TIME = 15.00 HRS
LOCAL WIND DIRECTION
RESID MODEL
f* (10⁻²)

VII.9 - VII.12

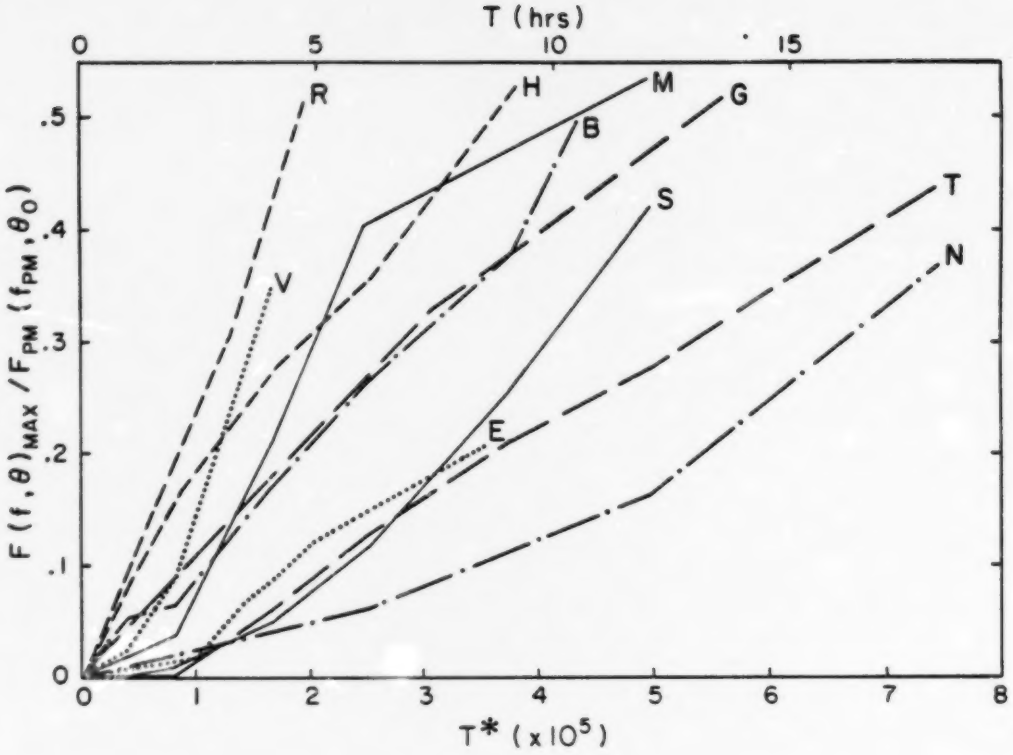
T (hrs)
0
5
10
15
R
H
M
G
B
S
T
N
V
E
.5
.4
.3
.2
.1
0
$F(f,\theta)_{MAX}/F_{PM}(f_{PM},\theta_0)$
0
1
2
3
4
5
6
7
8
T^* ($\times 10^5$)

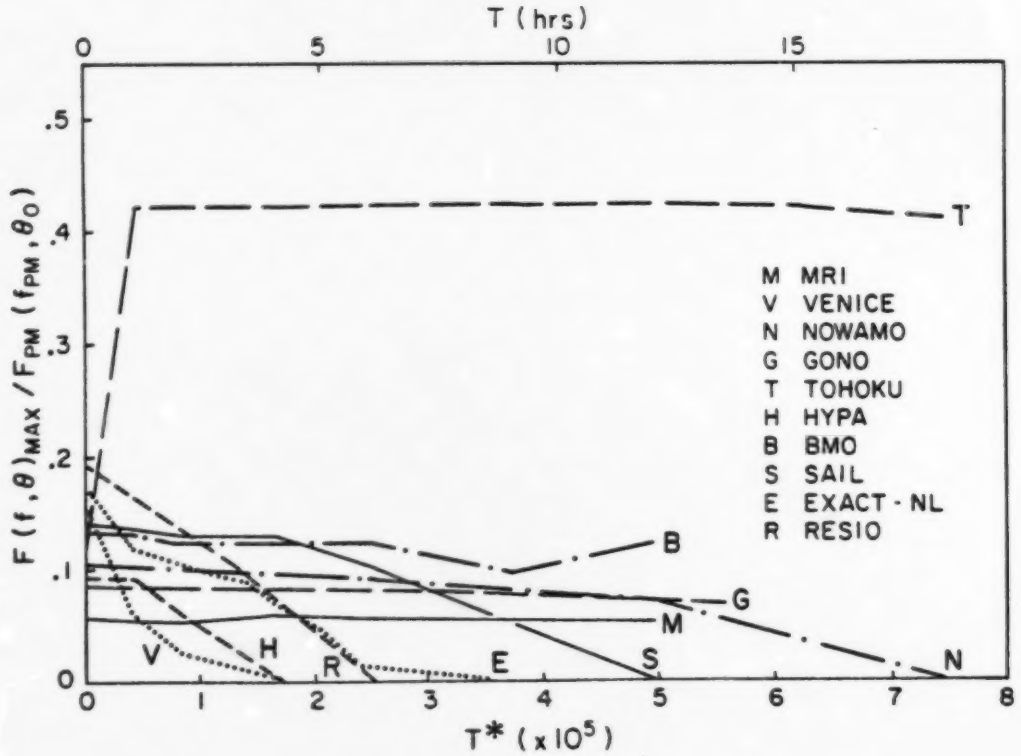
T (hrs)
0
5
10
15
T
M MRI
V VENICE
N NOWAMO
G GONO
T TOHOKU
H HYPA
B BMO
S SAIL
E EXACT - NL
R RESIO
B
G
M
V
H
R
E
S
N
.5
.4
.3
.2
.1
0
$F(f,\theta)_{MAX}/F_{PM}(f_{PM},\theta_0)$
0
1
2
3
4
5
6
7
8
T^* ($\times 10^5$)

VII.13 - VII.14

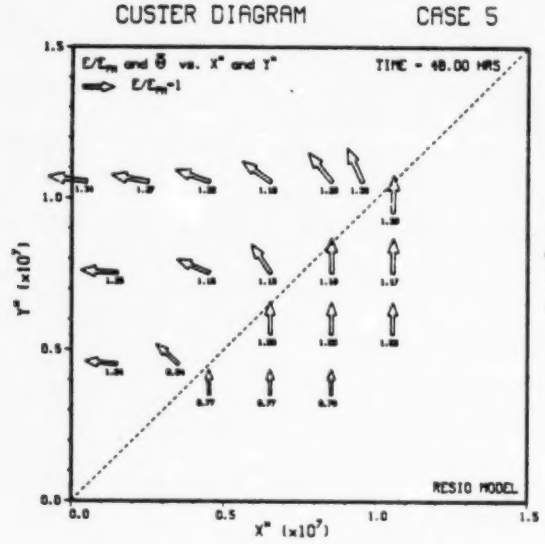
CUSTER DIAGRAM
CASE 5
TIME = 48.00 HRS
RESIO MODEL
X* (x10⁷)
Y* (x10⁷)

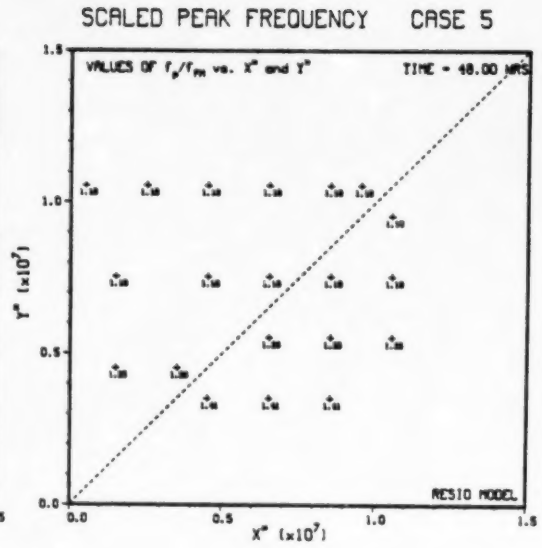
SCALED PEAK FREQUENCY
CASE 5
TIME = 48.00 HRS
RESIO MODEL
X* (x10⁷)
Y* (x10⁷)

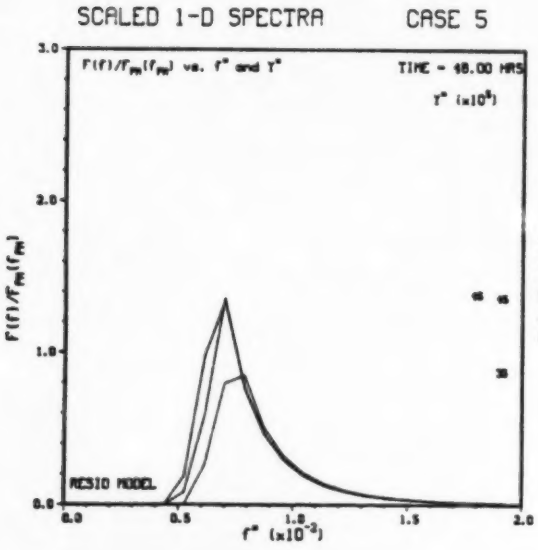
SCALED 1-D SPECTRA
CASE 5
TIME = 48.00 HRS
RESIO MODEL
f* (x10⁻²)

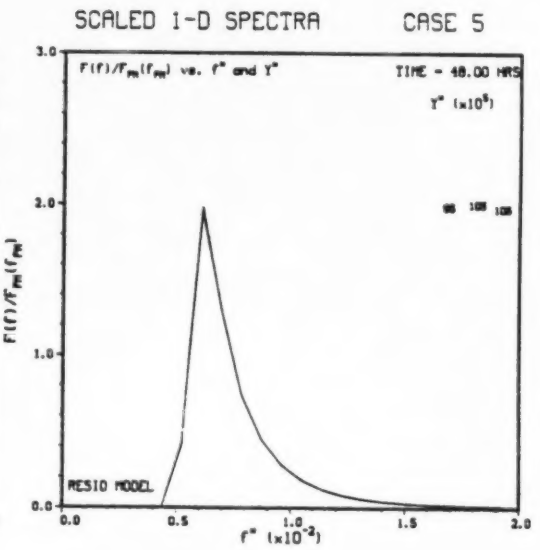
SCALED 1-D SPECTRA
CASE 5
TIME = 48.00 HRS
RESIO MODEL
f* (x10⁻²)

V.1 - V.4

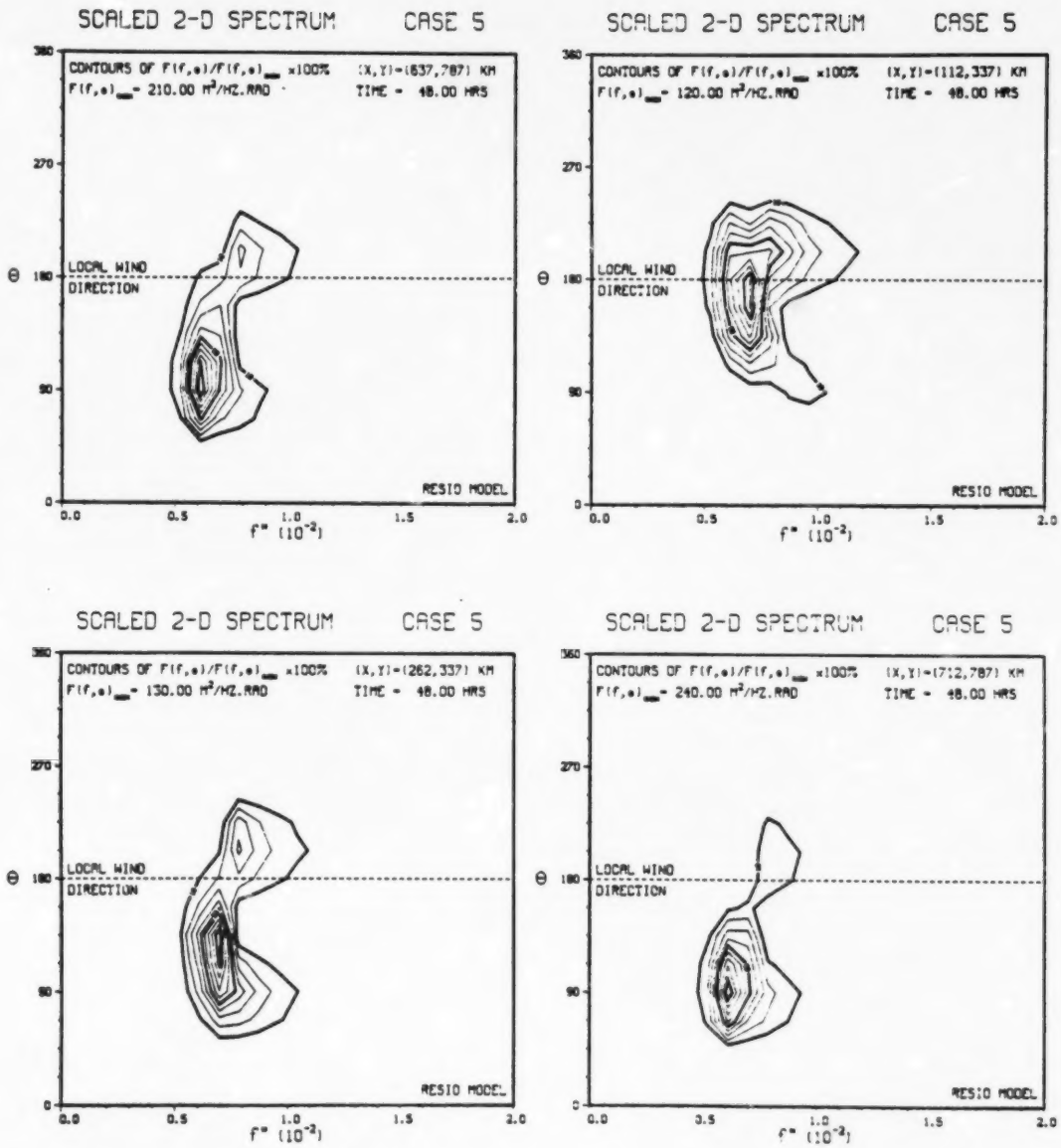
SCALED 2-D SPECTRUM CASE 5
CONTOURS OF F(f,θ)/F(f,θ)max ×100%
F(f,θ)max = 210.00 M²/HZ.RAD
(X,Y)=(637,787) KM
TIME = 48.00 HRS
LOCAL WIND DIRECTION
RESIO MODEL
θ
f* (10⁻²)
SCALED 2-D SPECTRUM CASE 5
CONTOURS OF F(f,θ)/F(f,θ)max ×100%
F(f,θ)max = 120.00 M²/HZ.RAD
(X,Y)=(112,337) KM
TIME = 48.00 HRS
LOCAL WIND DIRECTION
RESIO MODEL
θ
f* (10⁻²)
SCALED 2-D SPECTRUM CASE 5
CONTOURS OF F(f,θ)/F(f,θ)max ×100%
F(f,θ)max = 130.00 M²/HZ.RAD
(X,Y)=(262,337) KM
TIME = 48.00 HRS
LOCAL WIND DIRECTION
RESIO MODEL
θ
f* (10⁻²)
SCALED 2-D SPECTRUM CASE 5
CONTOURS OF F(f,θ)/F(f,θ)max ×100%
F(f,θ)max = 240.00 M²/HZ.RAD
(X,Y)=(712,787) KM
TIME = 48.00 HRS
LOCAL WIND DIRECTION
RESIO MODEL
θ
f* (10⁻²)

V.5 - V.8

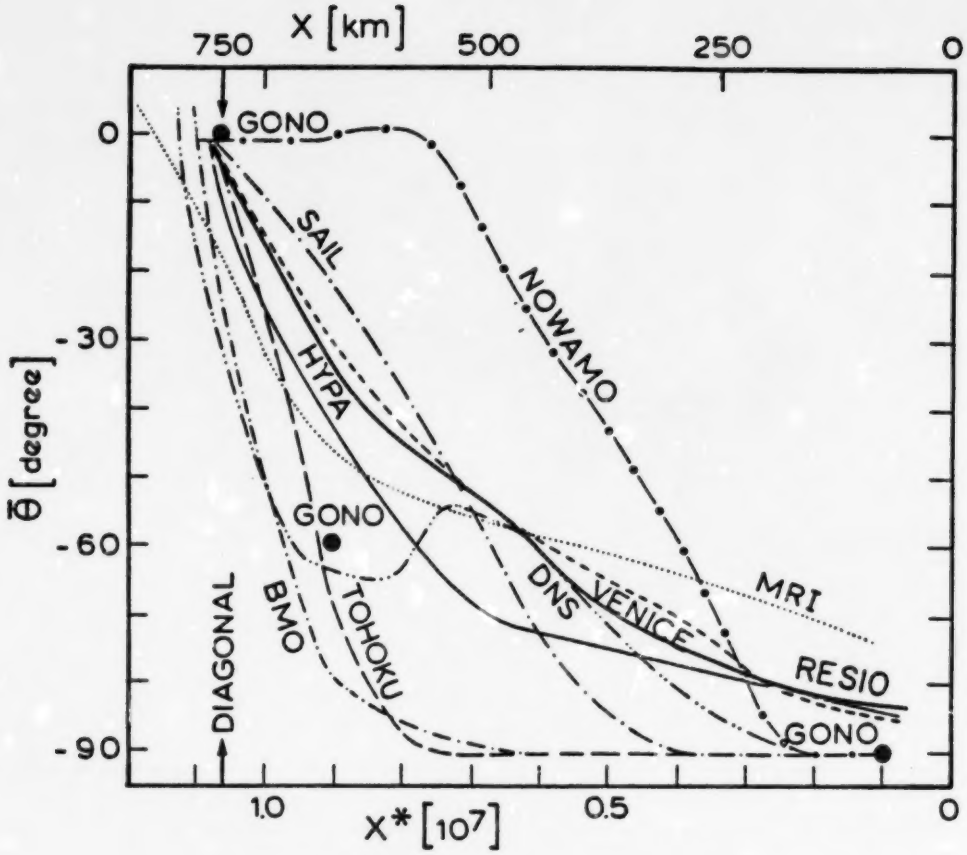
X [km]
750
500
250
0
0
-30
-60
-90
θ̄ [degree]
GONO
SAIL
NOWAMO
HYPA
GONO
BMO
TOHOKU
DNS
VENICE
MRI
RESIO
GONO
DIAGONAL
1.0
0.5
0
X* [10^7]

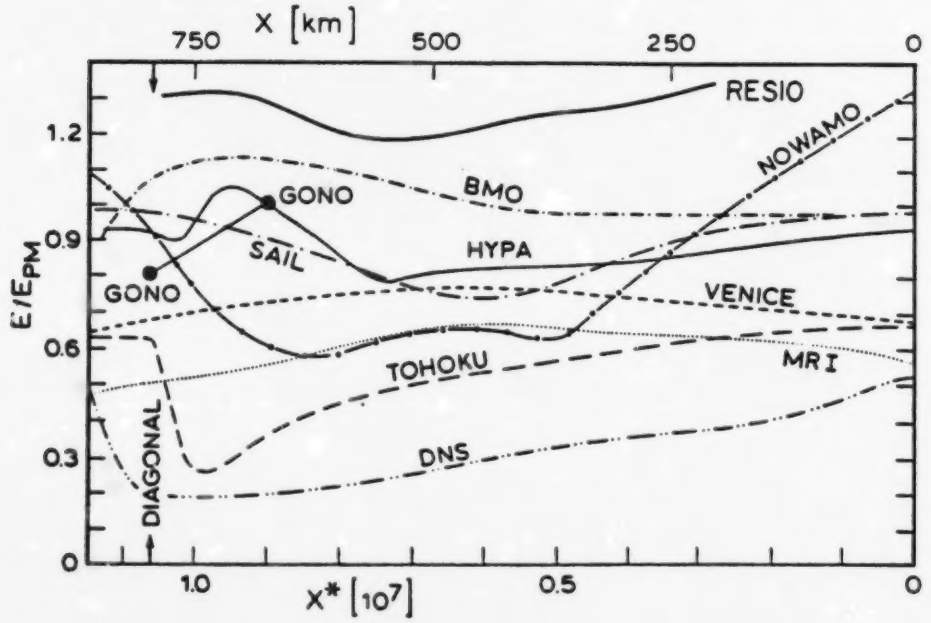
X [km]
750
500
250
0
RESIO
NOWAMO
1.2
BMO
GONO
0.9
SAIL
HYPA
GONO
VENICE
E/E_PM
0.6
TOHOKU
MRI
0.3
DNS
DIAGONAL
0
1.0
0.5
0
X* [10^7]

V.9 - V.10

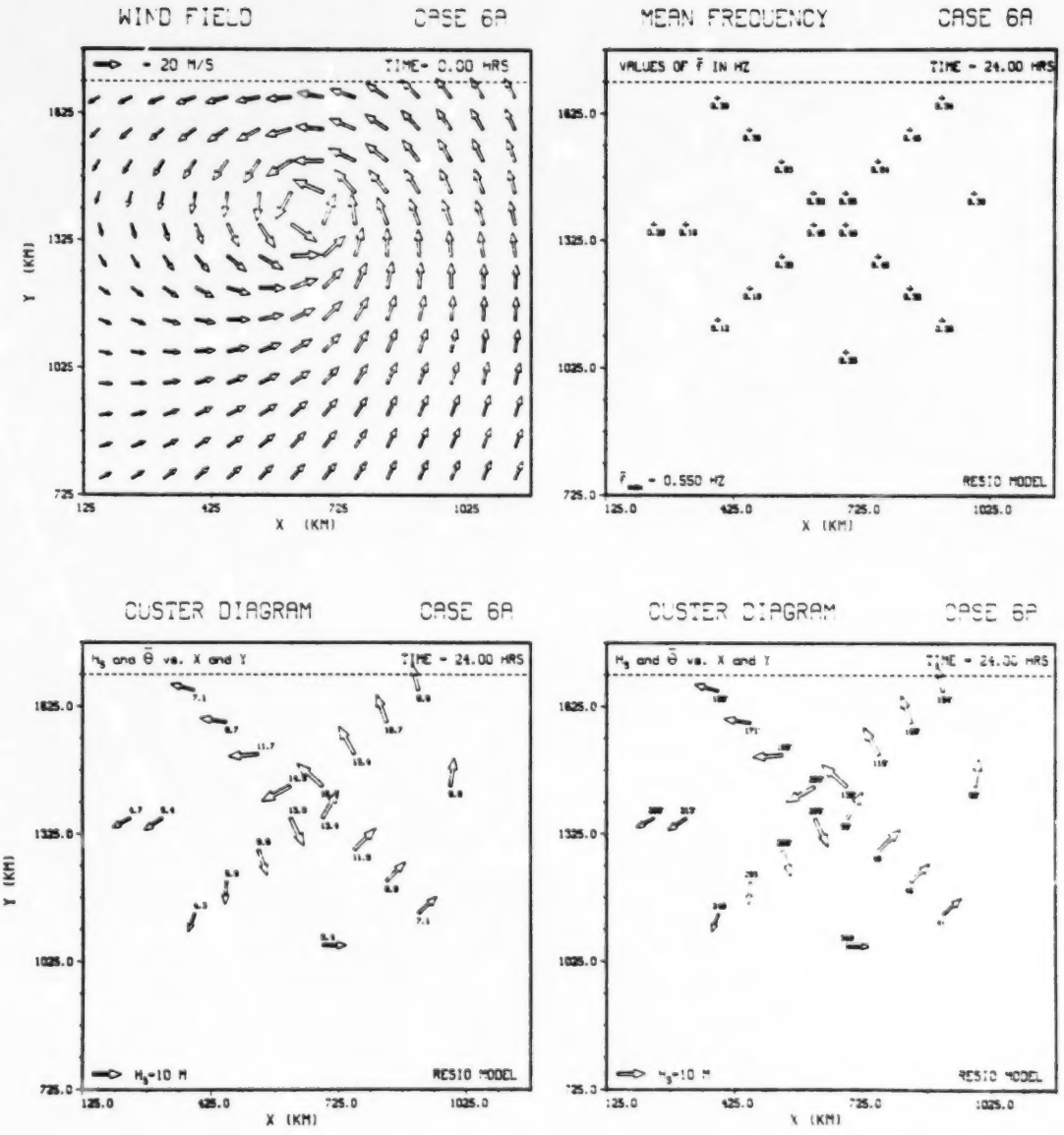
WIND FIELD
CASE 6A
- 20 M/S
TIME= 0.00 HRS
Y (KM)
X (KM)
MEAN FREQUENCY
CASE 6A
VALUES OF f̄ IN HZ
TIME = 24.00 HRS
f̄ = 0.550 HZ
RESIO MODEL
CUSTER DIAGRAM
CASE 6A
Hs and θ̄ vs. X and Y
TIME = 24.00 HRS
Hs=10 M
RESIO MODEL
CUSTER DIAGRAM
CASE 6P
Hs and θ̄ vs. X and Y
TIME = 24.00 HRS
Hs=10 M
RESIO MODEL

VI.1 - VI.4

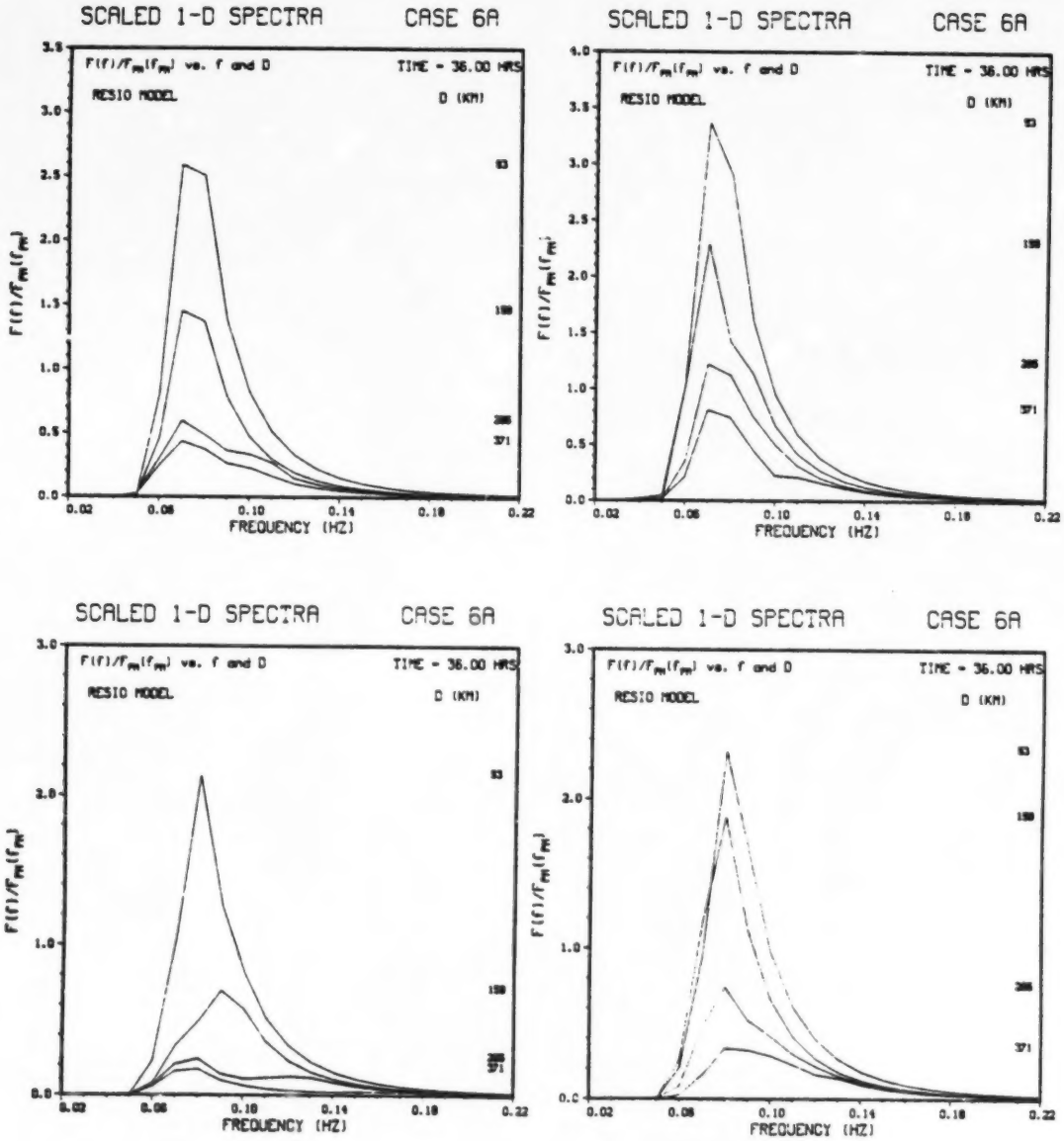
SCALED 1-D SPECTRA
CASE 6A
F(f)/F_m(f_m) vs. f and D
TIME = 36.00 HRS
RESIO MODEL
D (KM)
F(f)/F_m(f_m)
FREQUENCY (HZ)
SCALED 1-D SPECTRA
CASE 6A
F(f)/F_m(f_m) vs. f and D
TIME = 36.00 HRS
RESIO MODEL
D (KM)
F(f)/F_m(f_m)
FREQUENCY (HZ)
SCALED 1-D SPECTRA
CASE 6A
F(f)/F_m(f_m) vs. f and D
TIME = 36.00 HRS
RESIO MODEL
D (KM)
F(f)/F_m(f_m)
FREQUENCY (HZ)
SCALED 1-D SPECTRA
CASE 6A
F(f)/F_m(f_m) vs. f and D
TIME = 36.00 HRS
RESIO MODEL
D (KM)
F(f)/F_m(f_m)
FREQUENCY (HZ)

VI.5 - VI.8

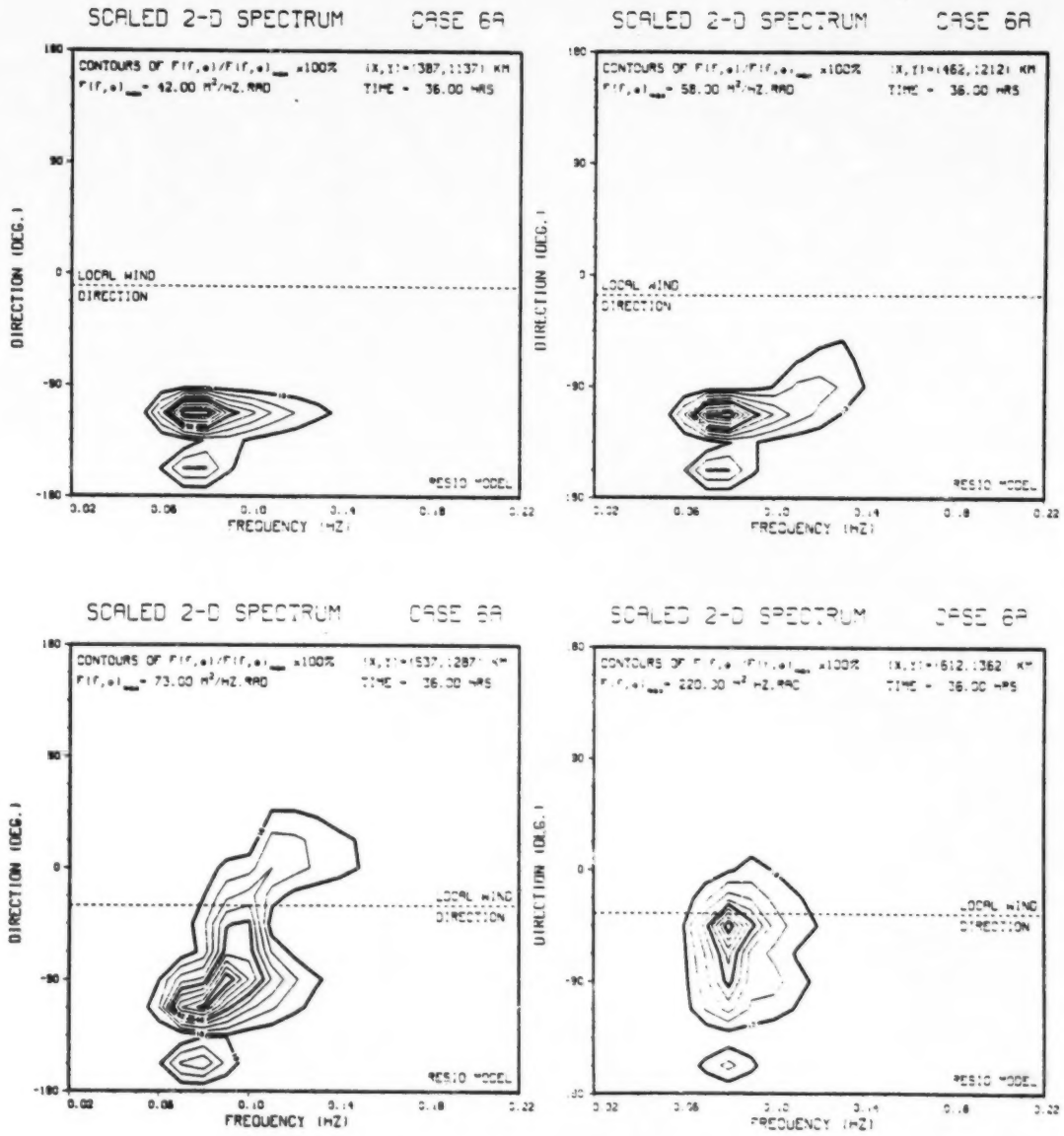
SCALED 2-D SPECTRUM CASE 6A
CONTOURS OF F(f,θ)/F(f,θ)max x100%
F(f,θ)max = 42.00 M²/HZ.RAD
TIME = 36.00 HRS
LOCAL WIND DIRECTION
DIRECTION (DEG.)
FREQUENCY (HZ)
RESID MODEL
SCALED 2-D SPECTRUM CASE 6A
CONTOURS OF F(f,θ)/F(f,θ)max x100%
F(f,θ)max = 58.00 M²/HZ.RAD
TIME = 36.00 HRS
LOCAL WIND DIRECTION
DIRECTION (DEG.)
FREQUENCY (HZ)
RESID MODEL
SCALED 2-D SPECTRUM CASE 6A
CONTOURS OF F(f,θ)/F(f,θ)max x100%
F(f,θ)max = 73.00 M²/HZ.RAD
TIME = 36.00 HRS
LOCAL WIND DIRECTION
DIRECTION (DEG.)
FREQUENCY (HZ)
RESID MODEL
SCALED 2-D SPECTRUM CASE 6A
CONTOURS OF F(f,θ)/F(f,θ)max x100%
F(f,θ)max = 220.00 M²/HZ.RAD
TIME = 36.00 HRS
LOCAL WIND DIRECTION
DIRECTION (DEG.)
FREQUENCY (HZ)
RESID MODEL

VI.9 - VI.12

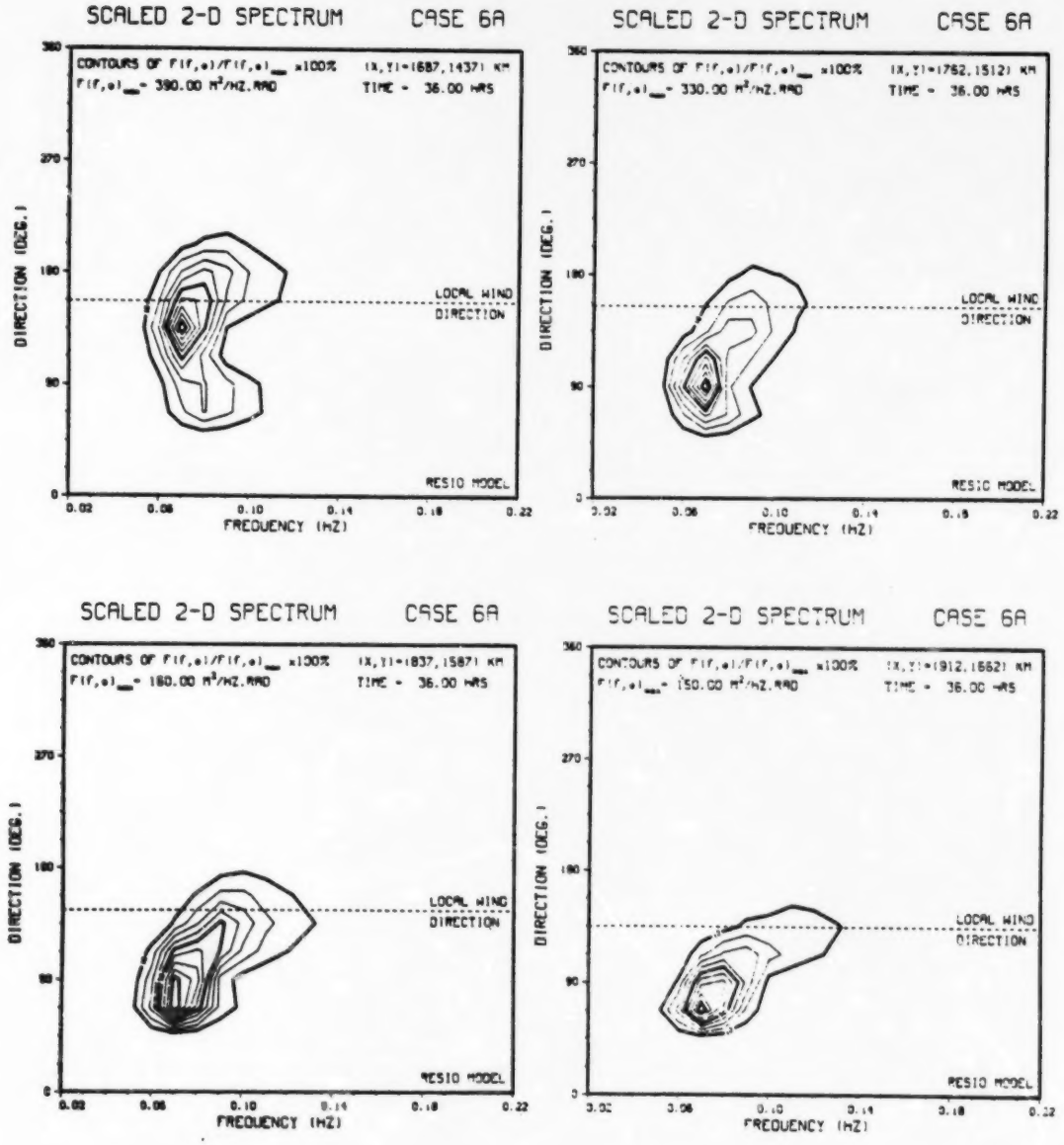
SCALED 2-D SPECTRUM CASE 6A
CONTOURS OF F(f,θ)/F(f,θ)__ x100%
F(f,θ)__ = 390.00 M²/HZ.RAD
(X,Y)=(687,1437) KM
TIME = 36.00 HRS
LOCAL WIND DIRECTION
RESIO MODEL
DIRECTION (DEG.)
FREQUENCY (HZ)
SCALED 2-D SPECTRUM CASE 6A
CONTOURS OF F(f,θ)/F(f,θ)__ x100%
F(f,θ)__ = 330.00 M²/HZ.RAD
(X,Y)=(762,1512) KM
TIME = 36.00 HRS
LOCAL WIND DIRECTION
RESIO MODEL
DIRECTION (DEG.)
FREQUENCY (HZ)
SCALED 2-D SPECTRUM CASE 6A
CONTOURS OF F(f,θ)/F(f,θ)__ x100%
F(f,θ)__ = 180.00 M²/HZ.RAD
(X,Y)=(837,1587) KM
TIME = 36.00 HRS
LOCAL WIND DIRECTION
RESIO MODEL
DIRECTION (DEG.)
FREQUENCY (HZ)
SCALED 2-D SPECTRUM CASE 6A
CONTOURS OF F(f,θ)/F(f,θ)__ x100%
F(f,θ)__ = 150.00 M²/HZ.RAD
(X,Y)=(912,1662) KM
TIME = 36.00 HRS
LOCAL WIND DIRECTION
RESIO MODEL
DIRECTION (DEG.)
FREQUENCY (HZ)

VI.13 - VI.16

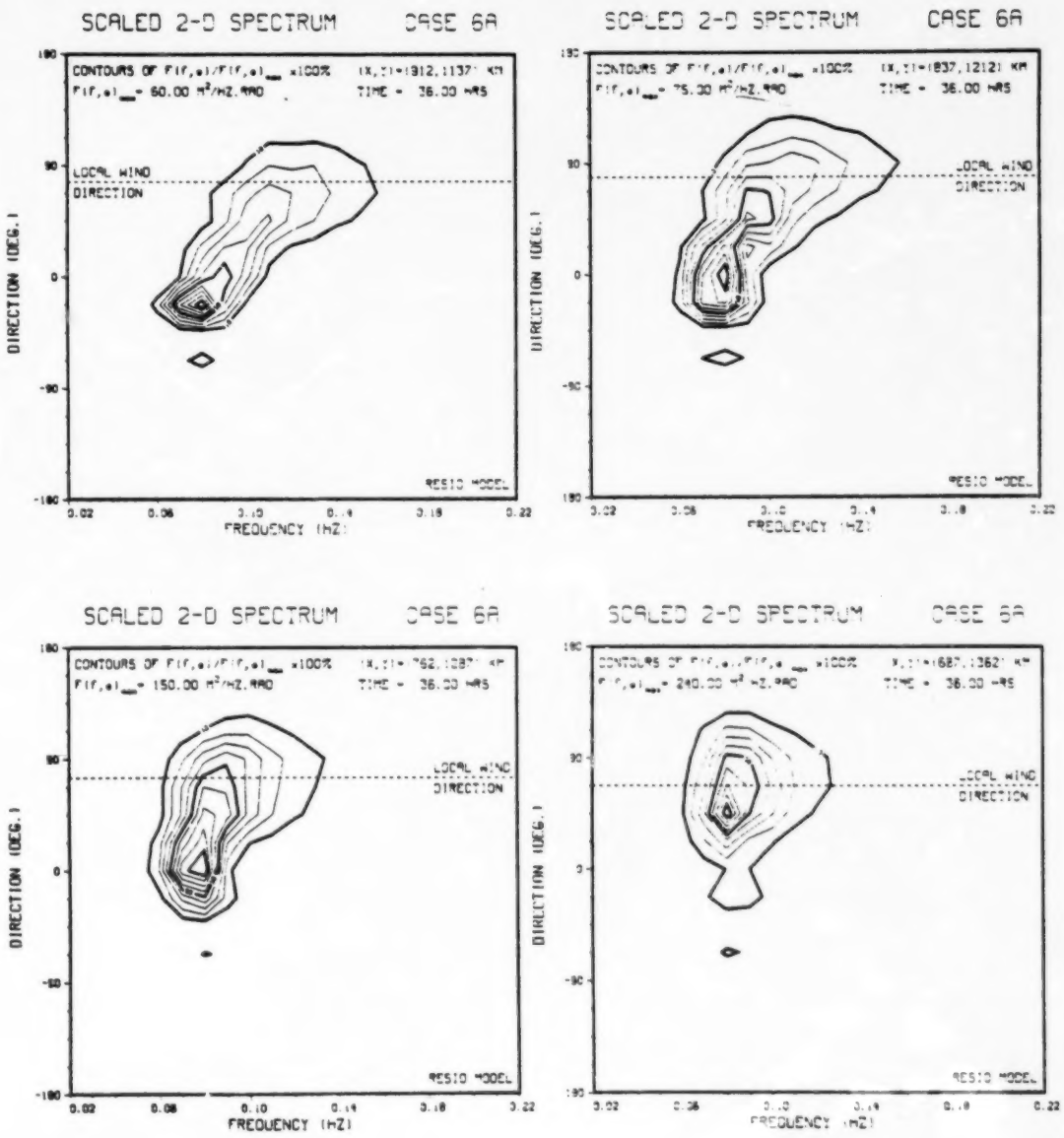
SCALED 2-D SPECTRUM CASE 6A
CONTOURS OF F(f,θ)/F(f,θ)max ×100%
F(f,θ)max = 60.00 M²/HZ.RAD
TIME = 36.00 HRS
LOCAL WIND DIRECTION
RESIO MODEL
DIRECTION (DEG.)
FREQUENCY (HZ)
SCALED 2-D SPECTRUM CASE 6A
CONTOURS OF F(f,θ)/F(f,θ)max ×100%
F(f,θ)max = 75.00 M²/HZ.RAD
TIME = 36.00 HRS
LOCAL WIND DIRECTION
RESIO MODEL
DIRECTION (DEG.)
FREQUENCY (HZ)
SCALED 2-D SPECTRUM CASE 6A
CONTOURS OF F(f,θ)/F(f,θ)max ×100%
F(f,θ)max = 150.00 M²/HZ.RAD
TIME = 36.00 HRS
LOCAL WIND DIRECTION
RESIO MODEL
DIRECTION (DEG.)
FREQUENCY (HZ)
SCALED 2-D SPECTRUM CASE 6A
CONTOURS OF F(f,θ)/F(f,θ)max ×100%
F(f,θ)max = 240.00 M²/HZ.RAD
TIME = 36.00 HRS
LOCAL WIND DIRECTION
RESIO MODEL
DIRECTION (DEG.)
FREQUENCY (HZ)

VI.17 - VI.20

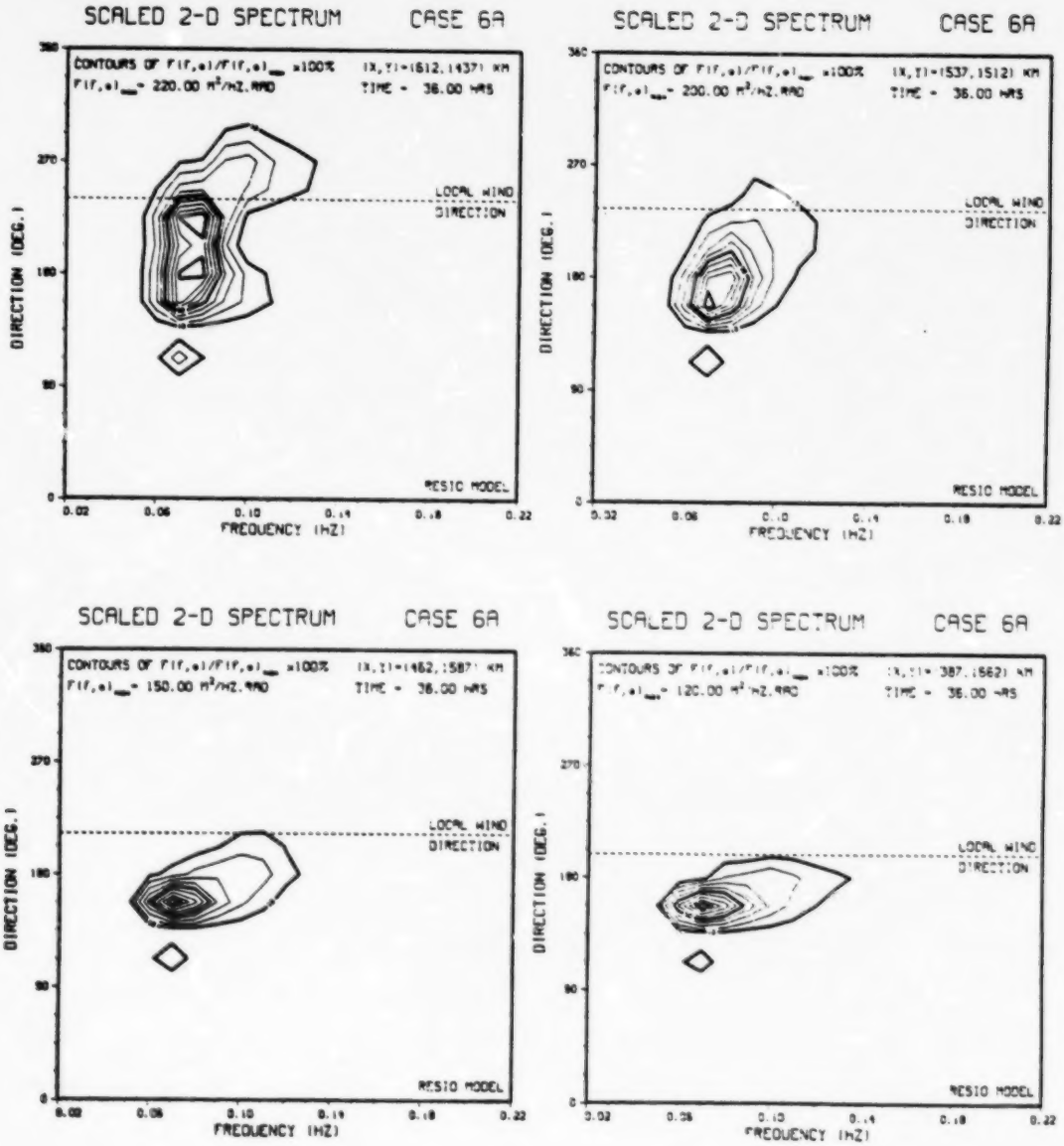
SCALED 2-D SPECTRUM CASE 6A
CONTOURS OF F(f,θ)/F(f,θ)max ×100%
F(f,θ)max = 220.00 M²/HZ.RAD
(X,Y)=(612,1437) KM
TIME = 36.00 HRS
LOCAL WIND DIRECTION
RESIO MODEL
DIRECTION (DEG.)
FREQUENCY (HZ)
SCALED 2-D SPECTRUM CASE 6A
CONTOURS OF F(f,θ)/F(f,θ)max ×100%
F(f,θ)max = 200.00 M²/HZ.RAD
(X,Y)=(537,1512) KM
TIME = 36.00 HRS
LOCAL WIND DIRECTION
RESIO MODEL
DIRECTION (DEG.)
FREQUENCY (HZ)
SCALED 2-D SPECTRUM CASE 6A
CONTOURS OF F(f,θ)/F(f,θ)max ×100%
F(f,θ)max = 150.00 M²/HZ.RAD
(X,Y)=(462,1587) KM
TIME = 36.00 HRS
LOCAL WIND DIRECTION
RESIO MODEL
DIRECTION (DEG.)
FREQUENCY (HZ)
SCALED 2-D SPECTRUM CASE 6A
CONTOURS OF F(f,θ)/F(f,θ)max ×100%
F(f,θ)max = 120.00 M²/HZ.RAD
(X,Y)=(387,1662) KM
TIME = 36.00 HRS
LOCAL WIND DIRECTION
RESIO MODEL
DIRECTION (DEG.)
FREQUENCY (HZ)

VI.21 - VI.24

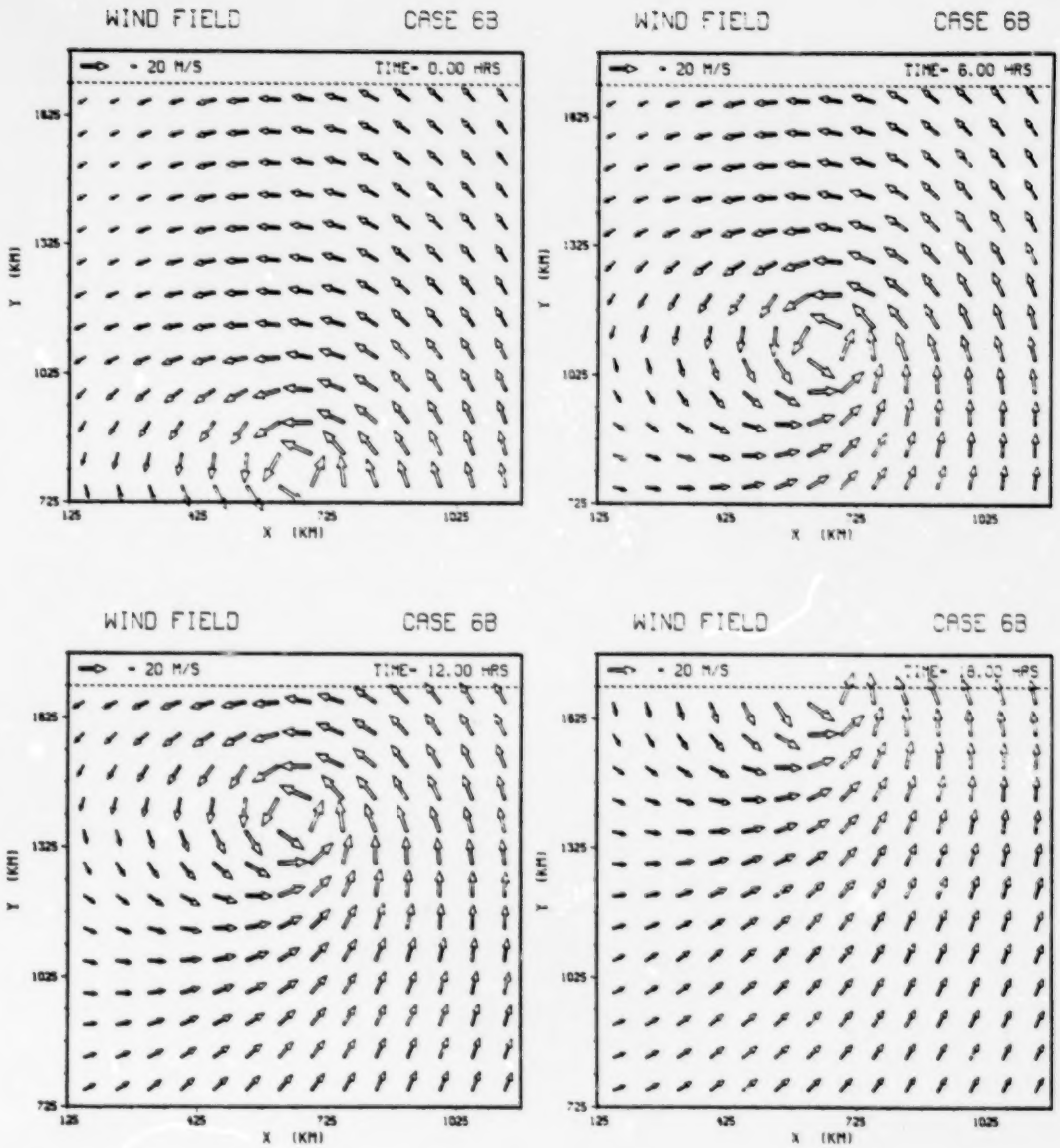
WIND FIELD
CASE 68
- 20 M/S
TIME- 0.00 HRS
WIND FIELD
CASE 68
- 20 M/S
TIME- 6.00 HRS
WIND FIELD
CASE 68
- 20 M/S
TIME- 12.00 HRS
WIND FIELD
CASE 68
- 20 M/S
TIME- 18.00 HRS
Y (KM)
X (KM)
125
425
725
1025
1325
1625

VI.25 - VI.28

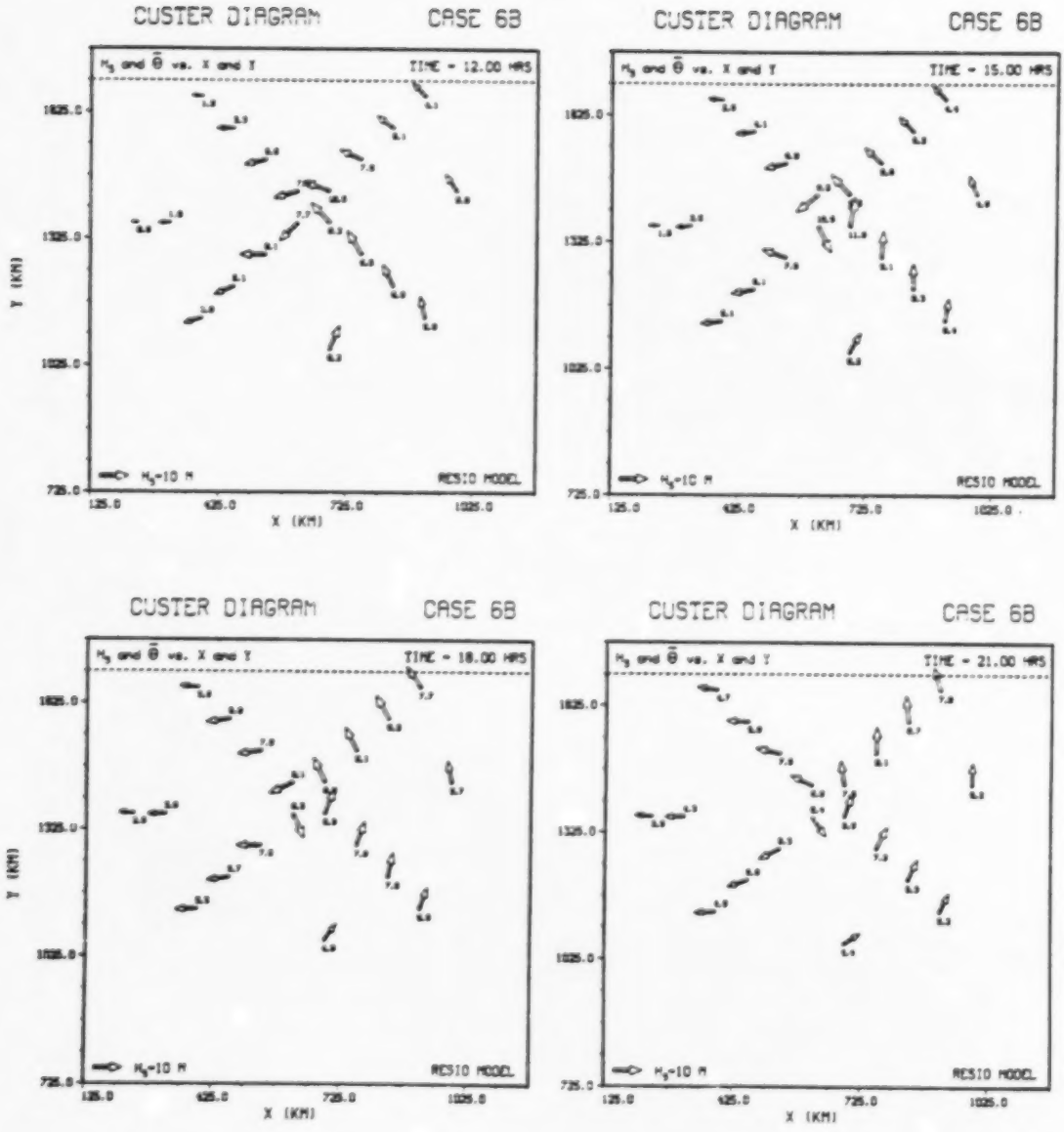
CUSTER DIAGRAM CASE 6B
H_s and $\bar{\theta}$ vs. X and Y
TIME = 12.00 HRS
H_s=10 M
RESIO MODEL
Y (KM)
X (KM)
CUSTER DIAGRAM CASE 6B
H_s and $\bar{\theta}$ vs. X and Y
TIME = 15.00 HRS
H_s=10 M
RESIO MODEL
X (KM)
CUSTER DIAGRAM CASE 6B
H_s and $\bar{\theta}$ vs. X and Y
TIME = 18.00 HRS
H_s=10 M
RESIO MODEL
Y (KM)
X (KM)
CUSTER DIAGRAM CASE 6B
H_s and $\bar{\theta}$ vs. X and Y
TIME = 21.00 HRS
H_s=10 M
RESIO MODEL
X (KM)

VI.29 - VI.32

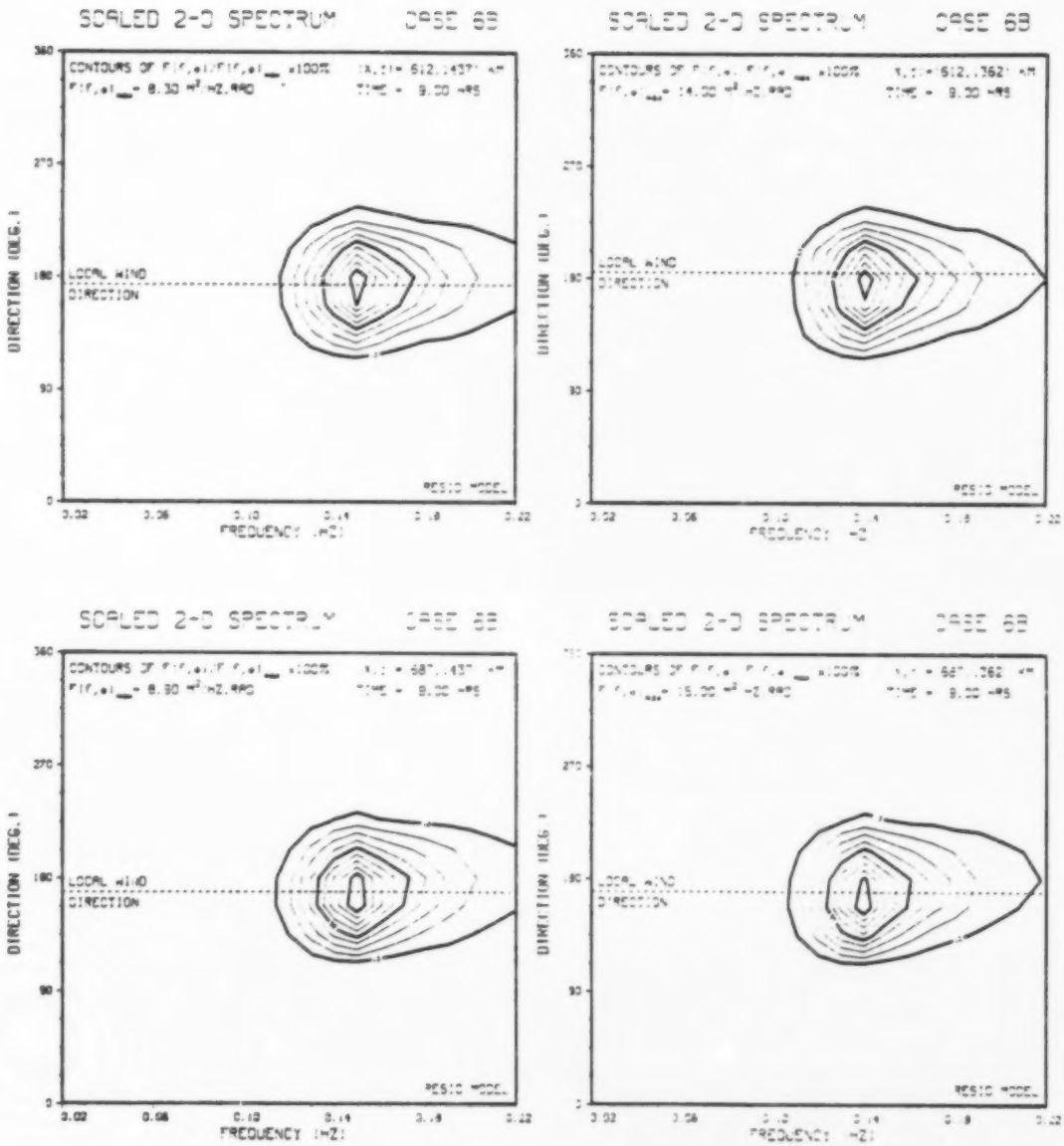
SCALED 2-D SPECTRUM
CASE 6B
DIRECTION (DEG.)
FREQUENCY (HZ)
LOCAL WIND DIRECTION
RESID MODEL

VI.33 - VI.36

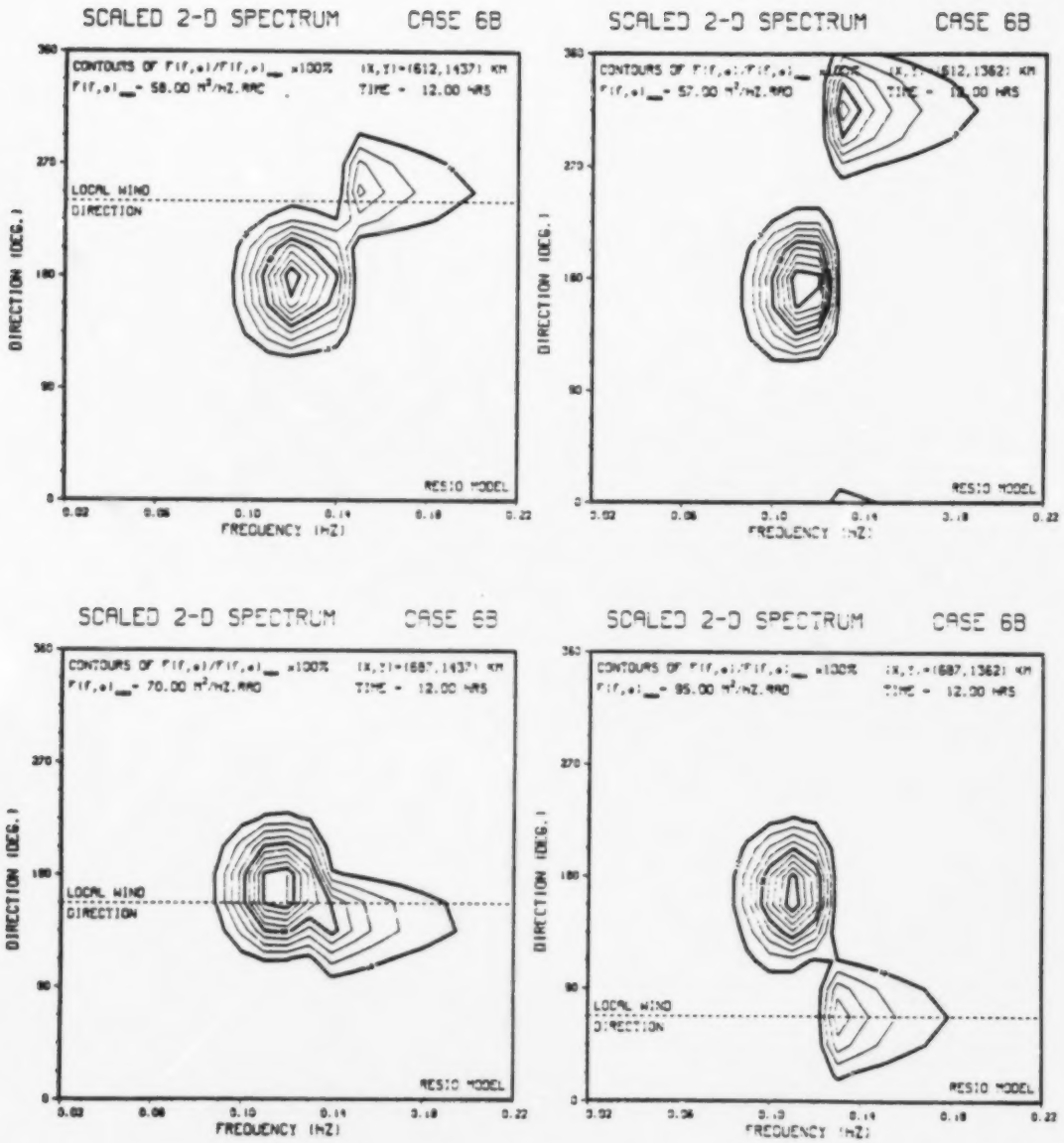
SCALED 2-D SPECTRUM CASE 6B
SCALED 2-D SPECTRUM CASE 6B
SCALED 2-D SPECTRUM CASE 6B
SCALED 2-D SPECTRUM CASE 6B
LOCAL WIND DIRECTION
RESID MODEL
DIRECTION (DEG.)
FREQUENCY (HZ)

VI.37 - VI.40

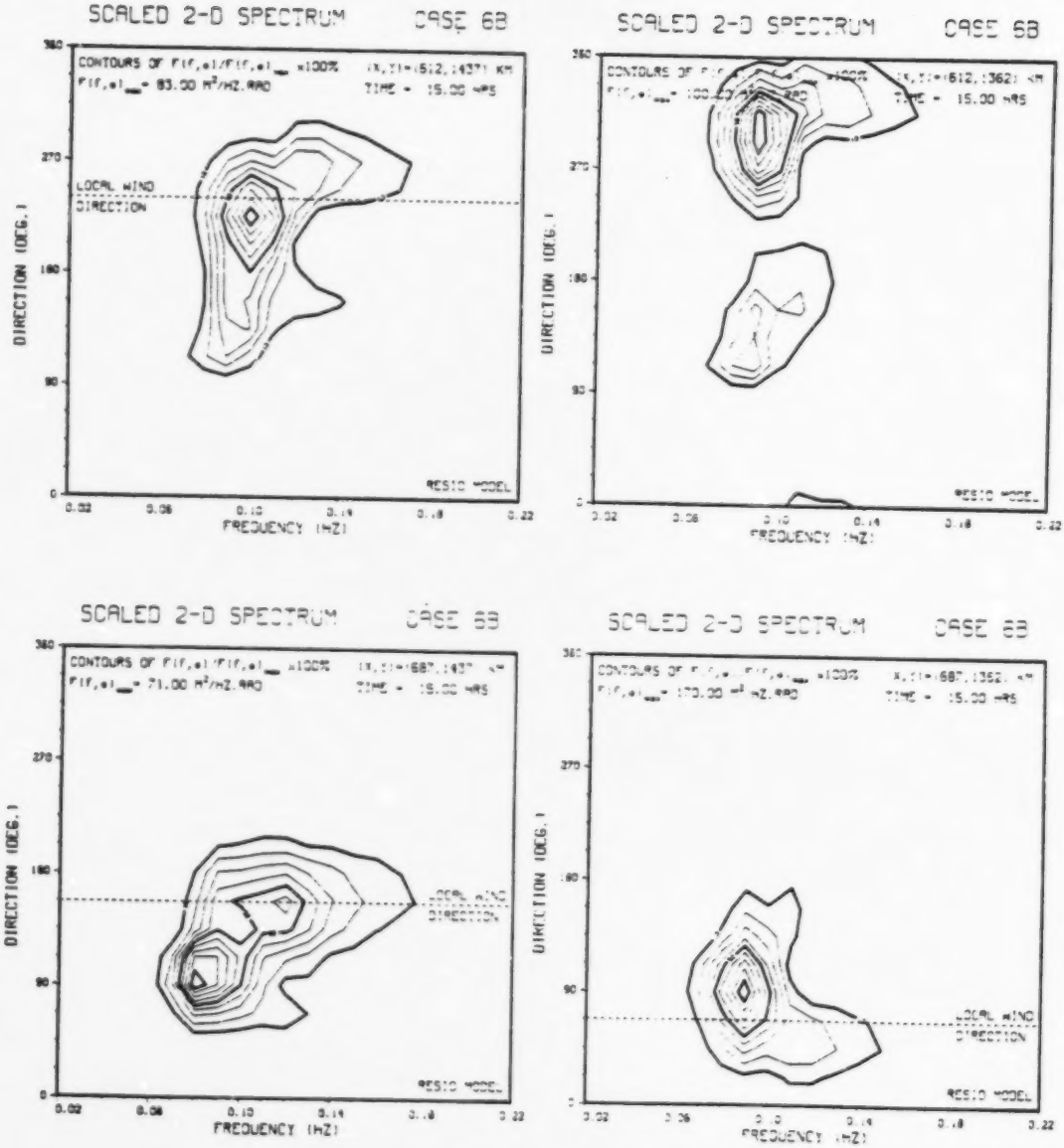
SCALED 2-D SPECTRUM CASE 6B
SCALED 2-D SPECTRUM CASE 6B
SCALED 2-D SPECTRUM CASE 8B
SCALED 2-D SPECTRUM CASE 8B
DIRECTION (DEG.)
FREQUENCY (HZ)
LOCAL WIND DIRECTION
RESID MODEL

VI.41 - VI.44

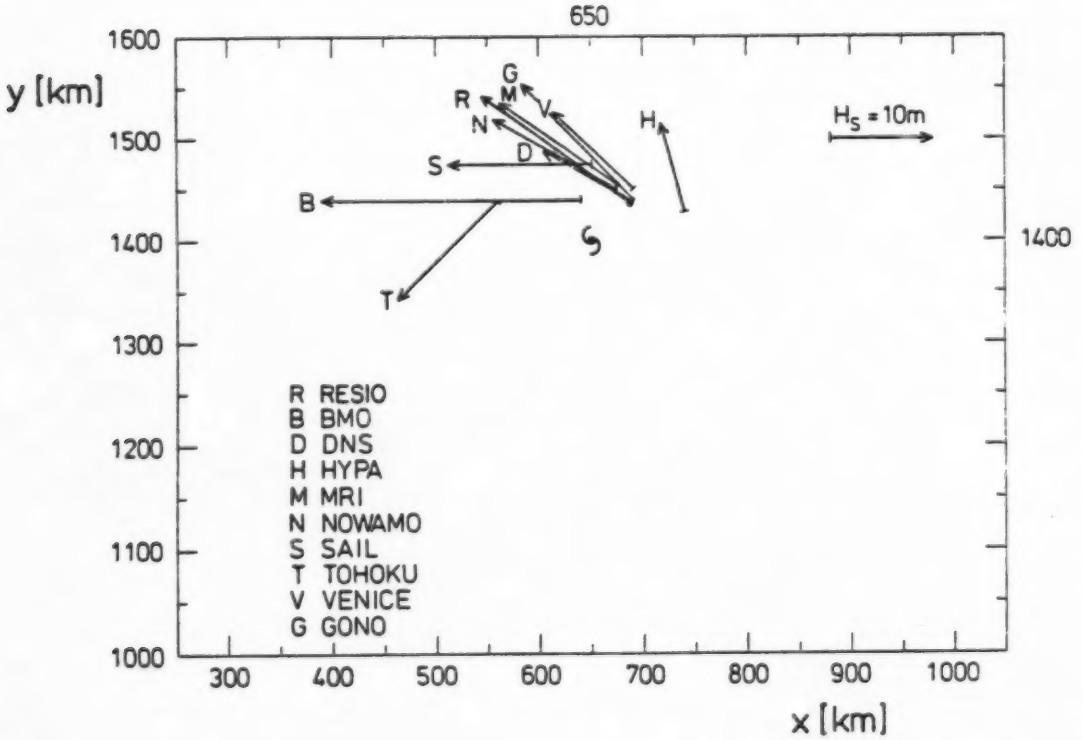
650
1600
1500
1400
1300
1200
1100
1000
y [km]
300
400
500
600
700
800
900
1000
x [km]
1400
G
M
R
V
N
H
D
S
B
T
H_S = 10m
R RESIO
B BMO
D DNS
H HYPA
M MRI
N NOWAMO
S SAIL
T TOHOKU
V VENICE
G GONO

VI.45